4-5-2016

Investigating Simple Shear Mechanics of Bovine Cartilage Using a Triaxial Shear Test Machine

Stephany Santos
stephany.santos@uconn.edu

Investigating Simple Shear Mechanics of Bovine Cartilage Using a Triaxial Shear Test Machine

Stephany Santos

B.S., University of Connecticut, 2012

A Thesis
Submitted in Partial Fulfillment of the
Requirements for the Degree of
Master of Science
at the
University of Connecticut
2016

APPROVAL PAGE

Master of Science Thesis

Investigating Simple Shear Mechanics of Bovine Cartilage Using a Triaxial Shear Test Machine

Presented by
Stephany Santos, B.S.

Major Advisor _____
Dr. David M. Pierce

Associate Advisor _____
Dr. Jiong Tang

Associate Advisor _____
Dr. Donald Peterson

University of Connecticut
2016

Acknowledgment

"Even if you fall on your face you're still moving forward." - Victor Kiam

After years of anticipation, this work is finally wrapped up and I can move to the next chapter.

Thank you to Dr. David M. Pierce, my current advisor, for pushing me, keeping me a realist, and for all the support. Thank you to Dr. Donald Peterson, my previous advisor, for giving me a strong foundation and opening the door to the world of biomechanics for me.

Thank you to Italy and the Politecnico di Milano, for re-introducing me to the beauty and simplicity of life. Thank you to Dr. Pasquale Vena, my Italian advisor, for the international support and advice in this global, interdisciplinary field. Thank you to my committee members, Federica Boschetti, Jose Feliz Rodriguez Matas and Jiong Tang for your time and guidance.

Thank you to Kevin McLaughlin, Sonya Renfro, and the Engineering Ambassadors, who remind me to think of the bigger picture, and understand how my piece fits into rest of the world. Thank you to Aida Ghiaei for pushing me forward, asking questions, and caring about my progress.

Thank you to Franz Maier, Jon Kaplan, and Bilal Kaleem, my labmates, who give tremendous support and insight in our experimental lab. Thank you to Deborah Dorcemus, my pseudo-labmate, for speaking my cartilage language, and helping me understand the fundamentals.

Thank you to Dr. James Grady for the tremendous help with the statistical analysis.

Thank you to Danica Chin, my best friend, and Jacques Pauleus, my fellow EAGLES scholar, for actually reading my thesis and giving me guidance and support.

Thank you to Patricia Santos, my sister, for the late night phone calls and favors and helping me when no one else was around. Thank you to my parents for praying and pushing me and believing in me.

Thank you to Davin English, my boyfriend, for being patient and supportive, and keeping me sane.

This is Part 1. Part 2 is the dissertation. Part 3 is the world.

Contents

List of Figures

List of Tables

Abstract

Objective: Articular cartilage is a non-homogeneous tissue with complex structure-function relationships. Damage to articular cartilage leads to traditionally irreparable conditions such as osteoarthritis, a disease that is both painful and debilitating to a large human population. The objective in this thesis is to perform triaxial mechanical tests on articular cartilage that are quasi-static and large-shear strains, in order to understand tissue mechanical behavior. ***Methods:*** Cartilage explants were taken from three healthy adult bovine femurs. Specimens were categorized by joint contact and contact stress regions with respect to the femoral condyle. Specimens were subject to applied shear parallel and perpendicular to the split line direction at $5\,\%$, $10\,\%$, $15\,\%$ and $20\,\%$ while submerged in phosphate buffered saline at $37\,^{\circ}\mathrm{C}$. Force and displacement were measured, and the shear stress and dissipation energy were calculated. ***Results:*** Joint contact region, governed by degrees of flexion, and thickness have significant effects on articular cartilage stiffness and the dissipation energy. There were no significant differences in results obtained from shearing parallel to the split line direction versus perpendicular, nor between high and low stress load-bearing regions. At 5% applied shear strain, $G = 412$ kPa, which is comparable to reported values for bovine by other groups.

1 Introduction

1.1 Motivation for Studying Knee Articular Cartilage

Understanding human body movements has been a topic of interest since the beginning of medical history. In recent years, there has been a shift from analyzing human body movements in a *qualitative* point of view to a *quantitative* point of view, merging the medical field with engineering principles and analysis (Lawson 1873, Buckwalter and Martin 1995, Peat et al. 2001). The human race has been plagued with mobility issues. For example, approximately one in five adults experience some form of painful physical limitation. The prevalence of disability tends to double in successive age groups (Brault et al. 2009, Ramos-Pichardo et al. 2014). Furthermore, a study published by the World Health Organization found that up to 76% of adults over the age of 65 report difficulty in walking one kilometer (Capistrant et al. 2014). The knee, one of the critical regions of the body, often induces this gait discomfort, ergo, the area of interest for this thesis.

The knee, a complex diarthrodal joint consisting of three joints - the lateral and medial tibio-femoral joints and the patello-femoral joint - has a relatively unstable configuration with respect to other joints, i.e. the ball-and-socket style hip and shoulder synovial joints (Blackburn and Craig 1980, Mow et al. 2005); hence, knee injuries are not unusual. Pain in the knee

can be caused by a number of sources such as acute injury, chronic trauma, or by intrinsic properties or diseases, such as arthritis. For many of these, cartilage can be designated as the primary site and root cause of discomfort (Atkinson et al. 1998, Peat et al. 2001, Logerstedt et al. 2010). The work presented in this thesis focuses on cartilage behavior as the crux to better understand and predict knee pain and disease.

Cartilage responds to both chemical and physical changes in the body. Thus, when a joint experiences a mechanical stimulus such as limb motion, inappropriate positions or loads, a cascade of changes could occur that ultimately lead to degradation of the fluid extracellular matrix and its solid constituents (Buckwalter 1997). It could also lead to damage of other joint structures such as the underlying bone, muscles, and tendons (Buckwalter and Martin 2006). Additionally, biochemical changes triggered by the mechanical stimulus often lead to a decreased presence of the proteins necessary for normal joint function. These biochemical changes contribute, as well as respond, to physical changes, thereby leading to further detrimental tissue transformations, and lending itself to a vicious cycle (Ewers et al. 2001, Julkunen et al. 2013).

Considering physical changes, cartilage degradation is categorized as the disease osteoarthritis (OA). The breakdown of cartilage leading to OA is due to a multitude of factors including genetic, mechanical, and chemical factors, and can be acute or chronic in nature (Mow et al. 2005). It is the most common joint disease affecting the human population, with up to 90% of adults over 40 showing signs of joint degeneration (Barbucci et al. 2002, Buckwalter and Martin 2006). Yet, there is no definitive cause of the disease. With OA being the second leading cause of disability in the United States, there is an evident need to determine the etiology of OA. The most comprehensive solutions involve the interdisciplinary approaches of both experimental and clinical practices (Griffin et al. 2014). The study described in this thesis uses

empirical clinical data to fuel experimental methods to analyze normal cartilage as a baseline for understanding OA-based knee issues.

For improved cognizance of the vicious cycle of destructive biochemical and physical changes, it is essential to understand the tissue's function in the body, considering both the ultrastructure and microstructure, and how the structure and function relate to each other and contribute to joint behavior. This will contribute to improved diagnostic tools and methods, as well as prognostic insight for potential disease prevention and care.

1.2 Cartilage Function: An Overview

Cartilage is a type of connective tissue that is found in various areas of the body. The tissue function is directly correlated to its morphology, which can be categorized into three types: Elastic, Hyaline and Fibrous. Elastic cartilage, the only type to contain elastin, provides flexible support and shape for various bodily structures, most notably the ear pinnae. Hyaline cartilage serves as a flexible yet firm protective agent on many interfaces, such as the rib cage, trachea, nose, and at joint articulations. Fibrocartilage is comprised of both flexible and rigid constituents, and provides stronger, shock-absorber-like support, as seen in intervertebral discs and the meniscus. (Mow et al. 2005, Buckwalter 1997, Heinegård and Paulsson 1987, Julkunen et al. 2013)

Ideally, cartilage tissue best performs as a low-friction, compliant, structure that dampens and distributes contact pressure evenly to the underlying bone. One specific type of hyaline cartilage, articular cartilage (AC), serves as the cushion between both long and sesamoid bones and prevents direct contact between the two bone surfaces, or periosteum (Mow et al. 2005). This allows our joints to move comfortably and freely. Osseous tissue is highly inner-

vated. Consequently, when direct contact stimulates the sensitive nociceptors, as with bone-bone/surface-bone contact, we feel severe pain. This anomaly occurs in patients with OA.

In the knee, AC covers the surfaces of the femoral condyles, tibial plateau, and the posterior face of the patella, as in Fig. 1.1, averaging a thickness of approximately 2 to 2.5 mm on average in humans, though the thickness varies throughout the surface up the tissue, as seen in Fig. 1.2 (Frisbie et al. 2006). Additionally, fibrocartilage -namely the menisci- serves as a“deep-dish socket" support on the tibial plateaus to provide a seat for the interfacing femur. The menisci are secured by a direct connection to capsular ligaments (Blackburn and Craig 1980). Therefore, to define function, the articular cartilage protects and lubricates, and the menisci provide further stability by holding the condyle in place.

1.3 Cartilage Structure: An Overview

Cartilage is a complex biological material. To the human-eye, healthy articular cartilage is a smooth, flexible, glistening translucent material, although, upon histological examination, it is heterogeneous on several accords. Approximately 70-85% of the weight of the tissue is water and electrolytes (fluid component), with the remainder comprising of the matrix proteins proteoglycans and collagen (solid components) (Mow et al. 2005, Buckwalter and Martin 2006, Julkunen et al. 2013). These constituents reside in a poroelastic medium with a dynamic composition. Due to its composition and its biomechanical behavior, some regard articular cartilage as “an inert hyperhydrated hydrogel" in nature (Eisenfeld et al. 1978).

Collagen, a fibrous protein, exists in over 16 forms. In articular cartilage, it primarily as fibers or fibril bundles of types I, II, and III (Gelse et al. 2003). Collagen fiber arrangement varies through the thickness of the tissue. This contributes to the anisotropic behavior. Car-

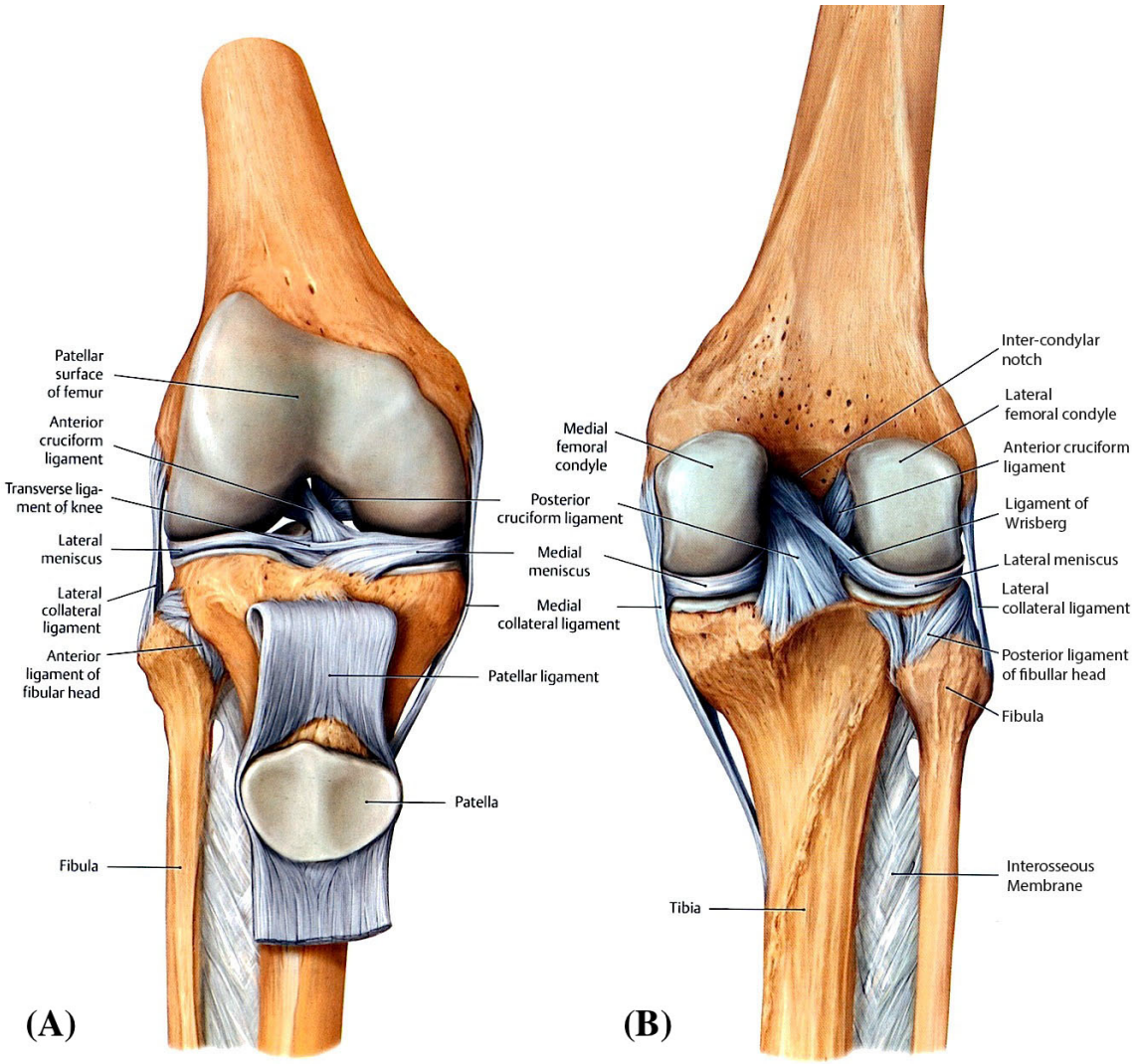

Figure 1.1: Anatomy of the human knee. **(A)** Anterior view. **(B)** Posterior view (Adapted from (Stannard and Luck 2015))

tilage can be divided into four major zones between the articular surface and the subchondral bone: Superficial/Tangential, Intermediate/Middle, Deep/Radiate, and Calcified Zones, as seen in Fig. 1.3 B. In the superficial zone, cartilage fibers are oriented approximately parallel to the surface. Specifically, the fibers are aligned in layers governed by the split-line direction.

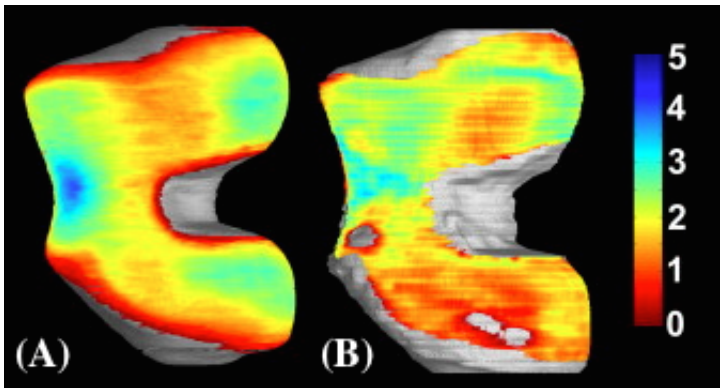

Figure 1.2: Human femoral head cartilage thickness map. **(A)** Normal **(B)** OA (Adapted from (Carballido-Gamio et al. 2008))

A gross depiction of split-lines can be seen in Fig. 1.4, and a more detailed representation in Fig. 1.5. Split lines are reference features made apparent by micro punctures on the surface of the cartilage, first demonstrated by Meachim (1972). Upon pricking the surface with a circular tool, an ellipsoidal hole transpires, confirming the general direction of the cartilage fibers. Split-line directions can vary within the articular surface, and are thus understood to have in-plane deviations. Split-line directions have been shown to precisely follow certain directions and orientations in greater load-bearing regions along the femoral condyle, though direct correlations between orientation and tissue behavior have yet to be investigated (Below et al. 2002). Considering depth deviations, in the intermediate zone, the fibers adjust radially, such that when transitioning deeper into the tissue, the fibers are randomly interwoven. In the deep zone, the fibers align themselves in a near-perpendicular fashion with respect to the subchondral bone surface. In addition to orientation shifts, the individual fiber thickness also varies with depth, such that the thinnest fibers are in the superficial zone, and exhibit increased thickness in the deeper zones (Mansour 2003, Julkunen et al. 2013).

On the microscale, keratan and chondroitin sulfates attach to a hyaluronic acid backbone to

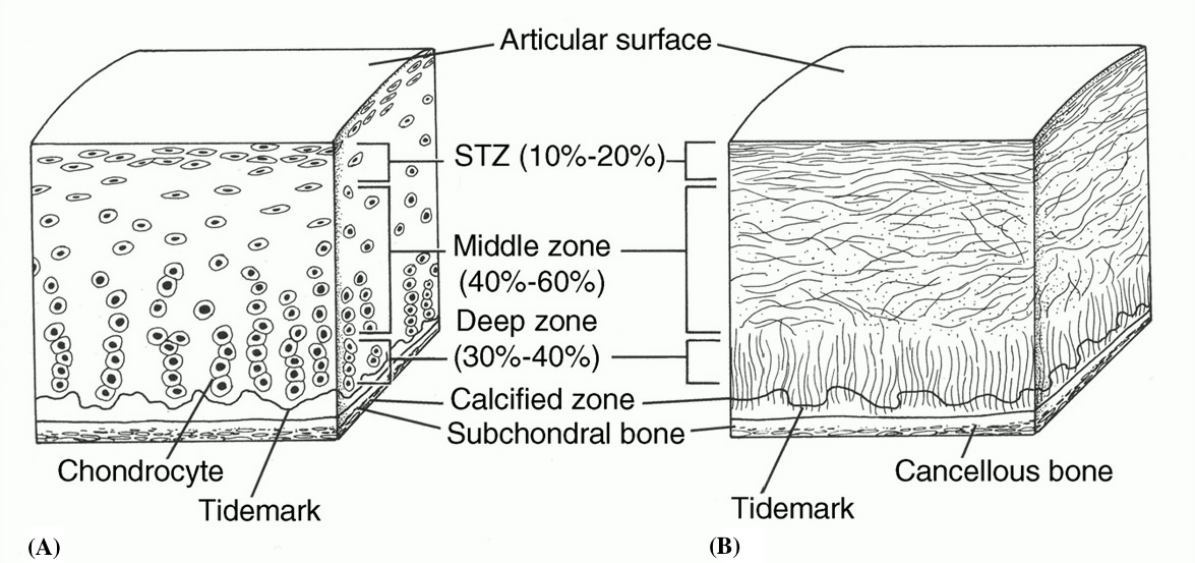

Figure 1.3: Cartilage structural morphology. **A,** Schematic showing the organization of chondrocytes in articular cartilage and the development of the three major uncalcified zones: superficial tangential zone (STZ), middle zone, and deep zone. The subchondral bone and tidemark are also shown. **B,** Schematic (sagittal cross-section) showing the collagen fiber orientation and alignment. The orientation shifts from superficial surface to the deep zone. (Reproduced from Buckwalter et al. (1994))

form the proteoglycan molecule. This macromolecule, often referred to as aggrecan, is suspended in the extracellular fluid and is intermixed between collagen fibers. The concentration of the aggrecan also varies through the thickness of the tissue, with the lowest concentration near the articular surface in the superficial zone, and increasing concentrations approaching the deep zone. Aggrecan dispersion additionally varies due to proximity to chondrocyte cells (Broom 1986, Jurvelin et al. 1997, Mow et al. 2005). Table 1.1 shows a summary of articular cartilage components.

Considering the cellular level, the cell type unique to cartilage tissue are called chondrocytes. The differentiation process of mesenchymal cells into chondrocytes, is vividly apparent

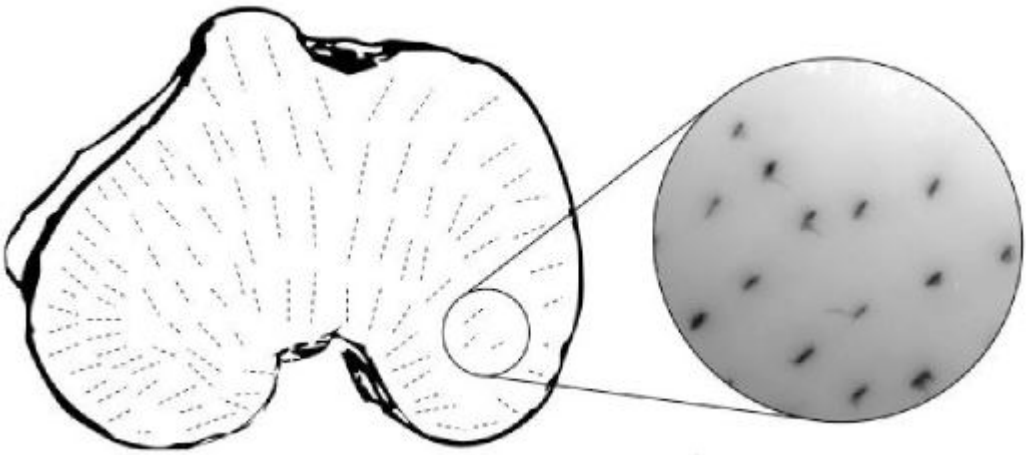

Figure 1.4: Split lines of the distal femur show the fiber orientation at the articular surface. The black lines are a result of India Ink needle piercing and staining to show the fiber orientation. (Reproduced from Athanasiou et al. (2013))

in the tissue structure, with newly differentiated chondrocytes near the superficial zone surface, and fully mature chondrocytes lining the calcified region. The chondrocytes are densely packed and relatively flat at the articular surface. They then shift towards a columnar orientation perpendicular to the calcified surface, as in Fig. 1.3 A. These ovoid chondrocytes form and maintain the fluid extracellular matrix of cartilage. The solid, fibrous pericellular matrix surrounding the chondrocytes help form the lacunae that is several microns long and is clearly visible in histological staining. Since cartilage is neither vascular nor innervated, chondrocytes provide the locus for fluid diffusion, which occurs in order to provide a nutrient supply to the tissue (Archer and Francis-West 2003). The nutrients come directly from the synovial fluid. Chondrocyte functions include the synthesis and secretion both proteoglycans and collagen. The chondrocyte matrix contains structures such as intracytoplasmic filaments, lipids, and cilia, all of which may have a role in sensing mechanical stimulation in the surrounding

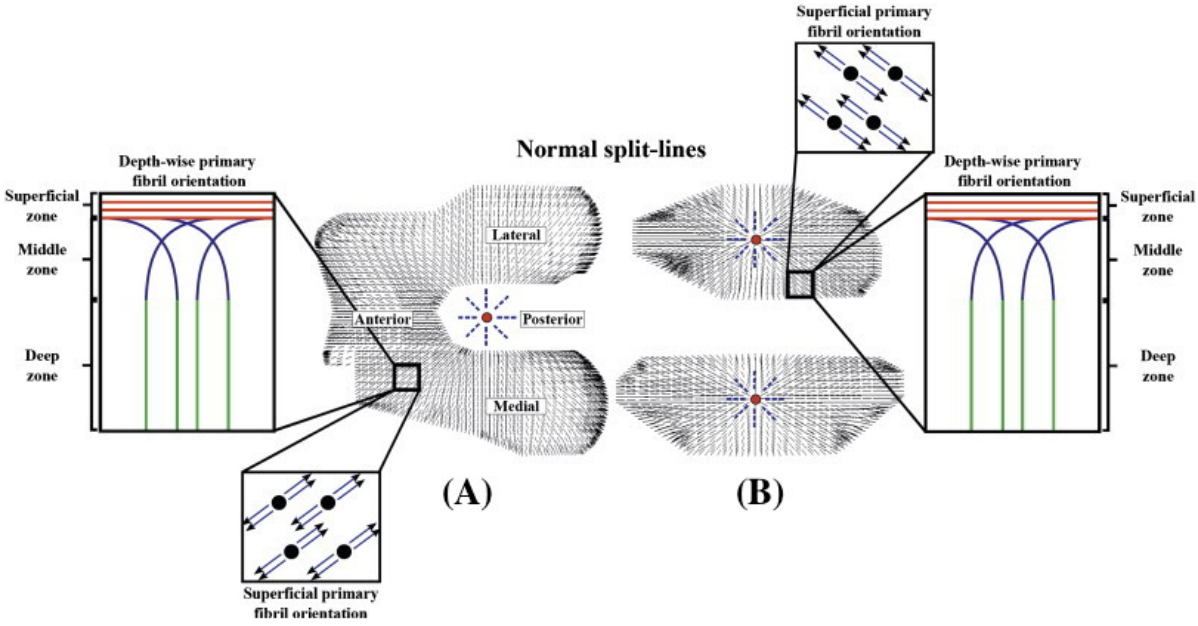

Figure 1.5: Normal split line patterns. Red circles indicate a reference point for pattern calculation. The zoomed subsections show localized split line behavior in both cross-sectional and top-views. **(A)** Normal femoral split line behavior. **(B)** Normal tibia split line behavior. (Reproduced from Mononen et al. (2012))

tissue.Compared to other cell types, chondrocytes have relatively low levels of metabolic activity, and has a lower response to mechanical stimuli or loads. Individual chondrocytes do have high metabolic levels, but considering total metabolic activity in the tissue, it is very low due to the low cell density (Buckwalter and Mankin 1998). Nonetheless, chondrocytes contribute significantly to AC behavior.

1.4 Cartilage Structure-Function Relationships

During human motion such as walking, the articular cartilage of the femur articulates and glides against the cartilage covering the tibial plateau (Wong and Sah 2010). In terms of all

Component	Wet Wt.(%)	Dry Wt.(%)	Distribution	Descriptor
Quantitatively Major				
Water	60-85		Throughout the tissue	
Collagen, type II	10-20	70	Throughout the tissue	Fibril forming molecule; 95% of total collagen
Aggrecan	5-10	30	Near surface, low concentration. Greatest concentration near subchondral surface	
Quantitatively Minor(<5%)				
Link protein				
Hyaluronan				
Collagen, type XI			Throughout the tissue	Fibril forming molecule; 3% of total collagen
Collagen, type VI			Throughout; May be concentrated pericellularly	Short-helix molecule; <1% of total collagen
Collagen, type IX			Throughout the tissue	Short-helix molecule; 1% of total collagen
Collagen, type X			Hypertrophic zone of growth plate and basal calcified zone of articular cartilage	Short-helix molecule; 1% of total collagen
Collagen, type V			Throughout; appears at the expense of type XI in mature cartilage	Short-helix molecule; <1% of total collagen

Table 1.1: Summary of articular cartilage components. (Adapted from Eyre (1991), Mansour (2003), Mow et al. (2005))

physiological motions, the knee can experience flexion-extension, anterior-posterior sliding, and medial-lateral rotation. The articular cartilage responds by serving as a load bearing interface that permits smooth motions of the joint, and typically lasts the majority of the human lifetime, or 60-90 years (Mow et al. 2005, Buckley et al. 2008). Its structure contributes to its functionality.

Considering overall load-bearing, the load distribution varies across the surface of the tissue, as seen in Fig. 1.6. The figures specifically show the areas of joint contact during varying degrees of flexion and extension. Conversely, the stress distribution can be seen in Fig. 1.7

The internal structure supports the local and global tissue function.

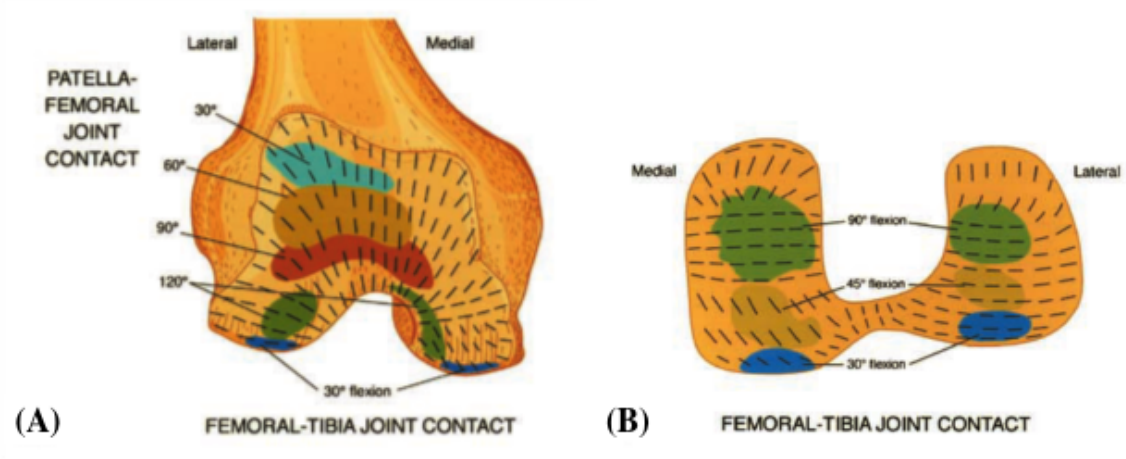

Figure 1.6: **(A)** Schematic drawing of the femoral head showing split-lines and areas of joint contact between the patella and distal femur. **(B)** Schematic drawing of the femoral head showing split-lines and areas of joint contact between the femur and tibia. (Adapted from Below et al. (2002))

As previously mentioned, the proteoglycan aggrecan, collagen, and other particles are suspended in a fluid matrix. When an impact occurs, the fluid is compressed, so suspended structures within the fluid matrix displace, reducing the distance between the particles. The proteoglycan aggregate of glycosaminoglycans and hyaluronic acid is negatively charged, thus, upon interaction with other aggrecan, repel each other. This repulsion is what causes the stiffness response of cartilage tissue, thereby providing stronger support when needed.

Furthermore, fluid permeability is very low through surface pores of cartilage tissue, and is greatly dependent upon the pore sizes, as well as the depth in the tissue. The frictional drag force of this interstitial fluid flow is an additional factor contributing to the tissue response behavior. Upon rapid compression, the fluid experiences difficulty flowing through the solid matrix pores. Some of the fluid is able to flow through the pores, albeit, a portion of the water that remains is absorbed by the collagen fibrils (Wilson et al. 2006). This allows the tissue to

generate hydrostatic pressure during compression, providing most of the support to the joint on shorter time scales.

Another contributor to the quantity of intrafibrillar water present in the cartilage is the fixed charge density from the proteoglycans. This fixed charge density affects the tissue swelling pressure, which controls the diameter of the fibrils, and thereby the amount of intrafibrillar water. Mow et al. (1989) attests that most intrafibrillar water is not eligible for transport in mechanical loading, which contributes to the normal osmotic pressure. This pressure is required for normal cartilage function.

The solid constituents and fluid matrix form the biphasic nature of cartilage. The two phases interact and contribute to the state of the other, yet they also are independently incompressible and have varied responses to mechanical stimuli (Mansour 2003). The biphasic nature can account for any and all inhomogeneities, isotropies, and variations in deformation (Mow et al. 1980, Ateshian et al. 1997, Wang et al. 2001).

Connecting the inherent structure with physiological function is two-thirds of the puzzle for completely understanding cartilage tissue. The structure and function is well-known in the biomedical community, but the third piece, mechanical properties, is still under investigation. This thesis probes knee cartilage mechanical properties as it relates to structure and function to contribute to the overall understanding of normal and diseased cartilage tissue.

1.5 Mechanical Properties of Cartilage

Standard knee motions such as rising from a deep bend require muscles to generate remarkably large mechanical moments and forces. These moments produce reaction forces in the knee joint that can reach up to 3 to 6 times body weight, which have been linked to causing

damage in the articular cartilage tissue and surrounding bone structures (Adams 2006). There are several factors that contribute to how tissue responds, such as thickness, contour map, and composition (Mow et al. 2005). These factors vary between individuals, as well as within a particular joint. It is important to understand exactly how the tissue, as a whole, and considering spatial variations, responds to mechanical loading.

Articular cartilage is both heterogeneous and anisotropic. The anisotropy is primarily due to the orientation of the collagen fibers, and the heterogeneity is attributed to the layer variation of the collagen and chondrocytes (Mow et al. 2005). Its depth-dependent composition contributes to nonlinear behaviors during knee compression and tension (Boschetti et al. 2004). The knee typically experiences 0 to $20\,\mathrm{MPa}$ during typical adult motion, which affects several component functions in the knee joint. Stress is a property that cannot be measured, but is rather calculated from measured forces during experimental procedures. Immobilization experiments have shown chondrocytes require normal loading to maintain homeostasis. Removing mechanical loads result in decreased chondrocyte proliferation and matrix synthesis, which often leads to cartilage thinning (Grodzinsky et al. 2000). Contrarily, increased exercise and loading increases matrix synthesis, and has proven to be a protective element for the knee articular cartilage. Specifically, an *in vitro* study found chondrocytes increased proteoglycan and collagen synthesis under increased cyclic tension.This positive effect only occurs until certain limits of magnitude and or frequency are reached. At this point, the mechanical loading has a destructive effect, causing the cartilage to potentially degenerate (Mow et al. 2005, Buckwalter and Martin 2006). Additionally, phenotypic expression can be altered during mechanical loads affecting the chondrocytes, further contributing to the detrimental effects immobilization or injury can have on cartilage (Mauck et al. 2000).

To describe cartilage mechanical behavior, material coefficients and constants such as Young's

modulus (E), shear modulus (μ or G), bulk modulus (K_o), aggregate modulus (H_A), permeability (ϕ or k), and Poisson's ratio (ν), can be used. The data analysis in Chapter 5 in this thesis will discuss particular parameters as it relates to experimental results and overall cartilage behavior. The aforementioned parameters are defined below and related to cartilage function and behavior.

Young's Modulus, also known as the tensile or elastic modulus, measures the stiffness of the material when exposed to uniaxial force. Materials with high Young's moduli, such as diamond (1220 GPa) or steel (200 GPa), are very rigid (Toolbox 2012). Cartilage typically has a Young's modulus of 0.45 to 0.80 MPa (Mansour 2003). Rubber, which is commonly compared to cartilage, exhibits a Young's modulus between 10 to 100 MPa under small strains. It is worth noting that the Young's modulus of an individual collagen fiber is between 30 to 800 MPa (Stein et al. 2010, Bar-On and Daniel Wagner 2012), which is more comparable to that of rubber.

The shear modulus is similar to the tensile (Young's) modulus, as it represents the stiffness of the material. The difference is that the shear modulus reports the stiffness of a material experiencing shear loads. Generally, shear loads are loads that are applied parallel to a surface while an equal and opposite force is experienced by the opposing surface. For example, a shear force causes a rectangular prism to deform into a parallelepiped. Water has a very small shear modulus of 1.3×10^{-11} MPa, while blood has a shear modulus approximately two orders of magnitude higher (Korenchenko and Beskachko 2008). Cartilage on the other hand has a significantly greater shear modulus between 0.06 to 0.18 MPa under equilibrium conditions and small strains(1% to 5%) (Wong et al. 2008), and rubber has a shear modulus of 0.6 MPa (Spanos 2003). Buckley et al. (2008) found the shear modulus is depth dependent, with variations of up to two magnitudes between the articular surface and the subchondral bone. This is

important when considering tissue anisotropy and zonal variations. Later on, the group determined the dynamic shear modulus, G^* to give the time- and depth-dependent elastic properties of cartilage. The dynamic shear modulus differs in principle from the static or equilibrium shear modulus in which the dynamic shear modulus is typically measured during sinusoidal shear application. Time-dependence is due to the change in mechanical behavior after initial loads are applied, and depth-dependence is due to the location within the tissue. In addition to the dynamic shear modulus, the local phase angle δ is measured as well as a reference. At the surface, Buckley et al. (2013) found the dynamic shear modulus to be approximately $1.5\,\mathrm{MPa}$ in the superficial zone, and 2.1 to $2.5\,\mathrm{MPa}$ in the deeper zones. Understanding the shear modulus, especially the depth-dependence and dynamic properties, lead to better understanding of the initiation and propagation of local diseases such as osteoarthritis.

The bulk modulus measures a material's resistance to uniform pressure or compression. For cartilage, it describes the change in volume due to isotropic stress, such as that due to osmotic pressure in the joint (Chen et al. 2001). An interpretation of the bulk modulus would be, a material with a bulk modulus of $1\,\mathrm{GPa}$ loses 1% of its volume when under an external pressure of $1\,\mathrm{GPa}$. Accordingly, a large bulk modulus implies a relatively incompressible material. Chen et al. (2001) found the bulk modulus to be between 0.8 to $2.4\,\mathrm{MPa}$ and that K increases with depth from the articular surface. The bulk moduli, though not sufficiently investigated, has given significant implication for load bearing properties and normal biomechanical behavior of articular cartilage.

The aggregate modulus measures the stiffness of a material at equilibrium, where equilibrium is defined as a state where there is no fluid flow. In cartilage, a region of with a low aggregate modulus may correlate with a region of localized finite deformation during loading (Wang et al. 2001). For cartilage, typical aggregate moduli values range between 0.5 to

$0.9\,\mathrm{MPa}$ (Jurvelin et al. 1997, Mansour 2003). This modulus describes the behavior of biological materials, so it cannot truly be compared with solid materials such as rubber or other commonly compared media.

Permeability describes a material's ability to resist fluid flow. For cartilage, it refers to fluid flow through the fibrillar matrix. Permeability is also referred to as the constant of proportionality, and in cartilage, ranges from 1×10^{-15} to $1 \times 10^{-16}\,\mathrm{m}^4/\mathrm{Ns}$ (Mansour 2003). This permeability is considered very low, which results in high interstitial fluid pressures during loading (Archer and Francis-West 2003). This is significant for joint support. Permeability is dependent on the pore size and the fixed charge density of proteoglycans, and is strain-dependent as well as depth-dependent (Wilson et al. 2006). Permeability is strain-dependent, such that permeability non-linearly decreases with applied compressive deformation (Boschetti et al. 2004, Mow et al. 1984). It is depth-dependent, such that the permeability decreases as the depth from the articular surface increases (Mow et al. 1984).Permeability variation gives tremendous insight to equilibrium and transient properties of articular cartilage.

Finally, Poisson's ratio is an intrinsic dimensionless parameter that gives the ratio of transverse strain to axial strain. Under axial compression, cartilage radially expands. The amount of lateral expansion can be characterized by Poisson's ratio (Athanasiou et al. 2013). It describes the tissue's tendency to physically distort rather than change in volume (Greaves et al. 2011). Poisson's ratio values are typically between -1 and 0.5 for stable materials, but anisotropic materials can have values greater than 0.5 (Wang et al. 2003). For materials where applied stress results in a change in shape, ν is approximately 0.5, and the material is considered incompressible. Cartilage can have ν values between 0 and 2.1 under certain load magnitudes and directions(Mow et al. 2005). Skin in comparison has an average Poisson's ratio of 1.0 (Lees et al. 1991). Poisson's ratio has a large effect on articular cartilage creep behavior

(Athanasiou et al. 1991), which is further described in the following sections.

According to Ateshian et al. (1997), the aforementioned six material parameters completely determine material behavior for a biphasic, isotropic, hyperelastic tissue. This model, along with other comprehensive models, pave the way for the future of computer-aided diagnostics. With accurate models, tissue behavior can be simulated for various periods of time under diverse loads, leading to a better understanding of human aging and tissue-based diseases such as osteoarthritis. These parameters must be calculated from experimental tests using appropriate stress-strain relationships and constituted laws (Mow et al. 2005). Thus, to better understand cartilage behavior *in vivo*, we perform *ex vivo* experimental procedures.

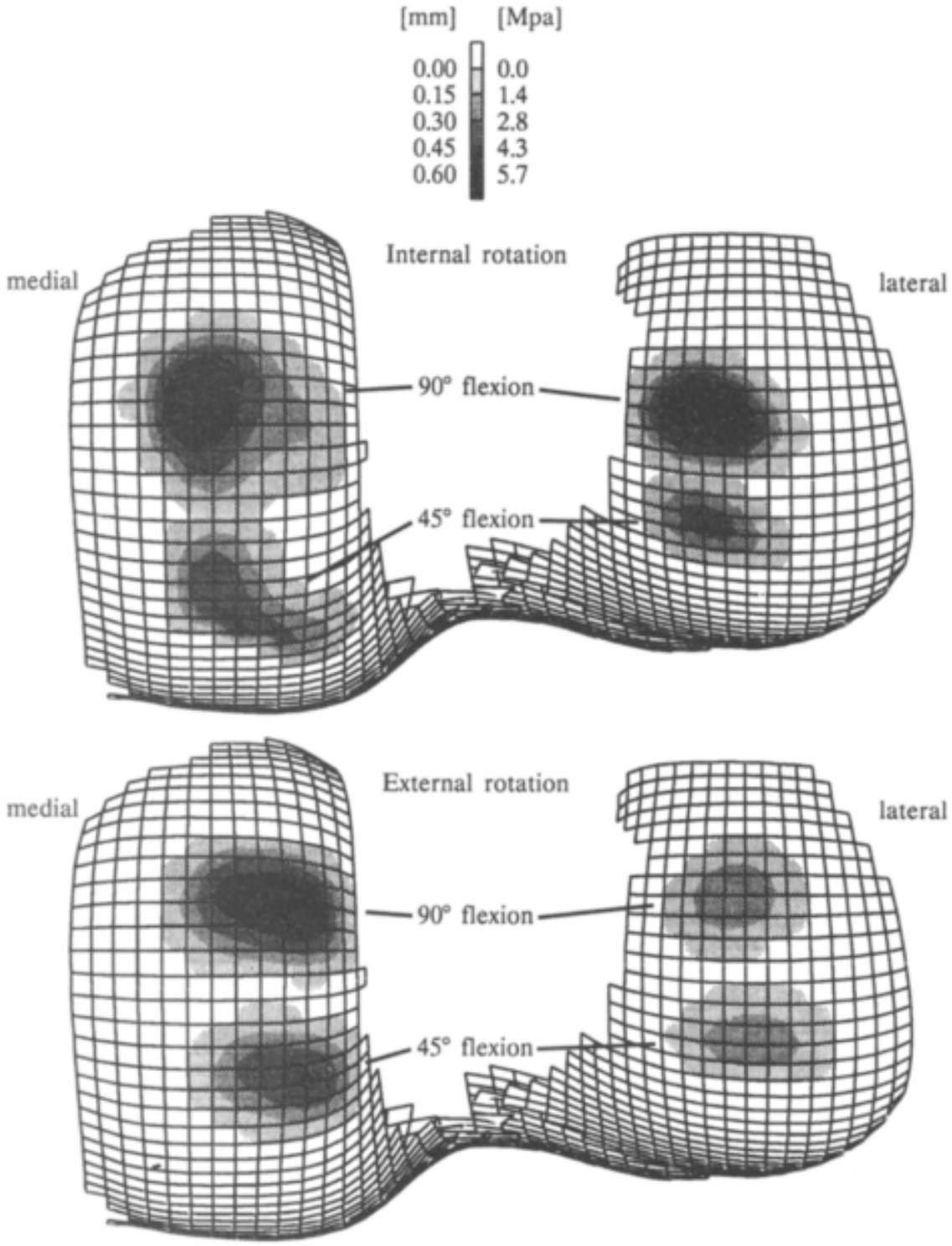

Figure 1.7: Surface displacements and surface stresses on the femoral condyle during 45° and 90° during flexion, internal rotation, and external rotation (Reproduced from Blankevoort et al. (1991)).

2 Experimental Studies of Cartilage Mechanics: Early Findings

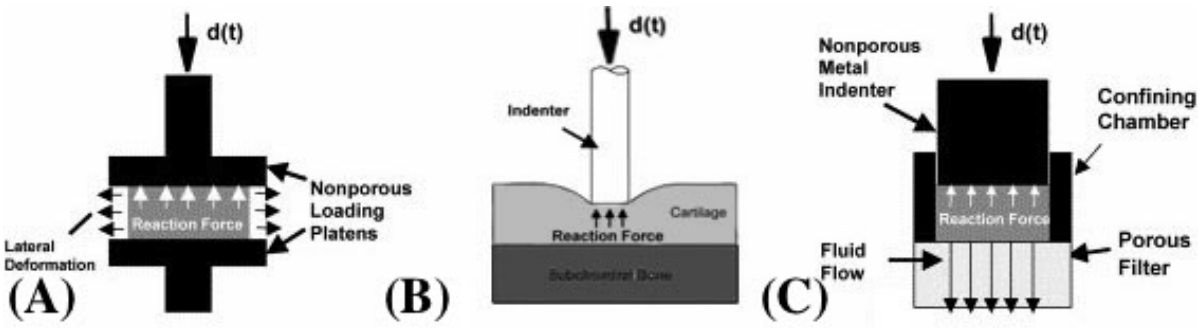

Figure 2.1: Schematics of three types of experimental setups for mechanically testing articular cartilage. **(A)** Unconfined compression **(B)** Indentation **(C)** Confined compression. (Adapted from DiSilvestro and Suh (001a))

2.1 Indentation Tests

One of the earliest mechanical tests conducted on cartilage were indentation tests to investigate cartilage deformability and stiffness. These indentation tests give insight to cartilage recovery characteristics of healthy and diseased tissue, as well as other elastic material constant infor-

mation. Additionally, indentation tests can show how stiffness varies across the joint articular surface (Kempson et al. 1970), which is fundamental when considering localized evidence of OA within a joint. Results from indentation tests have led to the general acceptance that cartilage is a viscoelastic material (Mow et al. 1980). Materials that are viscoelastic exhibit both viscous properties - i.e. resisting fluid flow, such as honey - and elastic properties - i.e. a tendency to return to its original shape after deformation, such as steel or rubber.

Experimental setup can vary, from using a small cylindrical explant of cartilage with subchondral bone still attached, as done by Clements et al. (2001), DiSilvestro and Suh (001a) in Fig. 2.1 (ii), to a complete femoral or tibial condyle as by Kempson et al. (1971). Notably, Lyyra et al. (1995) created an indentation instrument capable of taking measurements arthroscopically. This allows for the possibility of *in vivo* indentation tests, which gives clinicians a tool to evaluate cartilage stiffness and other mechanical properties by minimally invasive means. For typical *ex vivo* experiments, the tissue is submerged in saline solution at body temperature and the test is conducted with an impermeable indenter with either a planar or hemispherical end smaller than the diameter of the sample. The tip is assumed to be frictionless and shear tractions are assumed to be negligible. The indenter is lowered onto the articular surface and the load, displacement, and time are measured directly.

There are two types of indentation tests, producing either time-dependent creep deformation or stress relaxation responses (Hayes et al. 1972). Creep can be defined as the tendency of a solid material to deform under a constant mechanical load, and is a nod to viscous behavior of a material. Specifically, it is the increase in strain under constant stress. Stress relaxation on the other hand is the decrease in stress/force observed from a constant strain/deformation application (Purslow et al. 1998). Both of these loading conditions describe the kinetic behavior of cartilage, and can be seen in Fig. 2.2.

In creep, cartilage does not displace instantaneously, rather its displacement is dependent on time, due to fluid flow constraints through the tissue pores. Under the constant load, cartilage creep response is found to be rapid at first, then gradually slows down as it approaches a constant value and equilibrium. Typically, equilibrium is reached after several thousand seconds (Mansour 2003). In stress relaxation, the tissue is indented to a prescribed distance, and held at this deformed location. The force buildup within the tissue, namely the osmotic pressure, changes over time as interstitial fluid is released. This measured force change gives insight to the time-dependent nature of cartilage (Jurvelin et al. 1997).

Indentation tests may also be frequency dependent, where a sinusoidal or other oscillatory load or deformation is applied, and its response is recorded (Athanasiou et al. 2013). This experimental procedure intends to simulate natural conditions in the human body during motions such as walking, running, etc. Applying sinusoidal loads extended for millions of cycles can help us better understand how the cartilage tissue responds over time, and thus, lead to a better understanding of how the tissue degenerates as we age.

With the arthroscopic indenter by Lyyra et al. (1995), the group found a linear relationship between indenter force and the cartilage shear modulus, μ, and therefore a linear relationship between force and stiffness under shearing loads. Earlier *in situ* tests (Kempson et al. 1971, Hayes et al. 1972) assumed cartilage to be linear, isotropic, homogeneous and elastic, and able to be characterized by two out of the parameters E, ν, H_A, and μ, but more recent tests include the more accurate biphasic nature of cartilage, specifically the inclusion of the effects of interstitial fluid and thusly the heterogeneous behavior (Mow et al. 1989). The group was able to calculate H_A, ν, and k without any *a priori* assumptions by curve fitting experimental creep curves with a custom algorithm.

Further assumptions for indentation tests include (Kempson et al. 1971):

1. Indentation is reversible up to two seconds of loading

2. Anisotropic behavior exists in planes both parallel and perpendicular to articular surface.

The second assumption splits the tissue into two separate areas with respect to the planes perpendicular to the articular surface to analyze depth variations. The first segment captures articular surface properties, considering tissue up to $400\,\mu\mathrm{m}$ deep. This depth was chosen to represent the superficial zone where fiber orientations are parallel to planar surface and anisotropic behavior exists. The second region is the area beyond $400\,\mu\mathrm{m}$, which includes more random fiber orientation. In the latter region, the tissue tends to behave isotropically due to the random fiber orientation and dispersion (Kempson et al. 1971). This produces differences in stress distributions between the superficial zone and the deeper zones that need to be considered.

The following outlines the calculation of various constants and moduli from indentation test results as described by the literature.

Calculating the Shear Modulus, μ or G - from Lyyra et al. (1995)

$$G = \frac{P(1-v)}{4\alpha\omega\kappa} \tag{2.1}$$

G is shear modulus, P is the indenter force, v is Poisson's ratio, α is the indenter radius, ω is the deformation, κ is a correction function for the finite cartilage thickness. Thus, the shear modulus is directly proportional to Poisson's ratio. This means the shear modulus depends on the ratio of the area of the indenter to the tissue thickness, the deformation, and the independent material property v (Parsons and Black 1977).

Equation 2.1 can also be used to calculate the cartilage thickness if it is not known.

Calculating Creep Modulus, E - from Kempson et al. (1971)

For a hemisphere indenter

$$E = 1.28\left[\frac{1 - exp(\frac{-0.42^t}{a_t})}{d_t}\right]^{\frac{3}{2}} \tag{2.2}$$

E is the creep modulus, t is the time after load application, a_t is the contact area radius, d_t indentation distance for a sheet of finite thickness t.

For a planar indenter

$$E = 5.37\left[\frac{\phi(\frac{t}{R})}{d_t}\right] \tag{2.3}$$

$\phi(\frac{t}{R})$ is a function of the ratio of the sheet thickness to the indenter radius (R).

2.1.1 Shortcomings of Indentation Tests

There are three major shortcomings that arise during indentation tests. The first issue regards the assumptions made by the researchers. Several indentation tests require prior assumptions of values for Poisson's ratio and other constants (Mow et al. 1989, Fischenich et al. 2015). Further assumptions of either a single phase or biphasic material nature of cartilage can affect results (Mow et al. 1980, Mansour 2003). Further considerations to include viscoelastic dissipation from the solid matrix could also be considered. Mow et al. (1980) faced challenges when assuming there was constant deformation that was independent of permeability. These assumptions, along with the dependency of extrinsic material properties on specimen geometry, indenter geometry, and the overall procedure, make experiments difficult to reproduce or compare results. Furthermore, according to Parsons and Black (1977), it is "virtually

impossible" to compare the data from these distinct indentation tests.

The second issue regards post-processing data. Interpretation of experimental results from indentation tests is difficult because of the complex mechanical nature of articular cartilage, and the interdependent structural properties to consider (Woo et al. 1979). Additionally, Korhonen et al. (2002) found the size of the indenter produced different values for the elastic moduli, encountering a dependency between the two. Consequently, translation of results into clinical relevance or accurate theoretical models can be difficult.

The third flaw with indentation tests is the compaction effect, or loss of porosity, experienced by the tissue due to loading using a porous indenter (Park et al. 2004). Cartilage tends to compensate for compaction effects at the articular surface by continuing to propagate the effects into deeper zones (Mow et al. 1980), which can produce skewed stress-relaxation results.

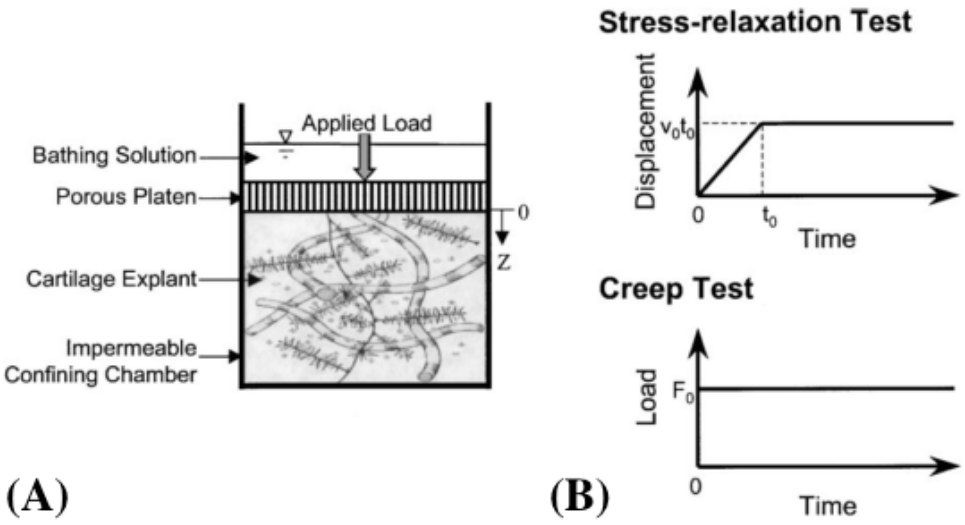

Figure 2.2: **(A)** One-dimensional schematic for confined compression. **(B)** Loading conditions for indentation and compression tests. (Adapted from Wang et al. (2001))

2.2 Confined Compression Tests

This method is one of the most commonly used tests to determine material properties of articular cartilage. It determines compressive properties of cartilage tissue, often times aiming to explain the non-linear strain-dependent permeability behavior (Mow et al. 1984). Confined compression tests also give cartilage viscoelastic responses, and insight to the motion and interaction between the solid matrix and interstitial fluid (Mow et al. 1980). Additionally, confined compression tests emulate *in vivo* conditions where surrounding tissue prevents large deformation. Physiological loading conditions for compression average between 5-20% during repeated knee flexion and running (Wong et al. 2008).

An excised osteochondral (with bone still attached) or purely cartilage plug is placed into a close-fitting well, as in Fig. 2.1 (i). The tissue is confined on all sides and is fit into the well such that the sides are flush and perfectly parallel to the tissue to ensure even load distributions (Athanasiou et al. 2013). The lateral sides are non-porous, whereas either the bottom or the top is a porous platen with an average pore size of $40\,\mu\text{m}$ that allows free flow of fluid(DiSilvestro and Suh 001a, Boschetti et al. 2004). The pores are typically located only at the articular surface (Mow et al. 1984). Unlike indentation tests, the width of the top platen is typically the same as the cartilage cylinder explant. Compression is applied normal to the articular surface.

Once placed in the confined well, there are two different approaches for applying a uniaxial load onto the tissue, equivalent to the modes previously mentioned for indentation tests in section 2.1. The first is creep mode, in which a constant load is applied to the load by a platen and the displacement over time is measured. The second is stress relaxation mode, in which a constant displacement is applied, and the force required to maintain the plate in that position is measured over time. The prevention of lateral expansion simplifies this compression prob-

lem as a one-dimensional test (Mow et al. 1984). The one-dimensional prevents measuring Poisson's ratio, so other methods, i.e. unconfined compression, must be used to determine this parameter (Jurvelin et al. 1997). The strain tensor can typically be calculated by (2.4), where u_z is the axial deformation (Soltz and Ateshian 2000).

$$\mathbf{E} = \begin{bmatrix} 0 & 0 & 0 \\ 0 & 0 & 0 \\ 0 & 0 & \frac{\partial u_z}{\partial z} \end{bmatrix} \tag{2.4}$$

The elastic stress tensor can be found by (2.5):

$$\sigma = \begin{bmatrix} \lambda_2 \frac{\partial u_z}{\partial z} & 0 & 0 \\ 0 & \lambda_2 \frac{\partial u_z}{\partial z} & 0 \\ 0 & 0 & H_{-A} \frac{\partial u_z}{\partial z} \end{bmatrix} \tag{2.5}$$

where H_{-A} is the confined compression modulus and λ_2 is a material parameter.

Since Mow et al. conducted the first successful publication to include both fluid and solid constituents in a coupled model in 1977, confined compression tests now typically include biphasic considerations to model the inhomogeneous nature (Hayes and Bodine 1978, Mow et al. 1980). Specifically, the solid matrix is assumed to be linear elastic, incompressible, and nondissipative. The fluid is assumed to be incompressible, and non-dissipative.

The governing equation for confined compression, originally derived from linear biphasic theory for isotropic homogeneous materials, is given by Mow et al. (1980), Soltz and Ateshian (1998)

$$\frac{\partial^2 u}{\partial z^2} - \frac{1}{H_A k_0} \frac{\partial u}{\partial t} = 0 \tag{2.6}$$

Where $u(z,t)$ is the solid phase displacement.

Average permeability can be calculated with the empirical law (Mow et al. 1984).

$$k = k_0 exp[\epsilon M] \tag{2.7}$$

Where k is the permeability, k_0 and M are intrinsic permeability parameters, and ϵ is the dilation of the solid matrix.

Confined compression tests have also been found to measure the aggregate modulus, H_A, with remarkable accuracy (Mow et al. 1984). The equation is given by

$$H_A = \lambda_s + 2\mu_s \tag{2.8}$$

Where λ_s and μ_s are the intrinsic elastic moduli for the solid phase.

The following three equations give boundary conditions with respect to experimental setup and settings. For a test setup where the bottom is impermeable, the boundary condition at the bottom is

$$u(0,t) = 0. \tag{2.9}$$

For stress relaxation tests, boundary conditions for the top permeable platen are,

$$u(h,t) = \begin{cases} -V_0 t & 0 \leqslant < t_o \text{ compression phase} \\ -V_0 t_0 & t_o \leqslant t \text{ relaxation phase} \end{cases} \tag{2.10}$$

where V_0 is the displacement rate.

For creep, the boundary condition is

$$H_A \frac{\partial u}{\partial z}\bigg|_{z=h} = -P_A \tag{2.11}$$

where P_A is the applied compressive load.

The Eqs. 2.8 and 2.11 are commonly applied to the biphasic theory equation that includes the nonlinearity and one-dimensional deformation and diffusion, giving to solve the creep problem(Mow et al. 1984)

$$H_A \frac{\partial^2 u}{\partial z^2} = k_o \exp\left(-M\frac{\partial u}{\partial z}\right)\frac{\partial u}{\partial t} \tag{2.12}$$

A significant result from creep experiments has shown that regardless of the initial force applied, the response of the tissue is proportional to $\sqrt{t}$.

Analogously, (2.10) is used to calculate the stress during relaxation by (Mow et al. 1984)

$$\begin{aligned} &\sigma_{zz}(t) \approx \sigma_p - M_r\sqrt{t-t_o} \\ &\text{where} \\ &\sigma_p = -\epsilon_0 H_A[1 + c_0\exp(\epsilon_0 M)] \\ &M_r = \frac{2h\epsilon_0 H_A}{t_0\sqrt{\pi H_A k_0 \exp(\epsilon_0 M)}} \end{aligned} \tag{2.13}$$

Results have shown that fluid redistribution causes the stress relaxation phenomenon. The fluid distribution is governed the decrease in permeability the tissue being in compression (Mow et al. 1984).

2.2.1 Shortcomings of Confined Compression Tests

There are three considerable shortcomings for confined compression tests. The first involves discrepancies due to experimental setup, which can be subdivided into human error and machine error. Human error from cutting the bottom face parallel to the articular surface could lead to misalignment and could give erroneous solutions to depth-dependent parameters. Additionally, “true" confined compression tests are difficult to execute, since the diameter of the explant needs to be slightly smaller than the confinement chamber bore. Therefore, initial responses from a confined compression test actually reflect Unconfined Compression Tests due to the tissue expanding to meet the chamber walls. With respect to machine error, Boschetti et al. (2004) argues a gap between the sides of the platen/indenter and the confinement walls alters results and causes an underestimation in calculated values for H_A and an overestimation for k. Nonetheless, the gap is necessary for proper “frictionless" indenter movement. Another machine-related error involves the interlocking and sticking of the articular surface into compressive platen pores (Korhonen et al. 2002). This interdigitation could increase resistance within the tissue, and is also a shortcoming for any porous surface in contact with cartilage.

The second shortcoming pertains to post-processing. Considering the lateral gap of the top platen, along with the assumption that no fluid flow at equilibrium, the data acquired is slightly tarnished. As a result, post processing to extrapolate the deformation during this time is usually required. (Mow et al. 1980).

The final shortcoming regards calculations of time-dependence properties. During confined compression tests, instantaneous deformations and responses are not possible; notwithstanding, instantaneous deformation is possible with unconfined compression tests, discussed in the next section, where the tissue can freely expand in the lateral direction.

2.3 Unconfined Compression Tests

Unconfined compression is very similar to Confined Compression Tests with the exception that the tissue is allowed to laterally expand freely; there is no confining well, as seen in Fig. 2.1 A. In contrary to the one-dimensional nature of confined compression tests, this is a two-dimensional problem, with the two dimensions being vertical and lateral variation. A 2D problem allows the Young's modulus to be calculated using constitutive stress-strain relationships, and the strain and stress tensors are given by (2.14-2.15),(Soltz and Ateshian 2000). Unconfined compression is typically the method of choice when desiring to produce near-physiological axial and lateral loading conditions over confined compression or Indentation Tests (Mauck et al. 2000). With unconfined compression tests, aforementioned approaches for load application protocols exist, though an additional approach with intentional varied displacement, or step-wise, as a function of time, can be considered. This test is typically used to find the tensile and compressive moduli, determine material symmetry, and to determine depth-dependent compressive properties (Krishnan et al. 2003). Furthermore, groups such as DiSilvestro and Suh (001a), Wang et al. (2003), Boschetti et al. (2004) use optical techniques to measure tissue expansion under compression and compare observations to experimental and simulated parameter values.

$$\mathbf{E} = \begin{bmatrix} \frac{\partial u_r}{\partial r} & 0 & 0 \\ 0 & \frac{u_r}{r} & 0 \\ 0 & 0 & \frac{\partial u_z}{\partial z} \end{bmatrix} \tag{2.14}$$

The elastic stress tensor can be found by (2.15):

$$\sigma = \begin{bmatrix} H_{+A}\frac{\partial u_r}{\partial r} + \lambda_2(\frac{u_r}{r} + \frac{\partial u_z}{\partial z}) & 0 & 0 \\ 0 & H_{+A}\frac{\partial u_r}{\partial r} + \lambda_2(\frac{\partial u_r}{\partial r} + \frac{\partial u_z}{\partial z}) & 0 \\ 0 & 0 & H_{+A}\frac{\partial u_r}{\partial r} + \lambda_2(\frac{u_r}{r} + \frac{\partial u_r}{\partial r}) \end{bmatrix} \quad (2.15)$$

Considering experimental set up, some groups (DiSilvestro and Suh 001a) use cartilage explants with underlying bone attached. These groups can observe mechanical matrix disruption due to high loads or loading rates. More often, groups remove the underlying bone (Wang et al. 2003, Park et al. 2004, Boschetti et al. 2004). There are several advantages to removing the subchondral bone, such as the use of lower loading rates to observe solid matrix damage, as well as chondrocyte metabolic response, including death (Ewers et al. 2001). Removal of bone to allow full cartilage expansion is not representative of *in vivo* conditions, but it does give valuable information for constitutive modeling (Park et al. 2004). Nevertheless, unconfined compression is more representative of *in vivo* conditions than confined compression or indentation tests due to the axial compression and lateral tension the cartilage is subjected to. Additionally, some groups (Krishnan et al. 2003) slice the cartilage into approximate zones to determine depth-depending properties such as Young's moduli and Poisson's ratio. In unconfined compression, the upper and lower platens are typically non-porous and impermeable (Athanasiou et al. 2013). Finally, synovial fluid can be applied between the platen-cartilage interfaces as a lubricant to reduce friction (Jurvelin et al. 1997).

During unconfined compression tests, it was found that cartilage is not functionally adapted for producing homogeneous stress, strain, or strain energy distributions. Additionally, maintaining interstitial fluid pressurization is required for cartilage functionality and integrity, and

support is greatest at the articular surface (Krishnan et al. 2003). It also seems that the underlying bone has a protective effect on the solid matrix during mechanical loading (Ewers et al. 2001). Finally, unconfined compression tests have shown the biphasic poroviscoelastic (BPVE) model accurately represents and simulates experimental results obtained for various moduli as well as the amount of lateral expansion that occurred (DiSilvestro and Suh 001a).

The biphasic constitutive model states the total tissue stress is a sum of the stresses from the solid component and fluid component, or

$$\sigma = \sigma^s + \sigma^f \tag{2.16}$$

In this model, the fluid term is

$$\sigma^f = -\phi^f p\mathbf{I} \tag{2.17}$$

where, ϕ^f is the volume fraction of the fluid, and p is the hydrostatic pressure.

The solid stress term takes into account the viscoelasticity of the solid phase, as shown in the unconfined compression test results. The stress is

$$\sigma^s = -\phi^s p\mathbf{I} + \tilde{\sigma}^s \tag{2.18}$$

where,ϕ^s is the volume fraction of the solid, and $\tilde{\sigma}^s$, the effective solid stress tensor, is

$$\tilde{\sigma}^s = B_s tr(\epsilon^s)\mathbf{I} + 2\mu_s \int_0^t G(t-\tau))\frac{\partial \mathbf{e}^s}{\partial \tau}d\tau \tag{2.19}$$

where B_s is the elastic bulk modulus, mu_s is the elastic shear modulus, τ is the relaxation time, ϵ^s is the solid strain tensor, and e^s is the deviatoric component of the solid strain tensor

(DiSilvestro et al. 001b).

These findings contribute to the development of a fully comprehensive model effectively able to predict behavior and determine cartilage pathology.

2.3.1 Shortcomings of Unconfined Compression Tests

There are three significant drawbacks with unconfined compression tests. The first is friction occurring during the test, which is intrinsic due to the nature of the experimental setup allowing tissue expansion. Specifically, friction between the tissue and the upper and lower platens can be an issue with unconfined compression tests (DiSilvestro and Suh 001a). In experiments, great care is taken to minimize this friction, including using synovial fluid. Friction is greatly reduced but is not eliminated, potentially influencing shear deformation. Groups could opt to use Phosphate Buffered Saline (PBS) solution as a lubricant, though notwithstanding, this has been found to elevates boundary friction (Wong et al. 2008).

The second flaw revolves around sample preparation. Physical artifacts from extracting the explant from the joint by cutting tools can affect tissue behavior and potentially produce reduced stiffness during unconfined compression tests (Korhonen et al. 2002). Furthermore, despite the fact that the majority of groups remove the subchondral layer before testing, Park et al. (2004) argues that removing the bone can disturb the collagen network, giving unrealistic responses. Wang et al. (2003) also argues many compression tests do not take the split-line orientation into account, and thereby ignore cartilage anisotropic properties. Fibril orientation directly impacts tissue compressive and tensile behaviors. Fiber arrangement and orientation vary with age, as in Fig. 2.3, so it is relevant to know the tissue state and fiber arrangement to accurately represent anisotropic behavior. The final issue regards model selection and pro-

cessing. Issues with accurately representing the stress relaxation response during unconfined compression with the linear biphasic elastic model has proved to been found (Boschetti et al. 2006). An example of a known issue is the inaccuracy of the ratio of stress experience between the peak and at equilibrium (Li et al. 1999). Additionally, many models assume constant fluid permeability for simplicity, which is not physiologically accurate. Wang et al. (2003) also found that linear orthotropic elasticity cannot characterize cartilage material symmetry nor the equilibrium response during unconfined compression. Finally, theoretical calculations were not commensurate with experimentally determined values for Poisson's ratio, so use of unconfined compression tests has been limited in comparison to other tests (Jurvelin et al. 1997).

2.4 Tension Tests

Tensile tests are not a commonly employed mechanical testing method for articular cartilage, but nevertheless they are useful for determining directional tensile properties and investigating the full effects of cartilage anisotropy (Woo et al. 1979). The strength exhibited by articular cartilage can greatly be attributed to collagen fibers (Athanasiou et al. 2013). It has been found that collagen fibers have high tensile strength and tremendous extensability, reaching up to 100% strain before fracturing (Shen et al. 2008). In addition to the collagen, proteoglycans have an indirect effect on cartilage tensile properties as well (Asanbaeva et al. 2008). Tension is required of cartilage in order to prevent excessive lateral expansion, maintaining the shape and structural integrity (Williamson et al. 2003). Tension balances the interstitial fluid pressure even when no external loads are applied to the joint (Fan and Waldman 2010). In cartilage, tension is experienced even under simple compression loads, along with shear and fluid pressure, contributing to a complex mechanical environment (Guilak and Mow 2000).

Specifically, tension has been investigated has one of the forces that influences chondrocyte proliferation and behavior. Therefore, in recent years, tension tests have also been utilized as a stimulation component in artificial cartilage growth (Fan and Waldman 2010). There are two types of tensile tests that can be conducted, which are elaborated on in the following sections.

2.4.1 Uniaxial Tension

The uniaxial tension method intends to apply loads to be able to observe cartilage extensability properties, as well as understand changes in fibril orientation and thickness. Cartilage harbors immense tension-compression response asymmetry, justifying the need for tensile experiments in addition to compression (Thomas et al. 2009). Furthermore, uniaxial tension tests can also confirm the longstanding belief that vertical cracks in cartilage are a result of high tensile physiological stresses on the articular surface (Mansour 2003).

For conventional experiments, an excised tissue sample is placed within two clamps, as in Fig. 2.4, and stretched to a given force or distance. The tissue is typically in the standard dumbbell or dog-bone shape classically used in mechanical testing of materials. The standardized dumbbell has a length to width ratio of no less than four at the center of the specimen (Woo et al. 1979). The tensile strips are frequently extracted with respect to split-line orientation. This experimental protocol, as with compression tests, can be conducted in both creep and relaxation modes. The tensile force and tensile stretch is recorded. Additionally, thickness reduction as the sample is stretched can be measured. A sinusoidal load application is also often conducted as well to understand tissue fatigue properties (Weightman 1976, Park and Ateshian 2006). For example, the fatigue life is lowered with both increased stress and increased age, independently. Furthermore, it has been confirmed that for any value of peak stress, older

individuals need a lower number of cycles to reach failure than younger individuals (Mansour 2003). In a fourth type of test protocol, cartilage is uniaxially stretched until failure, and the maximum stress reaches is determined. In this test, the dynamic tensile modulus can be measured to determine total tensile strength. (Williamson et al. 2003).

Initial uniaxial tension tests found that cartilage exhibits a directional non-linear response as well as differing stiffnesses among the three zones (Woo et al. 1979). It was also suggested that although stiffness varies, fluid flow is similar between zones. Additionally, with applied strain, the collagen network becomes more aligned with the direction of the applied tensile strain, transforming into a more anisotropic material (Mansour 2003). Moreover, the tensile strength can be associated with cross-linking between the collagen fibers, while the orientation and organization impact the tensile modulus (Williamson et al. 2003). Li et al. (2005) modeled collagen viscoelasticity during tensile tests and found fibrillar stresses are:

$$\sigma_r^F(t) = \sigma_r^F(0) + \int_0^t G_r(t-\tau))E_r^F(\epsilon_r)\frac{\partial \mathbf{e}^s}{\partial \tau}d\tau \tag{2.20}$$

where the subscript r indicates the radial directon, superscript F indicates it is the fibrillar component, and therefore E_r^F is the fibrillar strain-dependent tensile modulus (Young's modulus) in the radial direction. This is comparable to (2.19), with the addition of the tensile modulus term. Due to the strain dependence of this tensile modulus, (2.20) includes the nonlinear viscoelasticity of the tissue.

Considering links to OA, Kempson (1982) found that cartilage stiffness in the deep zone decreased with age during a longitudinal study testing individuals from 8 to 91. He also found that the tensile strength reached a peak value around the third decade of human life, decreasing thereafter. With OA being an age-related disease, this could be representative of changes in

cross-linking and fiber arrangement that occur with age.

Another application of uniaxial testing is to investigate mechanical response differences with respect to split-line variation on the articular surface. (Woo et al. 1979) extracted three groups of dog-bone samples for testing: parallel, perpendicular, or 45° to the split-line from the surface, middle and deep zones. The group found the stiffness of the tissue increased in the superficial and middle zones from 0° to 45° and 90°, and exhibited an increased stiffness overall in comparison to previous studies. The deep zone however had smaller directional difference. Sasazaki et al. (2006) and Bae et al. (2008) expanded the work by testing the directional response to understand zonal failure mechanisms of collagen fibers under tension. Both groups continued with using dog-bone samples, but Sasazaki et al. (2006) used confocal laser microscopy to observe collagen fibers as the samples were deformed. They learned that initial fiber rupture occurred at the surface under small tensile strains, and increased in depth with increasing strain. Prior to rupture there was fiber reorienation in the perpendicular group to align with the direction of the aligned strain. This gives insight to the preferred direction of fiber orientation under applied loads. Bae et al. (2008) also compared split-line orientations to wear-line orientations, and discovered wear-lines strongly impact tensile behavior. Wear-lines are simply evidence of surface fibrillation and disruption that can also be made apparent by India ink staining. Specimens with wear-lines are already experiencing cartilage degeneration. Split lines and wear lines are compared in Fig. 2.5.

Shen et al. (2008) and Tang et al. (2010) expanded on the principles of uniaxial testing and tested individual collagen fibrils for mechanical properties using a microtensile test machine using a microelectromechanical systems (MEMS) method. Collagen fibrils are approximately $100\,\mathrm{nm}$ in diameter, while fibers are approximately $1\,\mu\mathrm{m}$. Shen et al. (2008) reports strain hardening and strain recovery within the collagen fibrils. The hardening is a result of tensile

loading and water being removed from the fibrils. The recovery occurs after unloading and water is reabsorbed by the fibril. Both groups invoked large strains. Shen et al. (2008) also investigated the relevance of collagen to bone's resistance to crack initiation and propagation, providing further clinical relevance to obtained results. It was found that collagen fibers need to be included as structural components in material models. Tang et al. (2010) found peak stress behavior is dependent on fibril length and width, as well as the density of cross-linking between fibers. It was also found the failure or rupture of collagen fibril occurs when cross-links break, or when tropocollagen molecules (the basic structural unit of all collagen forms) rupture. As previously mentioned, cross-linking is a key contributor to overall cartilage tensile strength, so this finding is logical with respect to tissue degeneration.

Shortcomings of Uniaxial Tension Tests

The strains applied during many uniaxial tension tests are far greater than *in vivo* conditions, and are therefore too large to be physiologically relevant. Thus, expression of such strains are "inadequate" to describe articular cartilage mechanical properties (Woo et al. 1979). There is also significant variability in mechanical behavior among specimens (Shen et al. 2008). Furthermore, even though the tissue is kept moist in a saline bath, groups such as Woo et al. (1979) found significant water loss from a measured decrease in tissue volume. There was no relationship between stress and volume loss, suggesting different tests may be needed to confirm zonal water flow.

Tissue maturity, specifically the arrangement and development of the collagen fibers, can significantly affect test results (Thomas et al. 2009). Thus, it is imperative to keep track of age as well as location and orientation of extracted tissue samples. Tissue maturity also affects studies where elimination or depletion of certain tissue components are performed. This

occurs in (Asanbaeva et al. 2008) for example, where enzymes were used to digest collagen to examine fiber effects. In another depletion study, Thomas et al. (2009) also found correlations between glucosaminoglycan (GAG) and collagen that were contradictory of other studies, highlighting a need for more information and a consensus on the relationship.

Finally, for simplicity, cartilage is often regarded as an isotropic material, however, uniaxial tests by Woo et al. (1979) further confirm that this is neither feasible nor advisable. Woo et al. (1979) adds employing a single Poisson's ratio to characterize the tissue is fallacious, due to tissue inhomogeneity through the thickness.

2.4.2 Biaxial Tension

Biaxial tension tests are commonly used in testing anisotropic biological materials, such as the aorta or meniscus, to understand tissue behavior. With articular cartilge, biaxial testing is not typically used to understand tissue behavior, but rather to stimulate artifical cartilage growth. The only group to have conducted classical biaxial tension tests on articular cartilage is Kamalanathan and Broom (1993). Cruciform samples as shown in Fig.2.6 were taken from bovine knee cartilage such that the two orthogonal axes were aligned parallel and perpendicular to the split-line direction. The samples were attached to nylon fabric with cyanoacrylate adhesive, and simultaneously loaded in both directions.

Kamalanathan and Broom (1993) compares results from a uniaxial test in the same test apparatus but with no loads on the orthogonal arms. They describe biaxial results as proof of the "structural coupling" of the collagen fibers. The group argued that split-line direction is an indicator and potential correlation to the ability for rearrangement of the fiber ultrastructure. This is supported by findings of transversely applied loads having more of an effect on low

stress "toe regions" in a stress-strain curve than the high stress regions. Thus, increasing transverse loads has a minimal effect on the overall stiffness of the tissue, but does disturb the fiber matrix.

As previously mentioned, proteoglycan charges give rise to fluid swelling pressure. This needs to be balanced by tensile forces, thus, tension is necessary in the developmental stages of articular cartilage. Groups such as Amos et al. (2009), Wartella and Wayne (2009) and Fan and Waldman (2010) have used tension to accelerate the growth of new cartilage or cartilage-like tissues. Starting with uniaxial tension principles, Amos et al. (2009) found that mesenchymal cells cultured under tensile strain produce superior collagen scaffolds. Wartella and Wayne (2009) used a combination of compression and tension in perpendicular axes on incubated scaffolds and cell-seeded constructs, as shown in Fig.2.7. The scaffolds were seeded with bone marrow cells from the hip. With proper nutritional media, such as fetal bovine serum and glucose, as well mechanical stimulation, the cells could differentiate and proliferate into chondrocytes. Wartella and Wayne (2009) applied cyclic compression and cyclic tension, while Fan and Waldman (2010) applied intermittent radial and circumferential tensile strains on cylindrical cell cultures. Fan and Waldman (2010) validated the success of biaxial tension on stimulating more mechanically accurate artificial cartilage by testing products in unconfined indentation tests. The groups found that cell proliferation was not affected by the magnitude of applied tension, but rather the duration; however, biaxial tension did not influence collagen synthesis. The groups conclude that the improvements of formation under dynamic tensile strain versus static tensile strain reflect physiological conditions. These types of tests give great insight to future development of cartilage growth and repair.

Although Charlebois et al. (2004) conducted uniaxial tension and compression tests, the group is the only one in the available literature to mention a biaxial tensile modulus. The group

argues that axial compression causes the transverse plane to be in biaxial tension, supported by evidence of nonlinear force measurements in uniaxial tension. The biaxial tensile modulus is comparable to the Young's modulus (tensile modulus). Charlebois et al. (2004) states the biaxial tensile modulus could reach values several times greater than the Young's modulus, supporting the statement that axial compression creates biaxial tension, and thus generates greater forces in the orthogonal transverse directions.

Shortcomings of Biaxial Tension Testing

In human physiological conditions, joints experience forces in more than just one direction. Therefore, uniaxial tests are not the most accurate in terms of providing results that are comparable to *in vivo* loads. According to Charlebois et al. (2004) and Kamalanathan and Broom (1993), biaxial tension occurs in the human knee, yet only one group has investigated it. This lack of investigation raises questions as to whether or not the claims are valid.

Kamalanathan and Broom (1993) admits difficulty in precisely aligning the tensile axes with the split-line direction. This affects validity of any correlations with the split-line direction. Additionally, cartilage has shown to exhibit curvature, or curling, after extraction from the joint and removal from bone (Setton et al. 1998). Curvature has affected other groups conducting biaxial tests on biological tissues experience difficulties in interpreting data due to misalignment errors from the curved trajectory of the fibers (Billiar and Sacks 1999).

2.5 Summary

From the diversified mechanical tests presented in the Experimental Studies of Cartilage Mechanics: Early Findings chapter, we now know cartilage load-bearing behavior depends on

both the matrix components, as well as how the stress is transferred to matrix constituents. The collagen fibers, proteoglycans, and other molecules both play a significant role in the mechanics and chemistry of the tissue and how it responds to physiological loads (Asanbaeva et al. 2008). This chapter summarizes the results and methods for compression and tension tests, both of which comprise of more than 75% of cartilage mechanics literature. Physiological conditions are very difficult to mimic *in vitro*. Tests such as confined and unconfined compression tests do not allow for any variation in translational boundary conditions, which naturally occur in the physiological environment (Kallemeyn et al. 2006). Newer tests improve upon mimicking *in vivo* conditions, and further understanding the complex loads and responses of AC. The next chapter discusses shear testing, which has only been exclusively investigated since the mid-1990's, more than 50 years after the first mechanical tests on articular cartilage.

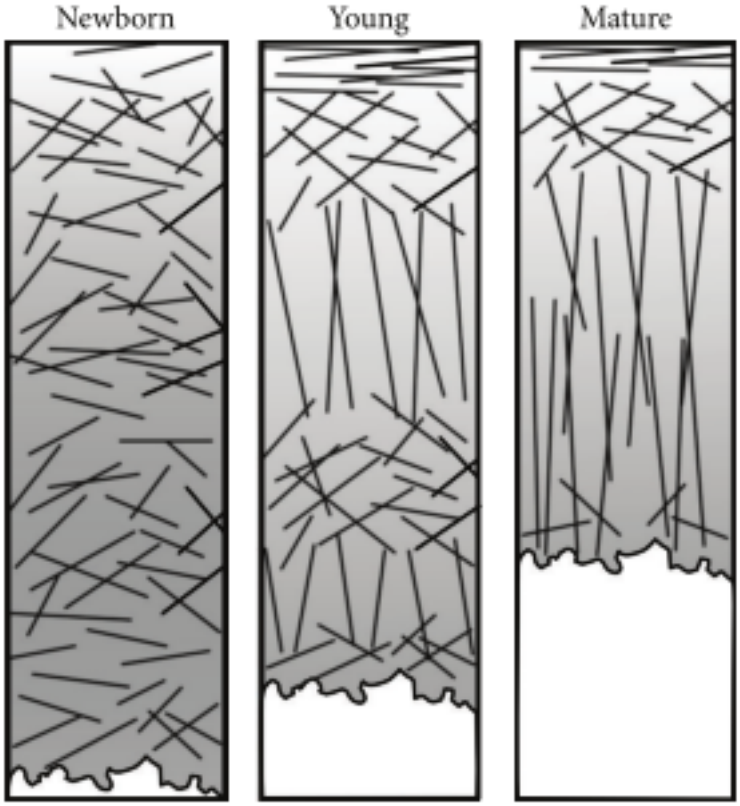

Figure 2.3: Collagen network organization in maturing articular cartilage. Over time, the structure resembles the traditional Benninghoff-type arrangement. (Reproduced from Julkunen et al. (2013))

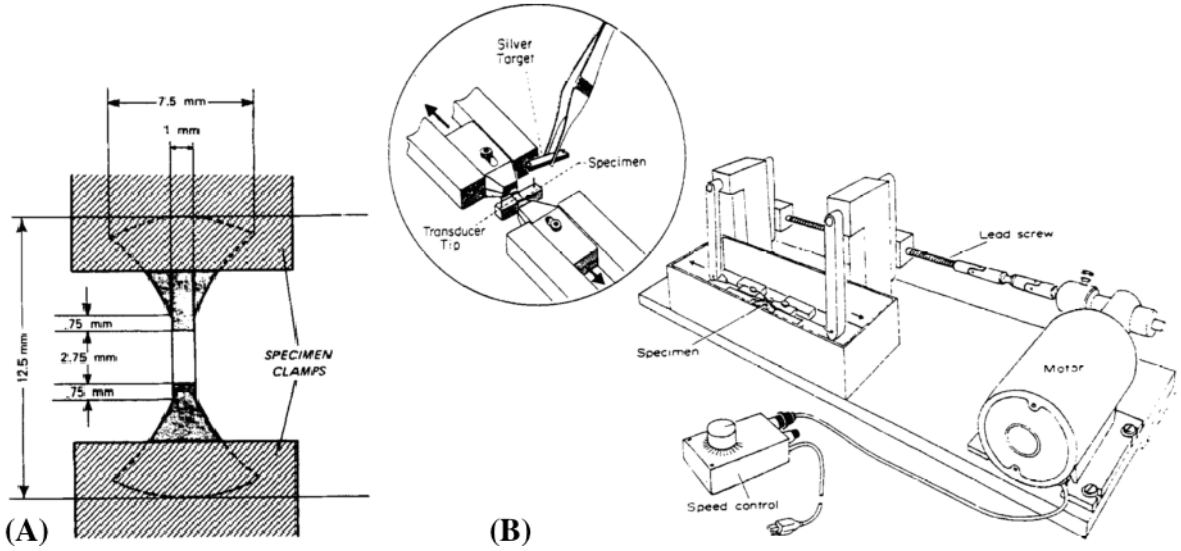

Figure 2.4: **(A)** Schematic of a standardized tensile specimen for cartilage uniaxial tension tests. The flanged ends are clamped while the inner strip of constant initial width is monitored during deformation. **(B)** An example experimental apparatus for a uniaxial tensile test machine. The specimen is typically submerged in a saline solution. (Adapted from Woo et al. (1976, 1979))

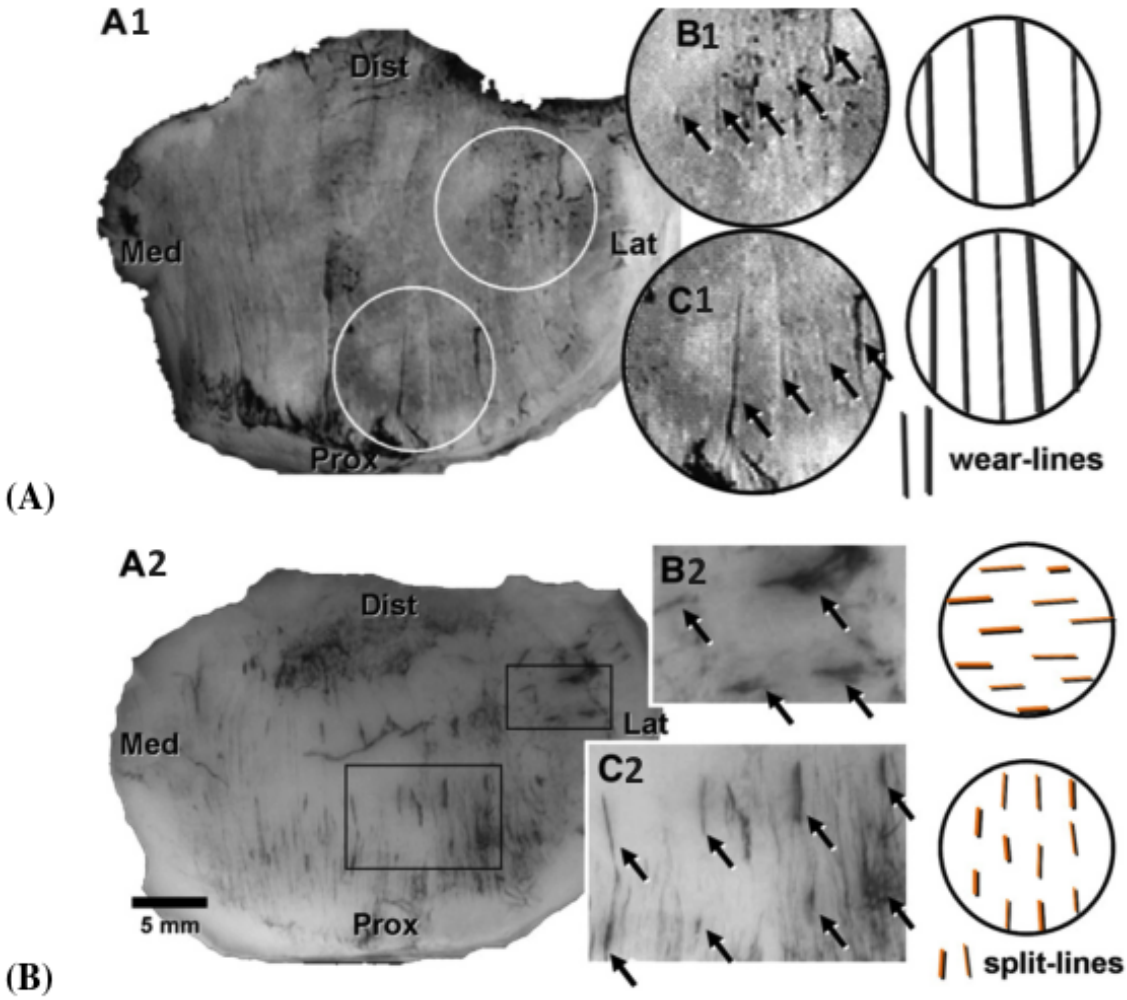

Figure 2.5: **(A)** Split lines in a human patella.**(B)** Wear lines in a human patella. (Adapted from Bae et al. (2008))

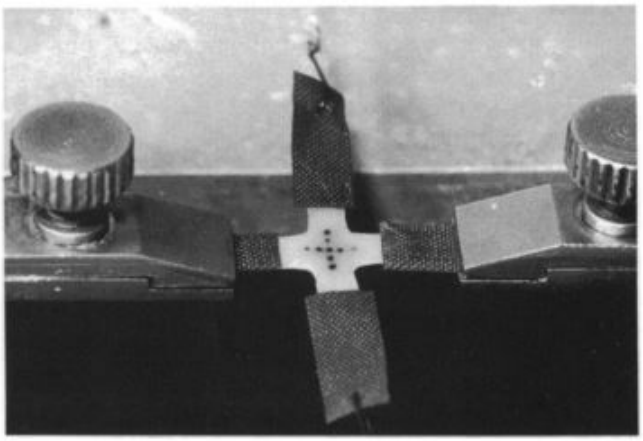

Figure 2.6: Cruciform-shaped specimen of bovine articular cartilage in a biaxial tension test machine at 2X magnification by Kamalanathan and Broom (1993).

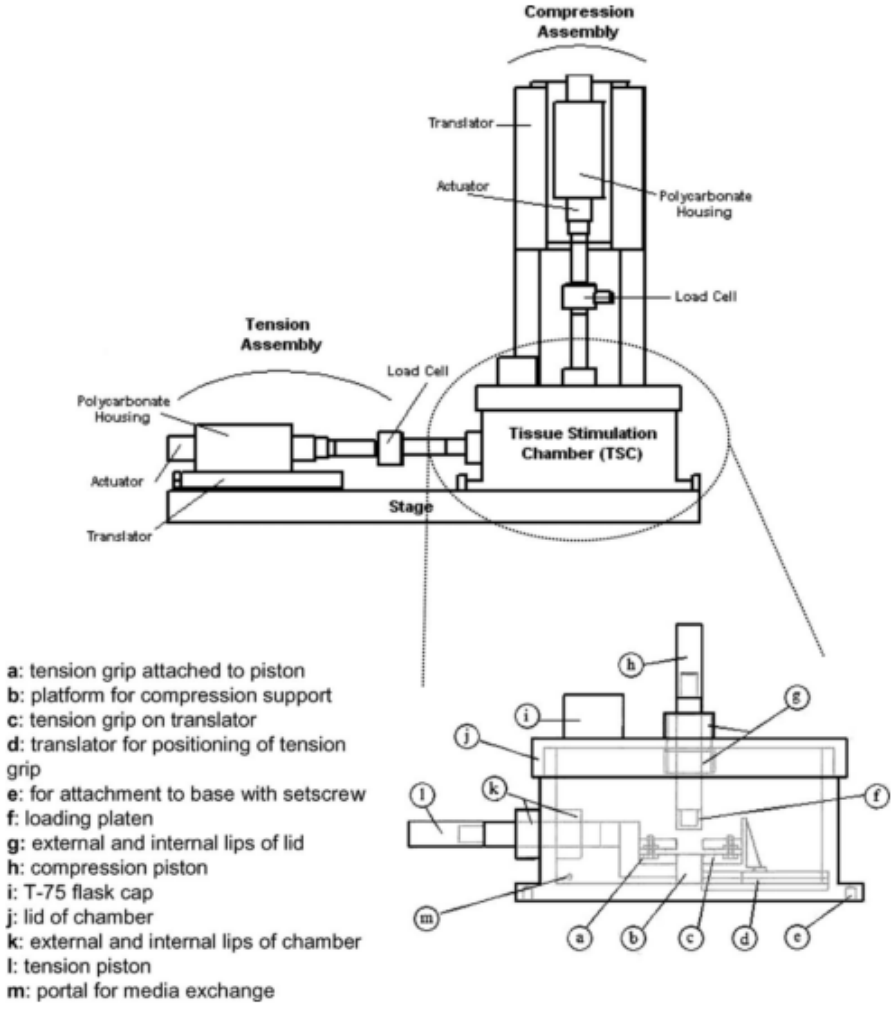

Figure 2.7: Schematic of the bioreactor for biaxial mechanical stimulation by Wartella and Wayne (2009). The bottom schematic is an exploded view of the tissue stimulation chamber.

3 Investigating Cartilage Shear Properties: Recent Findings and Proposed Work

The knee experiences complex loads in physiological conditions, namely compression, tension and shear. Cartilage degradation leading to OA originates from a multitude of sources. Collagen fibers are substantially weaker in shear forces, therefore lowering the integrity of the matrix and the stiffness of the tissue (Shen et al. 2008). Proteoglycans are less abundant, and water content increases in OA tissue, along with other pathophysiological changes that influence the AC mechanical properties (Zhu et al. 1993). Extensive work has been conducted investigating cartilage compressive and tensile properties. Though the longstanding theory that vertical cracks in cartilage are a result of high tensile physiological stresses on the articular surface, recent tests and models confirm that shearing initiates more cartilage failure than tensile loads (Mansour 2003). Only recently has mechanical shear testing entered the field of biomechanics, despite is resounding impact on tissue structure and function. The earliest shear experiments were investigated as an effect of compression and indentation tests(Parsons and Black 1977). This method, though representative of physiological conditions, does not

explicitly investigate the effect of shearing motion on cartilage. "Simple shear differs from pure shear only by a rotation," (Moreira and Nunes 2013), as seen by Fig. 3.1. Thus, there are two primary methods for applying shear on cartilage explants (Fig. 3.2).

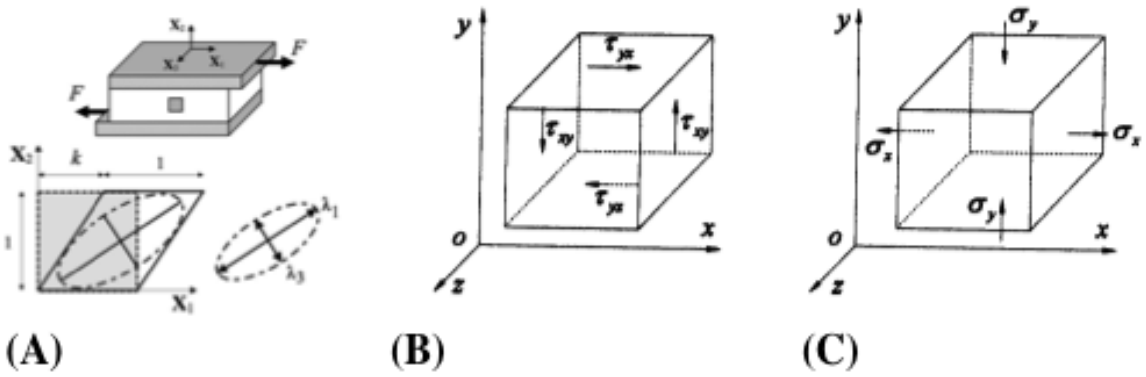

Figure 3.1: **(A)** Schematic of simple shear deformation of a rectangular block. (Adapted from Moreira and Nunes (2013)).**(B)** Simple shear stress state (Adapted from Tang et al. (2001))**(B)** Pure shear stress state (Adapted from Tang et al. (2001))

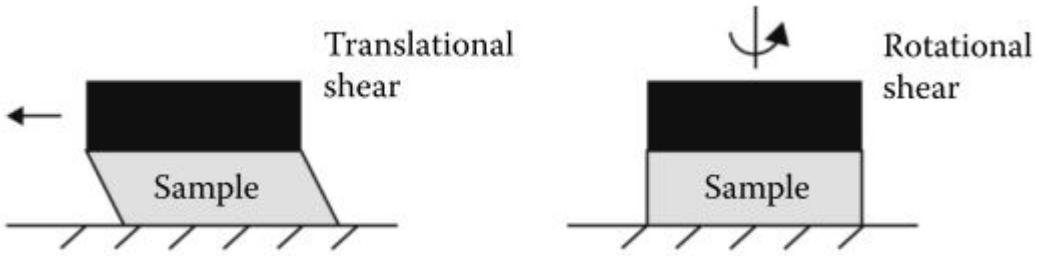

Figure 3.2: Types of experimentally applied shear on cartilage explants (Athanasiou et al. 2013).

3.1 Torsion Tests

Cartilage is weaker in tension in the direction perpendicular to shear (Kempson et al. 1971), making the tissue susceptible to torsional injuries (Athanasiou et al. 2013). Therefore, torsional shear tests are of interest. Torsion tests apply rotational strains by slightly compressing a cylindrical explant, then rotating about the z-axis (Athanasiou et al. 2013). This is also considered a biaxial load on the tissue, as there are two axes, in this case cylindrical coordinates, being simultaneously deformed.

Groups such as Soltz and Ateshian (2000), Setton et al. (1995), Zhu et al. (1993) use torsion tests to investigate tissue mechanical properties. Soltz and Ateshian (2000) conducted torsion tests in conjunction with confined and unconfined compression tests. In this problem, the strain and stress tensors are (3.1) - (3.2), respectively.

$$\mathbf{E} = \begin{bmatrix} 0 & 0 & 0 \\ 0 & 0 & \frac{1}{2}\frac{\partial u_\theta}{\partial z} \\ 0 & \frac{1}{2}\frac{\partial u_\theta}{\partial z} & 0 \end{bmatrix} \tag{3.1}$$

where u_θ is the circumferential displacement.

$$\sigma^{\mathbf{e}} = \begin{bmatrix} 0 & 0 & 0 \\ 0 & 0 & \mu\frac{\partial u_\theta}{\partial z} \\ 0 & \mu\frac{\partial u_\theta}{\partial z} & 0 \end{bmatrix} \tag{3.2}$$

Soltz and Ateshian (2000) conducted shear tests on a classical device, as shown in Fig. 3.3

Soltz and Ateshian (2000) tested healthy tissue while Zhu et al. (1993) and Setton et al. (1995) tested diseased or injured tissue. Soltz and Ateshian (2000) compressed the tissue to

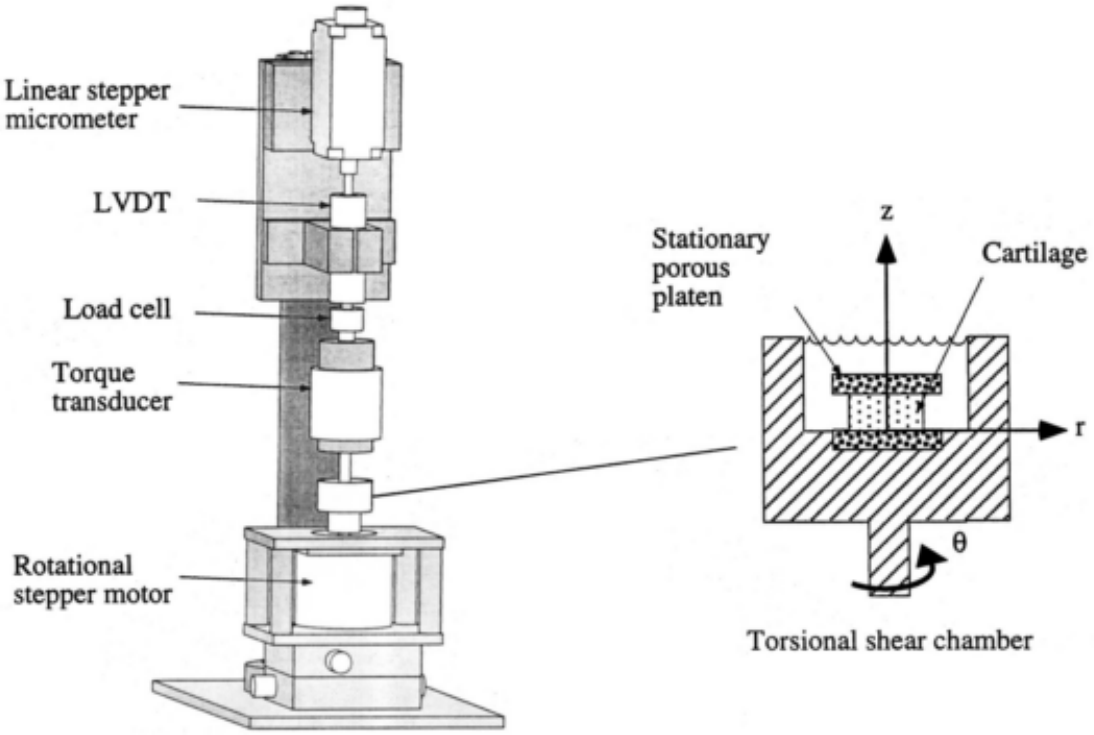

Figure 3.3: Schematic of an apparatus used for torsional shear testing by Soltz and Ateshian (2000).

0.89 N and applied step rotations at 0.016 rad. Soltz and Ateshian (2000) was able to successfully curve fit torsional shear data to a Conewise Linear Elasticity model, which proved the biphasic model could fit experimental data and produce accurate experimental material parameters.

(Zhu et al. 1993) tested cartilage explants at a range of frequencies 0.01 to 20 Hz, with multiple compressive strains 5 %, 9 %, 12 % and 16 %. The authors tested normal bovine tissue and tissue with chondroitinase and hyaluronidase to degrade proteoglycans. Shear strain amplitudes of 0.001 radians, ten-fold less than Soltz and Ateshian (2000), were applied. The

authors found G^* is strongly dependent on both the compressive strain and the frequency. The relationship between G^* and low frequencies is non-linear, and linear at high frequencies (20 to 1000 Hz). Hayes and Bodine (1978) and the authors agree on the relationship at 20 Hz. Additionally, strong correlations between collagen content and G^* show the importance of collagen fibers to overall cartilage shear response.

Setton et al. (1995) conducted torsion tests on healthy canine cartilage and cartilage from canines with ACL transections. The group investigated the effects of joint instability induced by ACL transection, and the response under (1) equilibrium compression-shear (2) transient shear experiments, and (3) dynamic shear experiments. In equilibrium shear measurements, the cartilage samples were held at static shear, and the response was measured after 1200 seconds. Transient shear experiments are where rapid changes in shear loads are applied, and are very common in rheology studies of multiphase materials. In this type of experiment, stress-relaxation results are recorded. All shear tests were brought to equilibrium of 1 kPa for 1200 seconds. Transient and dynamic shear experiments were conducted at 10% compression to minimize tissue slippage between the platens. Shear strains of 0.5, 1, 2 and $3\,\%$ were applied. The authors found that the short periods of instability from ACL transection greatly influenced AC mechanical properties, with substantial decreases in shear moduli and increase in water content. There was a correlation between increasing angular frequency and increasing shear modulus as well. Additionally, there were inconsequential differences in the magnitude of material parameters between explants from the distal portion of the knee, versus the the proximal area, where there is less load bearing surface contact at the joint (Fig. 3.4). The authors allude to this proving the frequency of contact is independent of these material parameters, but they fail to consider load-bearing weight distribution in the discussion. Shear

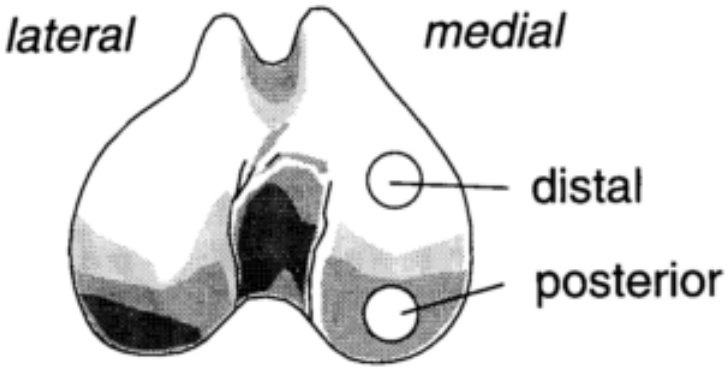

Figure 3.4: Sample extraction areas for Setton et al. (1995) torsion tests. Distal areas of the femoral head are considered more load bearing regions.

stress was calculated from the torque by (3.3), Setton et al. (1995)

$$\tau = \frac{Tr}{I_p} \tag{3.3}$$

where T is the torque, r is the radius of the sample, and $I_p = \pi r^4/2$.

If there is no volumetric change in the specimen, then it can be assumed there is no fluid-flow from the matrix. Therefore, the experimental results from torsion tests describe the solid collagen-proteoglycan matrix (Zhu et al. 1993). In these experiments, no adhesive was used; an initial compression was applied to ensure no slippage between the specimen and the platen. This compression affects the phase angle during torsion experiments.

3.2 Translational Shear

Numerous groups applied translational shear to animal and human specimens. In one of the earliest shear experiments, Hayes and Bodine (1978) used shear loading to directly determine

AC viscoelastic properties. The authors note the interstitial fluid is free and unbound, and therefore, it does not sustain shear stress.

The viscoelastic complex shear moduli describe the tissue response to varying sinusoidal strain.

$$G^*(\omega) = \frac{\tau^*}{\gamma^*} = G_1(\omega) + G_2(\omega) \tag{3.4}$$

where ω is the angular frequency, τ is the stress, and γ is the strain. The relationship between the complex shear modulus and other moduli can be seen in Fig.3.5. The storage modulus

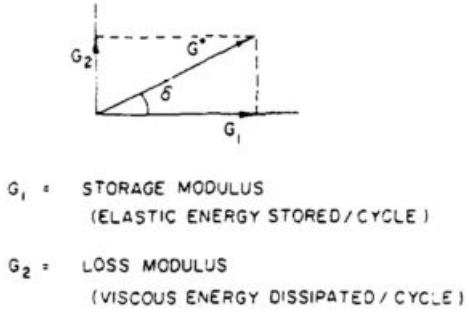

Figure 3.5: Relationship between storage modulus and loss modulus with respect to the viscoelastic complex shear modulus (Hayes and Bodine 1978).

defines the elastic energy stored due to applied strain. Conversely, the loss modulus relates to the dissipation energy by (3.5).

$$\Delta E = \int \tau d\gamma = \pi G_2 \gamma_0^2 \tag{3.5}$$

. Hayes and Bodine (1978) determined the uncoupled complex shear moduli using laterally applied sinusoidal shear. The bottom parallel plate was fixed while the top plate applied the shear longitudinally. The complex shear modulus G^* was extracted experimentally from the

force plate by (3.6):

$$F = AG^{*}x/b \tag{3.6}$$

where A is the specimen area, and $x = x_0 sin\omega t$.

In the Hayes and Bodine (1978) experiments, sinusoidal shear was applied to bovine patellae explants with bone removed and the deep zone milled flat. Additionally the surface zone removed, leaving 0.1 cm of transitional zone tested. The tissue was compressed 7% for to prevent slippage, and shear with amplitudes of 30×10^6 were applied. Biochemical changes as a function of frequency were analyzed, such as proteoglycan depletion, collagen digestion, and crosslink levels. The authors also altered biochemical levels in the cartilage to further understand biochemical effects. Hayes and Bodine (1978) found a decrease in the complex shear modulus when the tissue had reduced collagen or proteoglycan, suggesting that shear properties are highly dependent upon the matrix constituents.

Wong et al. (2008), Wong and Sah (2010) continued investigating biochemical effects on shear properties. The authors performed translational shear with a cartilage-cartilage interface from human tibia cadavers, as in Fig. 3.6. The specimens were stored in PBS and proteinase inhibitors until use. In the biaxial loading chamber, 13% compression was applied, and three lateral displacements $\pm 1\,\mathrm{mm}$ at $100\,\mu\mathrm{m\,s^{-1}}$ on specimens that 3 x 8 mm in size. The authors investigated slip properties and the effects of lubrication on shear properties. The authors determined the peak shear stress occurred at the articular surface, and decreased with depth. Additionally, when the articular surface had less lubrication or visible fibrillation, the surface shear increased drastically. This could contribute to the progression of OA. Finally, it was determined tibial cartilage is softer than femoral cartilage with respect to shear and axial deformation.

Considering long-term effects of shear loading on AC, Simon et al. (1982) conducted fatigue tests shear tests on $3\,\mathrm{mm}$ cylindrical samples of bovine explants. The bone was left attached to the samples, which brings the claim that this is a simple shear experiment into question. The sample was tested at 100 Hz (far greater than physiological conditions), and 0.5 mm shear displacement amplitude, which $\pm 3\,\%$ to $5\,\%$. The fatigue test lasted 6 hours, which produced approximately 10^6 cycles. With time, the area of the hysteresis on a stress-strain curve decreased, as well as the shear modulus. The hysteresis area is the dissipation energy, therefore the dissipation energy decreased over time. The authors hypothesized that the change was due to damage to the collagen network and proteoglycan depletion, though the authors did not confirm this like Hayes and Bodine (1978) did.

One group led by Dr. Itai Cohen from Cornell University recently conducted several studies on depth-dependent shear properties of AC (Buckley et al. 2008, 2010, 2013, Silverberg et al. 2013, 2014, Griffin et al. 2014). Sinusoidal translational shear displacements were applied on hemi-cylinders of degraded and undegraded immature bovine articular cartilage at 1 Hz and an amplitude of $16\,\mu\mathrm{m}$. Buckley et al. (2008) applied lateral shear of 1 to $3\,\%$ of the tissue thickness, which had the deep zone removed. Buckley et al. (2010) applied 10% axial compression, while Buckley et al. (2013) applied 20% compression. The groups intended to investigate AC depth-dependent properties, while Griffin et al. (2014) wanted to see the influence of trypsin or collegenase degradation on the tissue's viscoelastic properties. Trypsin depletes proteoglycans, while collagenase degrades collagen fibers. Confocal reflectance microscopy coupled with non-damaging photobleached line tracking was used to observe changes in collagen orientation and structure during the test (Fig. 3.7). Further imaging was conducted by Silverberg et al. (2014), who included Fourier transform infrared imaging (FTIR-I) and further investigated depth-dependent local shear properties.

Buckley et al. (2008) concluded that AC shear properties are incredibly inhomogeneous. Regions between the superficial zone and middle zones got increasingly stiffer under an increase in shear strain, and overall, the shear modulus varied with applied strains. Buckley et al. (2013) expanded on this inhomogeneity and confirmed the dynamic shear modulus reached both a minimum and maximum value approximately $100\,\mu m$ below the surface.

Confirming statements by Hayes and Bodine (1978) and Simon et al. (1982), Buckley et al. (2013) found induced enzymatic cartilage degeneration affected the total energy dissipation by a factor of 100. Increased digestion times resulted in greater energy dissipation. The validity of these results is questioned by Moody et al. (2006), who states there are many inconsistencies when using trypsin *in vitro*, and that at any given time, the change in proteoglycans due to trypsin varies tremendously. This variation can be due to depth, location in the joint space, and initial proteoglycan concentration values.

The group also found the local shear moduli also decreased significantly, along with decreased proteoglycan concentration at the surface. In this region, the shear modulus is much lower than surrounding areas. Buckley et al. (2008) calls this a notable energy dissipation region. All of these show the dependency of collagen. Another significant result is the distinct spatial patterning approximately $400\,\mu m$ below the articular surface. Additionally in this region, microscopy showed discontinuities in this ”transition zone", giving implications of collagen fiber buckling or crimping as a consequence of the high energy dissipation. Buckley et al. (2008) further hypothesizes that small strains effect collagen fibers by buckling into alignment, as in Fig. 3.8. (Buckley et al. 2013, Griffin et al. 2014) claim that if this region were to be removed from the tissue, the cartilage, and therefore the joint, would be more vulnerable to severe damage. Considering it has been shown proteoglycans are capable of storing deformational energy, the true effect and existence of the energy dissipation region needs fur-

ther investigation (Hardingham et al. 1987, Zhu et al. 1993). Additionally, relevance to adult articular cartilage behavior is questionable because neonatal bovine cartilage was used. Recall from Fig.2.3 the vast difference in collagen fiber orientation and distribution between newborn and adult articular cartilage. Despite the fact that Silverberg et al. (2014) suggests the depth-dependent shear modulus is similar in young bovine and adult human, the ”transition zone" may also simply be a phenomenon of the use of newborn tissue.

Stress-strain curves produced by Buckley et al. (2013) exhibited hysteresis and were elliptical in shape, as in Fig.3.9.

In the most recent paper published by the group, Silverberg et al. (2014) used a biopolymer rheology model, or rigidity percolation model, in conjunction with experimental results, to model AC characteristics. Instead of standard square or triangular lattices, a kagome lattice, as in Fig. 3.10, was chosen because mechanical properties are independent of orientation. The authors chose to model the fibers as linear elastic rods, and the matrix as a simple reinforcing elastic medium that resists collagen fiber microscale transverse displacement. The model functions on the assumptions that the shear modulus of the medium supports the tissue, while the rheology of the nonpercolating model provides the primary responses. This new model is an extension of previous biphasic models, and captures behaviors such as fiber buckling in the model at small strains.

Continuing the trend of conducting compression-shear tests with live-optical tracking, Motavalli et al. (2013) used new approaches similar to Buckley et al. (2010) to understand depth-dependent shear properties. Buckley et al. (2008, 2010) used numerical differentiation to calculate shear strain, which could increase noise. Motavalli et al. (2013) used analytical approaches on high resolution pixel displacement data and calculating the first derivative to eliminate the noise. Experimentally, the authors applied translational shear with a step size

of $20\,\mu m$ with 0% compressive strain, held for 2 min, then allowed to relax. To analyze their pixels, the group compared polynomials, cubic splines, and non-parametric loess curves. The group determined that a 6th or 7th order polynomial fits the shear displacement data extraordinarily well, as shown in Fig. 3.11. Experimentally the group found that cartilage exhibits internal failure at the articular surface at approximately 25% applied shear.

3.3 Shear Stimulation of Natural and Artificial Cartilage

Frank et al. (2000) and Jin et al. (2001) used compression and torsion to stimulate bovine explants. (Frank et al. 2000) applied small strains (0.4 to 1.6 %), while Jin et al. (2001) applied 3% sinusoidal rotational shear on bovine explants at varying frequencies between 0.1 to 1 Hz. The authors intended to stimulate chondrocyte biosynthesis through shear deformation with minimal intratissue fluid flow or pressure gradients. Protein and proteoglycan synthesis increased greatly with shear stimulation in comparison to a control group held statically under the same conditions. Additionally, the shear modulus appeared to decrease with increasing strain (up to 1.2%). Two years later (Jin et al. 2003), the group applied 0.5 to 6 % at 0.1 Hz to the middle zones of newborn bovine cartilage explants treated with growth factor stimulation to determine effects on chondrocyte matrix synthesis. The authors found independent positive effects, but no interaction between the biomechanical and biochemical stimuli, thus dynamic shear does not enhance transport of large molecules such as IGF-I.

Waldman et al. (2003) and Waldman et al. (2007) used compression and translational shear on cartilaginous tissue generated from chondrocytes extracted from bovine tissue. Mechanical tests were performed on the tissue cultures after 4 weeks of incubation. Cultures were compressed and sheared at all combinations of 2% and 5% at either 0.5 Hz or 1 Hz for up to

four weeks. Chemical and Mechanical analysis of this tissue showed that low shearing strains (2%) inhibited the development of the extracellular matrix, while high strains (5%) fostered increased matrix synthesis. Intermediate testing to determine a neutral point, i.e. the point where there is neither inhibition nor improvement, was not done. Overall, the shear modulus increased 1.75-fold after four weeks of compression-shear stimulation.

3.4 Surface Shear Properties

Some groups, such as Seror et al. (2012) used shear testing to understand tissue behavior at the surface. Seror et al. (2012) found that hyaluronan, aggrecan and link protein from AC are not the sole contributors to the lubrication at the articular surface, contrary to what has previously understood. This was found through an experiment where these components were extracted from bovine femurs, attached to a mica sheet, and measuring the shear interactions through frictional force measurements after applying translational shear. Results showed these components work in conjunction with other features at the articular surface to provide seamless lubrication.

3.5 Shortcomings of Previous Shear Studies

The Cohen group from Cornell University conducted extensive transverse shear tests on AC; however all of their investigations used neonatal bovine tissue, confirmed to be isotropic after split-line testing (Silverberg et al. 2013). Although this ensures the tissue is directionally independent, it is not representative of mature AC. Therefore, results cannot be used in biphasic models, or ultimately in understanding the progression of OA.

Additionally, all of the tests described in this section were conducted using small strains, which is not true of physiological conditions. Many tests also relied on surface friction from compression, which could still produce microscale slippage that invalidates assumptions and results.

The majority of the tests conducted did not use full-thickness samples of cartilage; either the superficial or the deep zone was removed. The precise depth of each cartilage zone varies tremendously. Often times, the removal of these zones is based on a fixed depth, thus, authors cannot ensure only a particular zone is removed. This compromised the integrity of the tissue. Additionally, further destruction of the collagen fiber matrix could influence mechanical response. Thus, these methods, though useful in identifying general regional properties, are not refined enough for the claims made by the authors.

Finally, groups such as Silverberg et al. (2013) compare the mechanical behavior between femoral, tibial, and patellar cartilage, but fail to analyze spatial variation within a region with varying load-bearing contacts. For example, the group harvested samples from the femoral condyle, but cartilage on the condyle can vary extensively in terms thickness, split-line severity, and degree of load-bearing on the surface.

All of these considerations lead to the selection of triaxial shear application under quasi-static, large strain, shear loads. The experiment is described in the next chapter.

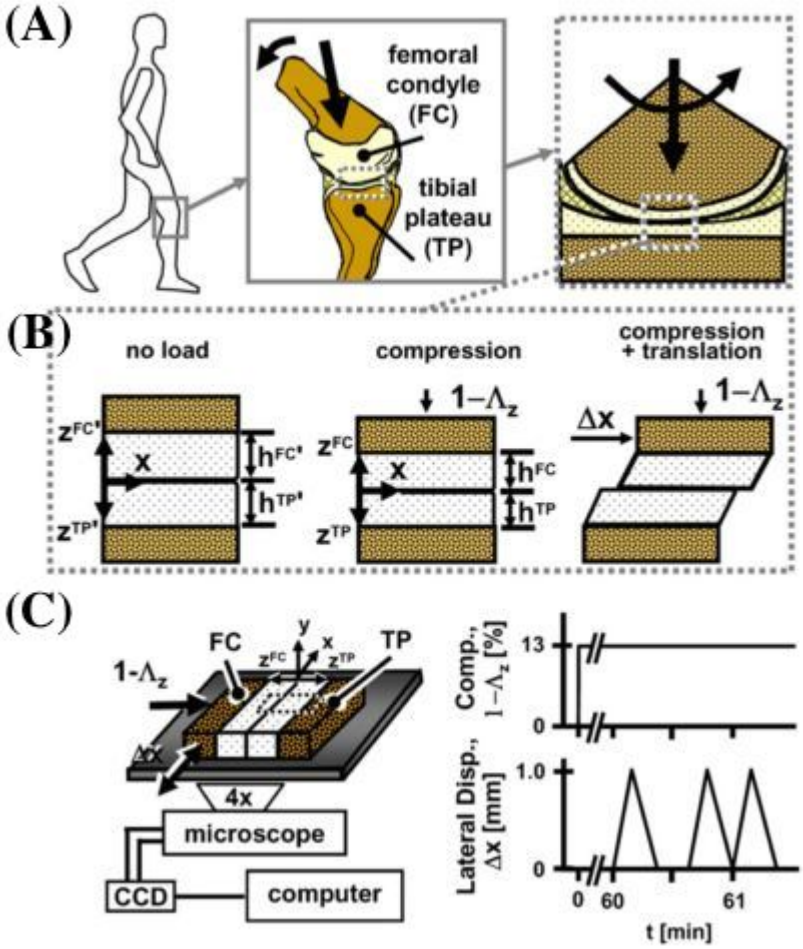

Figure 3.6: **(A)** Knee joint movements ant multiple scales, **(B)**, Cartilage deformation with no load, compression, and compression and translation, **(C)**, Experimental setup and loading (Wong and Sah 2010).

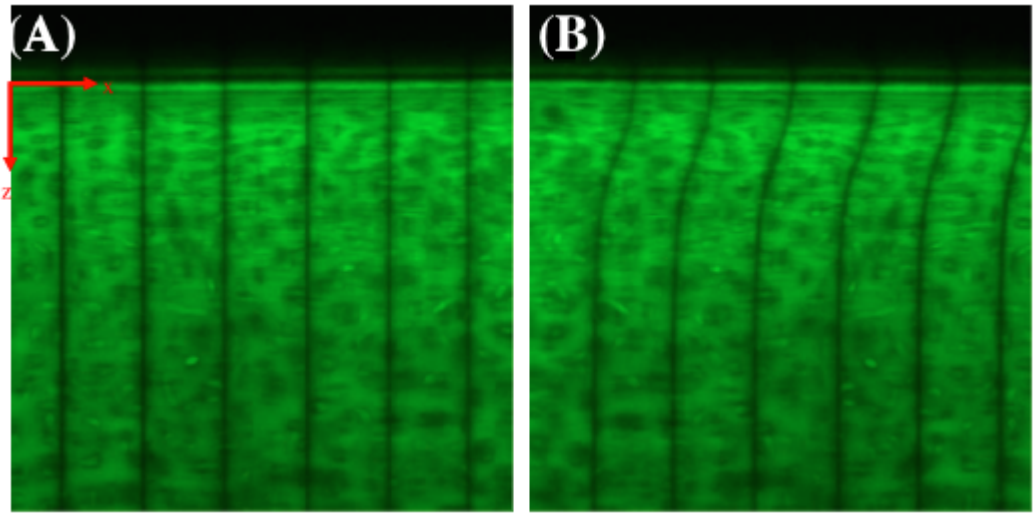

Figure 3.7: Confocal microscopy of articular cartilage samples 5-DTAF stained and photo-bleached for deformation tracking **(A)** before shear applicaton **(B)** during shear application, (Buckley et al. 2010).

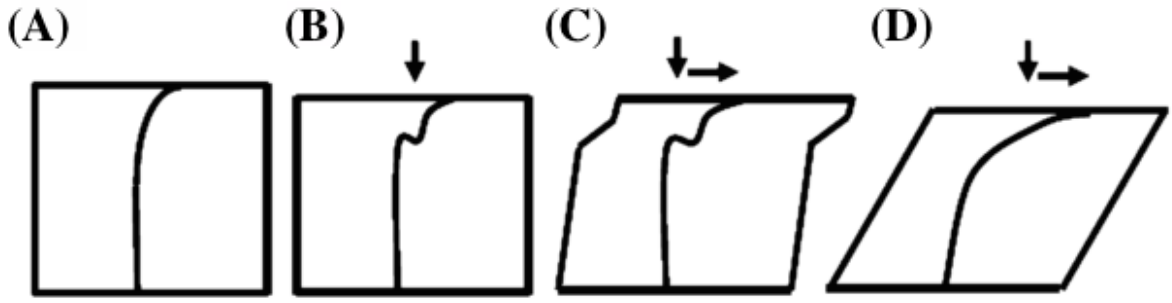

Figure 3.8: A schematic representation of collagen fiber behavior under small strains during **(A)**, no load **(B)**, compression, **(C)**, compression and early-stage shear, and **(D)**, compression and lates-stage shear (Buckley et al. 2008).

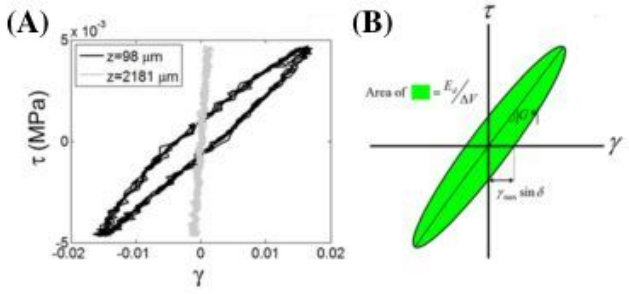

Figure 3.9: **(A)**, Shear stress vs shear strain at depths $98\,\mu\mathrm{m}$ and $2181\,\mu\mathrm{m}$ below the articular surface at 1 Hz **(B)**, G^* is extracted from the stress-strain curves as the slope of the elliptical major axis and the x-intercept (Adapted from Buckley et al. (2013)).

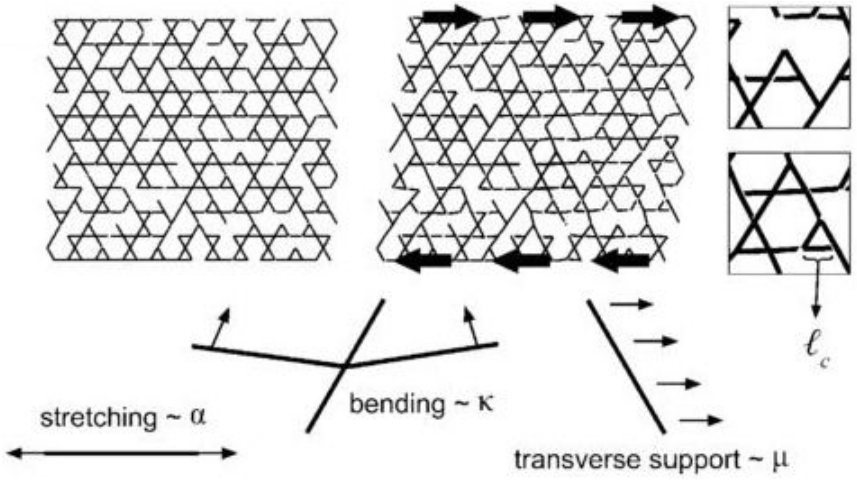

Figure 3.10: Kagome lattice before (left) and after (right) shear deformation. Black lines represent collagen fibers (Adapted from Silverberg et al. (2014)).

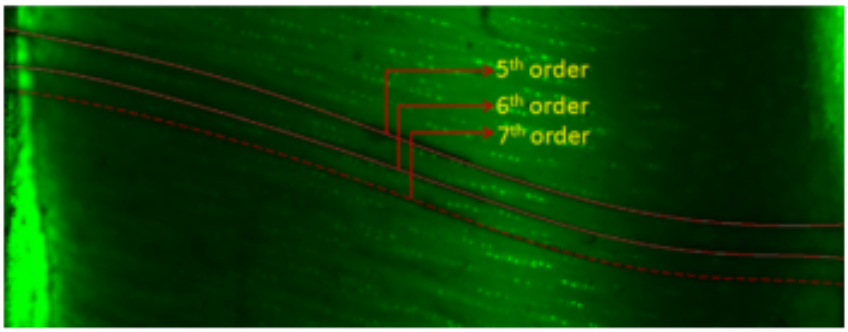

Figure 3.11: An overlay of 5th-7th order polynomials on photobleached lines in confocal imaging of articular cartilage during shear deformation. The articular surface is on the right side of the image (Motavalli et al. 2013).

4 Methods and Materials

4.1 Triaxial Shear

Research implicates shear forces to be a critical factor in the destruction of cartilage tissue, yet few studies have been conducted on cartilage undergoing mechanical shear. In order to make accurate stress predictions in finite element models of cartilage tissue, we seek to calibrate our custom constitutive models using data generated under shear loading. This shear loading will be applied using a triaxial shear test machine.

Triaxial shear machines extend current applications of compression and transverse shear into the third lateral dimension. In this machine, tissue compression can be controlled and held fixed or variable by a moving head. During maintained compression, deformation can be applied in the X and Y directions. These applied stretches contribute to shear stresses in the tissue, namely γ_{xz} and γ_{yz}. This triaxial approach is much more realistic than other test methods, as axial and lateral displacements can be independently controlled (Kallemeyn et al. 2006).

4.2 Materials

Previous work shows mechanical similarities between young bovine (< 2 years) and adult human cartilage (Buckley et al. 2013). Therefore, eighteen specimens mature bovine metacarpals (Animal Technologies, Inc., Tyler, TX) were used. Specifically, samples from only the lateral femoral condyle and tibial plateau were excised from the bovine knees. Bovine samples not tested within 24 hours of slaughter were sealed in phosphate buffered saline (PBS) ($137\,\mathrm{mM}$ NaCl, $2.7\,\mathrm{mM}$ KCl, $10\,\mathrm{mM}$ Na_2HPO_4, $1.8\,\mathrm{mM}$ KH_2PO_4) and maintained at either $4\,^{\circ}\mathrm{C}$. Human tissue will be sealed and maintained in original preservative fluid at $4\,^{\circ}\mathrm{C}$. Frozen tissues will be transferred to $4\,^{\circ}\mathrm{C}$ for one day, then thawed in PBS at room temperature the day of scheduled testing.

4.2.1 Material Preparation

Split-Line Testing

Prior to excising tissue samples, we used the split-line test to determine the orientation and suitability of tissue use. After rinsing with PBS, we pricked the condyle surface with a circular awl dipped in India Ink, similar to methods used by Silverberg et al. (2013). Only samples with visible split-lines were used for testing, as visible lines indicate anisotropic surface behavior. We define the x direction as the direction parallel to the split-line. A representative condyle with split lines is in Fig. 4.1.

Figure 4.1: Representative sample of bovine distal femoral condyle with visible split-lines

Sample Excision

We carefully aligned the bottom edge of a custom square cutting tool of side length $3\,\mathrm{mm}$ with the split-line direction. Using the tool, we punched square samples from the joint, maintaining 0.2 to $1.5\,\mathrm{mm}$ of subchondral bone attached. Further trimming of the subchondral bone with a surgical scalpel ensured proper length and alignment with the AC surface. The scalpel resulted in an estimated surface roughness of $0.0025\,\mathrm{cm}$ with remaining bone, if any, measuring less than $0.2\,\mathrm{mm}$ (Hayes and Bodine 1978). Samples were immediately washed with PBS, and thickness was measured using a digital micrometer (Carrera Precision, resolution $0.01\,\mathrm{mm}$).

Samples were excised in adjacent pairs, such that one sample was reserved for mechanical testing, and the other was sent for histological examination and imaging.

Sample Categories

Samples were additionally categorized based on estimated joint contact areas and contact stress regions, as shown in Figs. 4.2 - 4.3. In Fig. 4.2, regions 1, 2, and 3 were approximately the joint contact areas during 30°, 90° and 45° flexion respectively, based on Below et al. (2002). In Fig. 4.3, region 1 corresponds to approximate low stress regions, while region 2 corresponds to high stress regions, based on Blankevoort et al. (1991).

A summary of samples and the measured thickness and categorized regions is in Table 4.1.

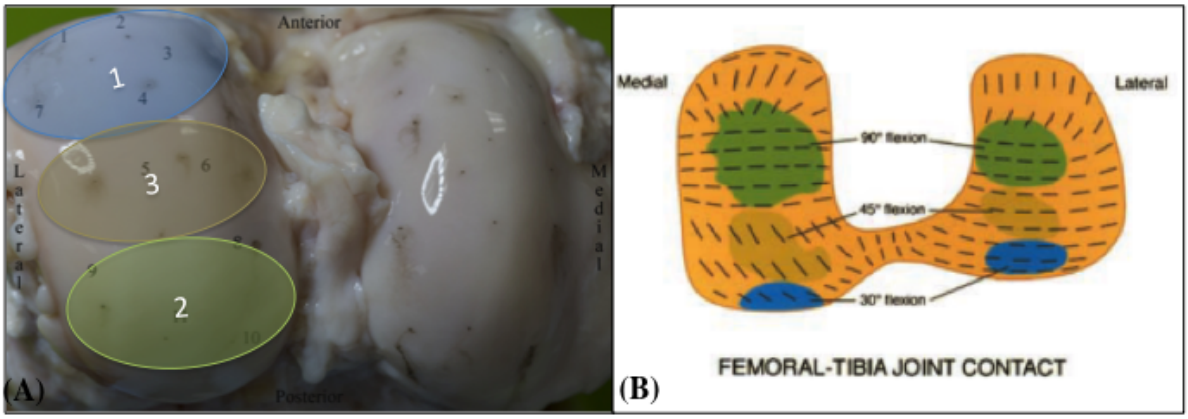

Figure 4.2: **(A)** Representative sample of bovine distal femoral condyle with joint contact regions, visible split-lines, and excised samples based on **(B)** femoral-tibia joint contact areas from Below et al. (2002).

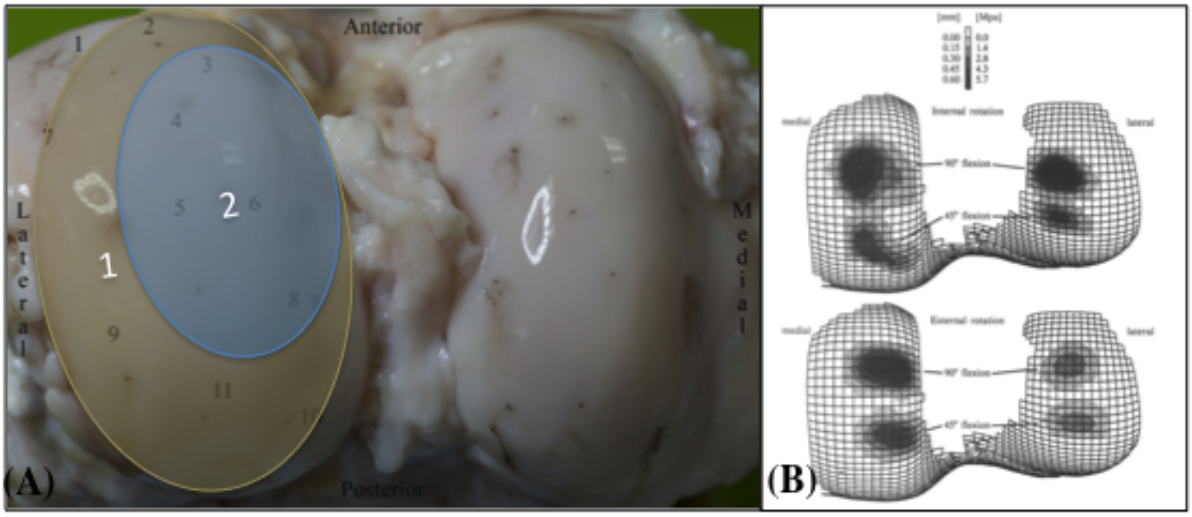

Figure 4.3: **(A)**Representative sample of bovine distal femoral condyle with contact stress regions visible split-lines, and excised samples based on **(B)** femoral-tibia joint contact stresses from Blankevoort et al. (1991).

4.3 Experimental Setup

Mechanical tests were performed using a custom-built triaxial shear testing device (Messphysik Materials Testing, Fürstenfeld, Austria and Zwick/Roell, Ulm, Germany), Fig. 4.4. This device, a high-precision, low-load machine, was designed specifically for compressive and shear microscale testing of soft biological tissues (Sommer et al. 2013). The device featured a standard uniaxial tension machine configuration for displacements in the z direction. Coupled with this were two platforms, each controlled by actuators to allow for translation in both the x and y directions. There are two points of attachment from the sample to the machine. The upper specimen mount, controlled solely by the $0.04\,\mu\mathrm{m}$ stroke resolution z actuator, was attached to a $\pm 50\,\mathrm{N}$ capacity 3-axis force sensor ($\pm 1\,\%$ accuracy class). The lower specimen mount sat in a circular bath for PBS, with temperature set to maintain $37\,^{\circ}\mathrm{C}$

Patient	Specimen	Thickness	Joint Contact Region	Contact Stress Region
1	1	2.75	2	2
1	5	2.2	1	1
1	6	2.5	1	1
1	7	2.5	1	2
1	10	1.8	3	2
1	11	2.45	3	1
2	2	2.6	2	2
2	4	2.5	2	1
2	5	2.55	1	1
2	9	2.8	3	2
2	12	2.5	1	1
2	13	2.8	3	2
3	3	1.75	1	2
3	4	1.7	3	1
3	5	1.85	1	1
3	6	2	2	1
3	7	1.5	2	2
3	9	1.4	2	2

Table 4.1: Summary of patient thickness, joint contact region, and contact stress region, by specimen.

(Lauda-Brinkman EcoSilver, Delran, NJ). The x and y actuators both had a stroke resolution of $0.25\,\mu\mathrm{m}$. Motor control was performed using a Windows-based PC operating the testXpert II software (Zwick/Roell, Ulm, Germany).

4.3.1 Experimental Sample Preparation

The excised $3\,\mathrm{mm} \times 3\,\mathrm{mm} \times \leq 2.5\,\mathrm{mm}$ sample was affixed to the lower mount using a small amount of cyanoacrylate adhesive on the previous subchondral bone face. The shear modulus is not affected by using adhesive to bone remnants, in comparison to non-glued cartilage without bone (Hayes and Bodine 1978). The split-line was oriented such that it was aligned with

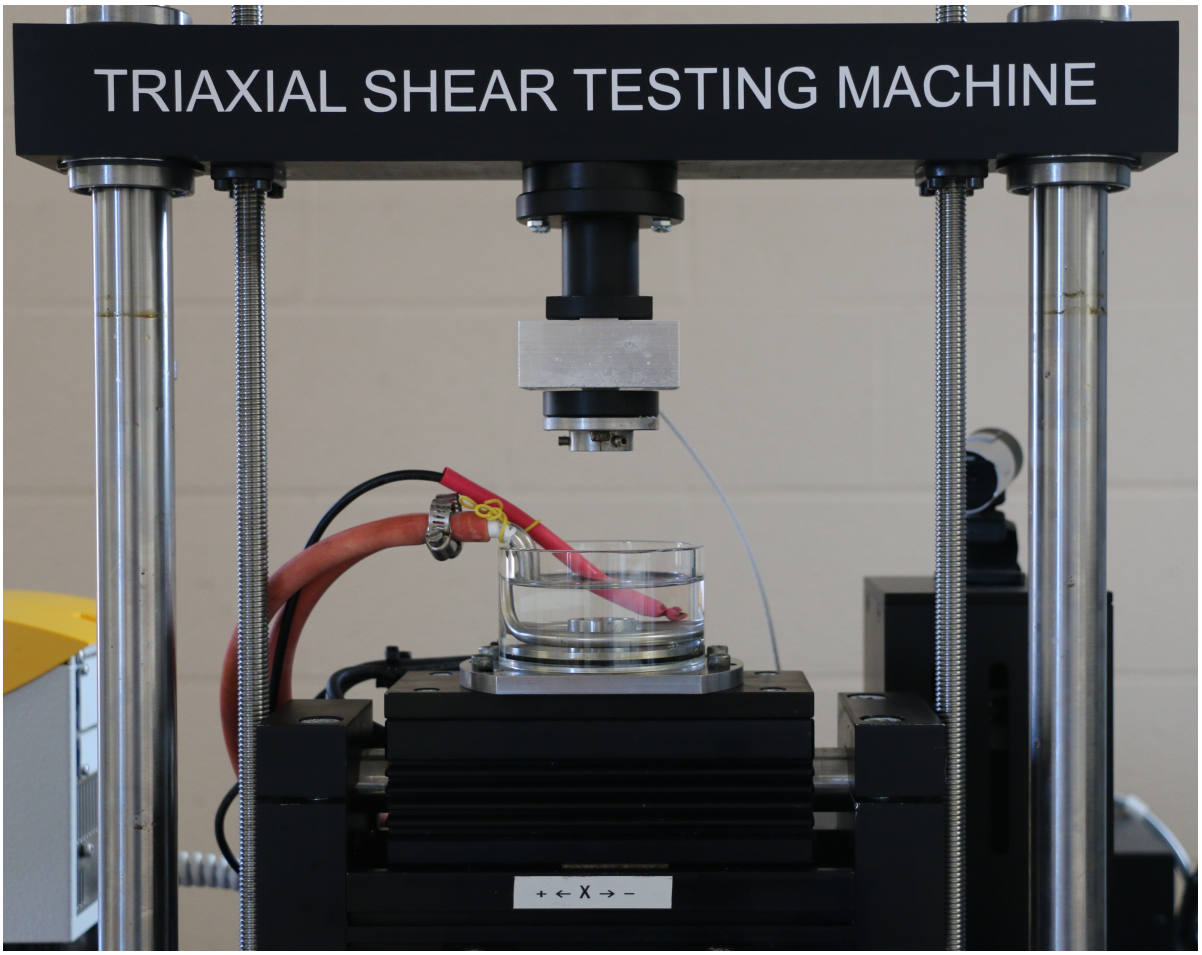

Figure 4.4: Image of the Triaxial Shear Test Machine

a notch on the upper mount indicating the x direction. Once secured, additional cyanoacrylate adhesive was applied to the exposed AC surface, and the sample was immediately lowered onto the bottom mount until $0.125\,\mathrm{N}$ compression (z direction). This compression was maintained for 120 seconds until the adhesive cured.

4.3.2 Procedure

PBS solution was added, and the tissue was held in 1% compression with respect to the total thickness until mechanical equilibrium was reached. For shear testing, a quasi-static pre-conditioning compressive load of $1\,\%$ was applied for $3000\,\mathrm{s}$. Sinusoidal shear deformation was applied at a rate of $0.1\,\mathrm{mm/min}$ producing E_{xz} strain of $\pm 5\,\%$. After 3 pre-conditioning cycles, 6 cycles of sinusoidal shear were recorded.When the shear was completed in the x direction, the tissue was allowed to rest and return to equilibrium for 3000 seconds before beginning the protocol in the y direction E_{yz} strain of $\pm 5\,\%$. This cycle was repeated with applied strains of 5, 10, 15 and $20\,\%$.

4.3.3 Experimental Data Analysis

Results were processed using MATLAB (The Mathworks, Inc., Natick, MA). From the displacement measurements, shear strain γ was calculated by (4.1), where Δl denotes the shear displacement, and L is the thickness of the sample.

$$\gamma = \frac{\Delta l}{L} \tag{4.1}$$

The shear stress τ is calculated by (4.2) where F is the applied shear stress on the surface, and A is the surface are. In this study, the articular surface had an area of approximately $9\,\mathrm{mm}^2$.

$$\tau = \frac{F}{A} \tag{4.2}$$

The stress shift to compensate for drifts as in Fig. 6.1 was a simple linear regression given

by (4.3). τ_{shift} denotes the uniform drift compensation for each data point. n represents the data point of the data segment of interest, such that n_0 is the first point in the segment, and n is the last. The new τ is calculated from adjustments to the original stress τ_0.

$$\begin{aligned} \tau_{shift} &= \frac{\tau(n) - \tau(n_0)}{n - n_0} \\ \tau &= \tau_0 - (\tau_0(n_0) + \tau_{shift}) \end{aligned} \tag{4.3}$$

Built in MATLAB functions were used to calculate the maximum stress and minimum stress, as well as the area enclosed by the hysteresis loop. Specifically, `polyarea` was used to individually calculate the area of each loop, whereby averages were taken for the entire strain application cycle.

The shear modulus G is defined by (4.4) ((Buckley et al. 2008)).

$$G = \frac{\tau}{\gamma} \tag{4.4}$$

This modulus was calculated at 5% strain in order to compare values with other groups.

4.3.4 Statistical Analysis

Patients (1, 2, 3) and regions (1, 2, 3) were considered grouped categorical variables in the analysis. To assess the associations of the numeric outcomes of peak to peak stress and energy dissipation with the grouping variables (e.g., region or patient) we conducted a one-factor analysis of variance (ANOVA), followed by poc hoc tests, if the overall F-test was significant (p <0.05), using Tukey's Honest Significant Difference (HSD) test, with alpha=0.05. For assessing the strength of the linear relationship between numeric variables, for example thickness

and peak to peak stress, we present Pearson's correlation coefficients. We also used a paired t-test test to examine the hypothesis of whether parallel and perpendicular orientations are the same. Statistical analyses were completed using SAS® 9.4 (SAS Institute Inc., Cary, NC) statistical software using the CORR, and ANOVA procedures. The alpha level of significance for all tests was 0.05. Statistical correlations were investigated in:

1. **Inter-patient variability.** Can a given data point be traced back to the original patient, indicating significant differences between patient stress and energy values?

2. **Differences between applied shear parallel and perpendicular to the split line.** Is there a significant difference in the response with respect to the split line direction?

3. **Effects of joint contact region.** Does variability along the anterior-posterior axis correlate with stress and energy values?

4. **Effects of contact stress region.** Do samples taken from high load-bearing regions have significantly different responses to shear?

5. **Effects of sample thickness.** Does the sample thickness have statistical correlation to the stress and energy values?

5 Results

5.1 Experimental Results

The Triaxial Shear Test Machine gives data in terms of force and displacement. Data from a representative sample can be seen in Fig. 5.1. Circled stars represent zero points in time used to identify different phases in the test protocol. For all patients and specimens, results were analyzed and interpreted using stress-strain curves. A representative specimen can be seen in Figs. 5.2 - 5.3. The peak stress values are only shown in Fig. 5.3. The dissipation energy was calculated from the enclosed area between the hysteresis curves for each cycle. Tables 5.1 - 5.6 give the average peak to peak stresses and dissipation energies categorized by patient, joint contact region, and contact stress region. The shear modulus G was calculated at 5% shear strain. The average shear modulus is presented in Fig. 5.4.

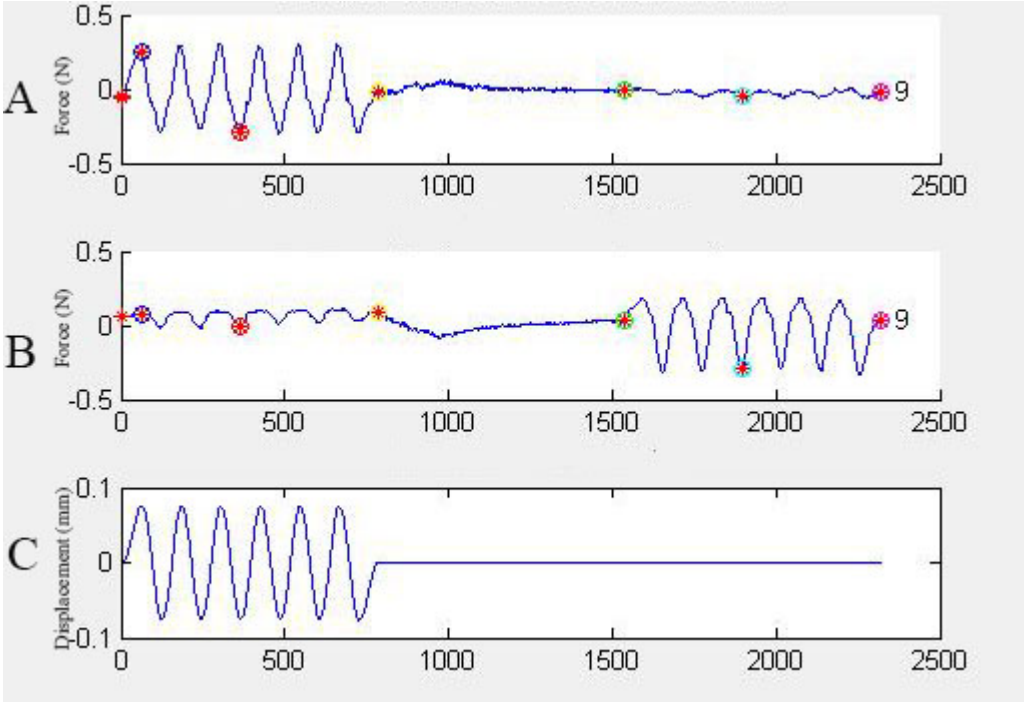

Figure 5.1: Data from a representative bovine cartilage sample.**(A)** Measured force data during applied shear parallel to the split line **(B)** Measured force data during applied shear perpendicular to the split line **(C)** Applied displacement parallel to split line direction, simultaneous to (A) response.

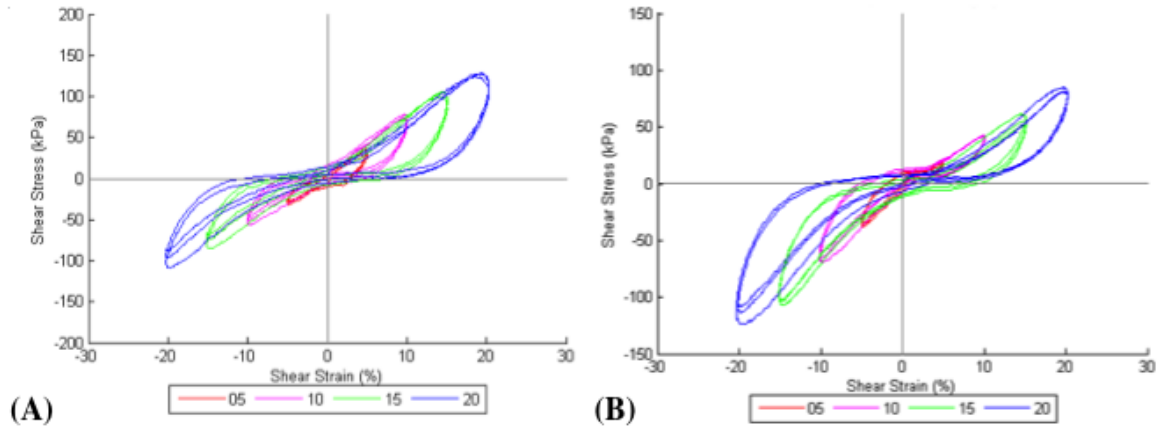

Figure 5.2: Stress-strain curves from a representative bovine cartilage sample during preconditioning cycles **(A)** parallel to split line (X) **(B)** perpendicular to split line (Y).

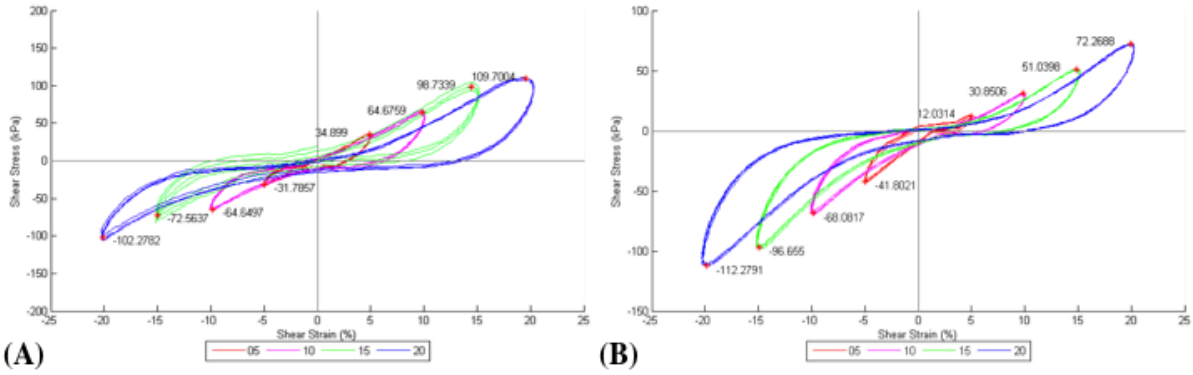

Figure 5.3: Stress-strain curves from a representative bovine cartilage sample during non-preconditioning cycles **(A)** parallel to split line (X) **(B)** perpendicular to split line (Y).

Strain (%)	Patient	Avg. Peak to Peak Stress (kPa)	
		Parallel	Perpendicular
5	1	41.31 ± 22.96	41.78 ± 19.78
	2	25.19 ±10.97	24.04 ± 10.13
	3	39.02 ± 19.95	33.79 ± 15.95
10	1	73.75 ± 35.65	69.47 ± 32.10
	2	49.11 ± 22.80	47.56 ± 21.96
	3	71.98 ± 38.76	67.38 ± 33.24
15	1	97.56 ± 42.81	89.25 ± 31.63
	2	81.38 ± 40.43	77.10 ± 36.44
	3	112.59 ± 48.39	110.40 ± 52.06
20	1	106.78 ± 39.27	101.59 ± 33.62
	2	105.2283 ± 47.35	97.15 ± 37.42
	3	160.77 ± 61.39	153.74 ± 70.47

Table 5.1: Comparing Average Peak to Peak Stress Parallel and Perpendicular to the Split Line by Patient

Strain (%)	Patient	Avg. Dissipation Energy (mJ/mm^2)	
		Parallel	Perpendicular
5	1	100.62 ± 55.93	87.61 ± 41.42
	2	34.27 ± 16.31	36.47 ± 18.27
	3	76.37 ± 46.22	71.86 ± 37.31
10	1	283.48 ± 127.32	263.72 ± 122.87
	2	133.92 ± 56.64	134.37 ± 63.57
	3	267.91 ± 149.99	241.21 ± 109.21
15	1	534.73 ± 223.63	496.55 ± 175.20
	2	326.97 ± 142.45	318.97 ± 164.29
	3	541.91 ± 276.92	513.86 ± 380.93
20	1	755.84 ± 291.88	718.21 ± 254.16
	2	572.73 ± 234.38	553.70 ± 251.65
	3	892.05 ± 400.42	858.49 ± 380.93

Table 5.2: Comparing Average Dissipation Energies Parallel and Perpendicular to the Split Line by Patient. Standard deviations are also given.

Strain (%)	Joint Contact Region	Avg. Peak to Peak Stress (kPa)	
		Parallel	Perpendicular
5	1	39.35 ± 20.22	38.05 ± 17.29
	2	40.60 ± 19.06	38.42 ± 14.92
	3	22.68 ± 14.02	20.16 ± 12.27
10	1	71.90 ± 28.55	68.36 ± 25.21
	2	79.97 ± 37.74	75.99 ± 31.21
	3	37.18 ± 17.13	34.42 ± 15.04
15	1	105.00 ± 31.70	94.50 ± 21.93
	2	120.97 ± 50.80	121.04 ± 50.04
	3	57.70 ± 18.85	54.57 ± 16.52
20	1	122.55 ± 39.69	111.20 ± 23.91
	2	158.63 ± 68.64	158.87 ± 71.49
	3	85.40 ± 22.95	76.66 ± 19.32

Table 5.3: Comparing Average Peak to Peak Stress Parallel and Perpendicular to the Split Line by Joint Contact Region. Standard deviations are also given.

Strain (%)	Joint Contact Region	Avg. Dissipation Energy (mJ/mm^2)	
		Parallel	Perpendicular
5	1	84.70 ± 48.96	69.55 ± 30.52
	2	68.95 ± 48.01	71.00 ± 41.44
	3	52.19 ± 55.17	52.54 ± 50.33
10	1	244.48 ± 113.26	238.79 ± 99.79
	2	262.81 ± 152.40	237.06 ± 121.26
	3	164.72 ± 130.79	148.37 ± 112.17
15	1	506.72 ± 176.01	484.14 ± 131.03
	2	555.21 ± 277.27	509.96 ± 238.82
	3	308.66 ± 200.25	305.49 ± 183.65
20	1	780.47 ± 255.38	746.80 ± 162.81
	2	880.82 ± 397.84	872.58 ± 403.40
	3	515.08 ± 247.15	463.86 ± 224.02

Table 5.4: Comparing Average Dissipation Energies Parallel and Perpendicular to the Split Line by Joint Contact Region. Standard deviations are also given.

Strain(%)	Contact Stress Region	Avg. Peak to Peak Stress (kPa)	
		Parallel	Perpendicular
5	1	28.16 ± 9.83	28.10 ± 7.55
	2	42.19 ± 23.67	38.31 ± 21.69
10	1	54.48 ± 20.84	53.49 ± 14.31
	2	75.41 ± 40.75	69.46 ± 38.82
15	1	86.55 ± 34.45	84.56 ± 22.90
	2	107.81 ± 50.55	99.94 ± 54.02
20	1	113.15 ± 44.75	107.23 ± 25.47
	2	135.37 ± 62.77	127.76 ± 72.70

Table 5.5: Comparing Average Peak to Peak Stress Parallel and Perpendicular to the Split Line by Contact Stress Region. Standard deviations are also given.

Strain(%)	Contact Stress Region	Avg. Dissipation Energy (mJ/mm^2)	
		Parallel	Perpendicular
5	1	55.57 ± 41.19	50.05 ± 13.15
	2	85.26 ± 54.37	80.57 ± 49.83
10	1	171.85 ± 57.79	168.86 ± 35.57
	2	285.02 ± 160.61	257.34 ± 144.59
15	1	381.41 ± 129.18	394.01 ± 80.18
	2	554.33 ± 284.11	492.23 ± 264.94
20	1	638.10 ± 228.53	630.162 ± 162.95
	2	842.31 ± 388.10	790.19 ± 405.69

Table 5.6: Comparing Average Dissipation Energy Parallel and Perpendicular to the Split Line by Contact Stress Region. Standard deviations are also given.

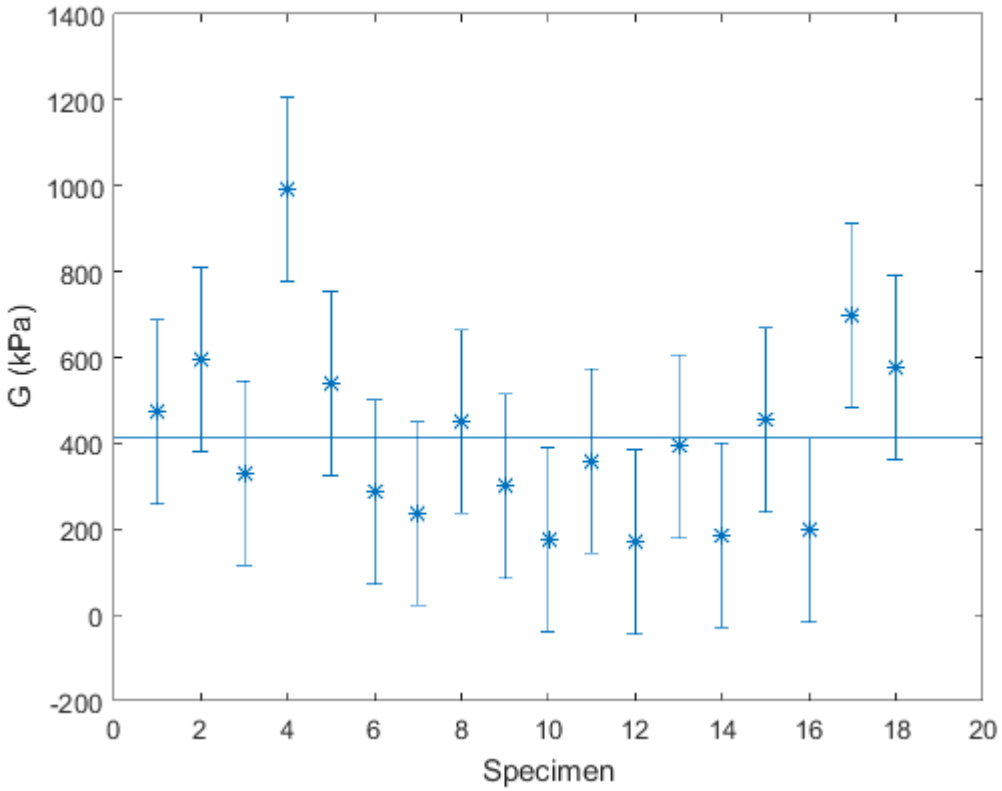

Figure 5.4: Shear modulus G by specimen at 5% shear strain. Average shear modulus is given by the solid line.

5.2 Statistical Analysis

5.2.1 Inter-patient Variability

Tables 5.7 - 5.8 give the statistical analysis of relationships between bovine patients and calculated peak to peak stress and dissipation energy, respectively. Fig.5.5 visually shows the average peak to peak stress and dissipation energy by patient for applied shear both parallel and perpendicular to the split line.

Strain (%)	p-value Parallel	Significance	p-value Perpendicular	Significance
5	0.29	None	0.18	None
10	0.39	None	0.38	None
15	0.49	None	0.39	None
20	0.13	None	0.13	None

Table 5.7: Analysis of correlations between patients and peak to peak stress using ANOVA and Tukey's HSD. p-values less than 0.05 are significant.

Strain(%)	p-value Parallel	Significance	p-value Perpendicular	Significance
5	0.05	1-2	0.05	1-2
10	0.09	None	0.09	None
15	0.20	None	0.17	None
20	0.25	None	0.25	None

Table 5.8: Analysis of correlations between patients and dissipation energy using ANOVA and Tukey's HSD. p-values less than 0.05 are significant.

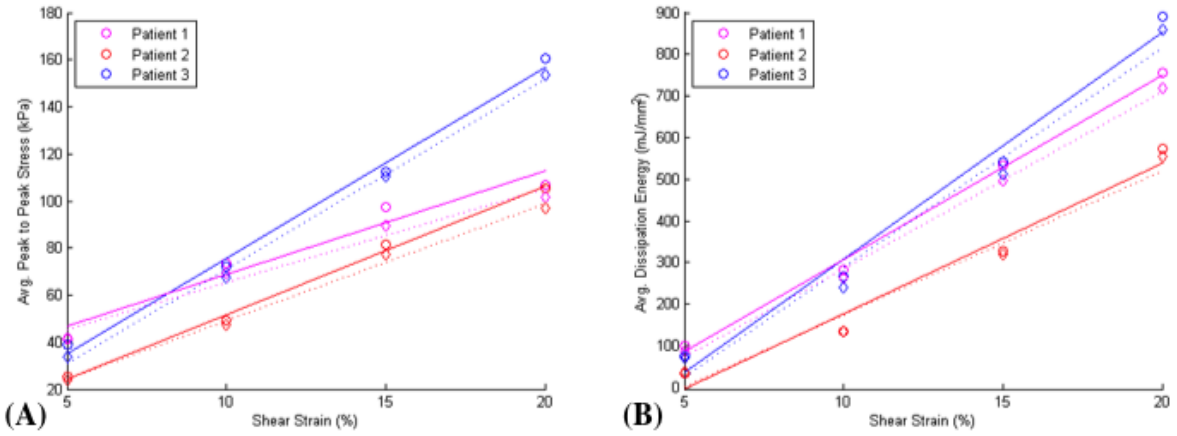

Figure 5.5: Average values by patient. Solid lines with circle markers represent shear applied parallel to the split line. Dotted lines with diamond markers represent shear applied perpendicular to split line.**(A)** Average peak to peak stress versus strain graph by patient. **(B)** Average dissipation energy versus strain graph by patient

5.2.2 Differences Between Applied Shear Parallel or Perpendicular to the Split Line

Box plots showing the distribution of peak to peak stress and energy are shown in Fig. 5.6 with interpretation directions in Table 5.9. Tables 5.10 - 5.11 give results from Pearson's

Group Summary Statistic	Group Summary Statistic Feature of Box-and-Whiskers Plot
maximum	endpoint of upper whisker
third quartile (75th percentile)	upper edge of box
median (50th percentile)	line inside box
mean	symbol marker
first quartile (25th percentile)	lower edge of box
minimum	endpoint of lower whisker

Table 5.9: How to interpret box and whisker plots

correlation and paired t-tests between shear applied in parallel and perpendicular directions

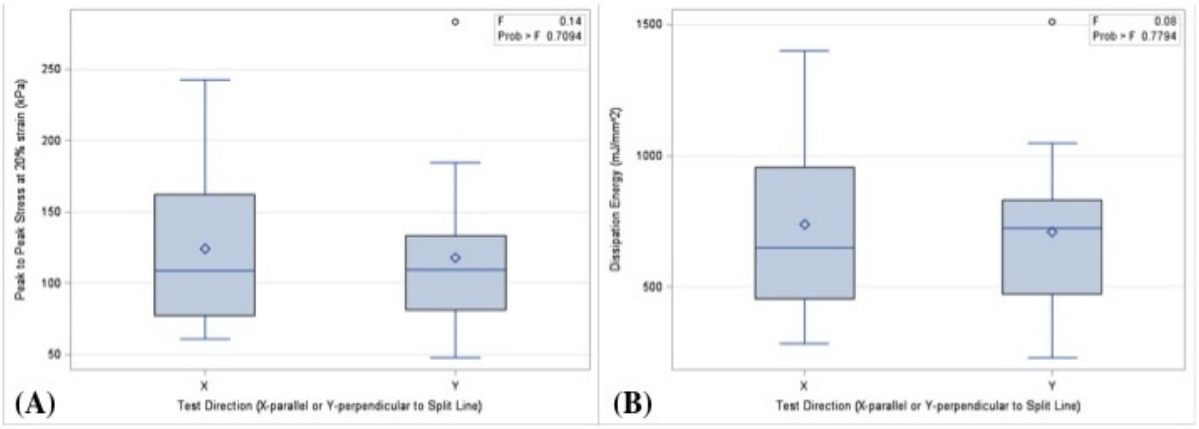

Figure 5.6: Box plots showing **(A)** Peak to Peak Stress **(B)** Dissipation Energy, by shear application direction

with respect to the split line. For Pearson's correlation $p < 0.05$ indicates there is statistically significant correlation between the two groups. For paired t-tests, $p > 0.05$ indicates there is no statistically significant difference between the two groups.

	Correlation Test		Paired t-Test	
Strain(%)	r-value	p-value	t-value	p-value
5	0.94	<.0001	1.3	0.21
10	0.94	<.0001	1.25	0.23
15	0.90	<.0001	1.11	0.28
20	0.91	<.0001	1.28	0.22

Table 5.10: Analysis of correlation between X (parallel) and Y (perpendicular) shear application for peak to peak stress using Pearson's correlation and paired t-tests

Figs.5.7 - 5.10 show the relationship between peak to peak stresses and dissipation energies obtained from shearing parallel and perpendicular to the split line for all applied strains. The solid line represents a 1-1 ratio.

	Correlation Test		Paired t-Test	
Strain(%)	r-value	p-value	t-value	p-value
5	0.89	<.0001	0.94	0.36
10	0.95	<.0001	1.51	0.15
15	0.93	<.0001	1.22	0.24
20	0.89	<.0001	0.84	0.41

Table 5.11: Analysis of correlation between X (parallel) and Y (perpendicular) shear application for dissipation energy using Pearson's correlation and paired t-tests

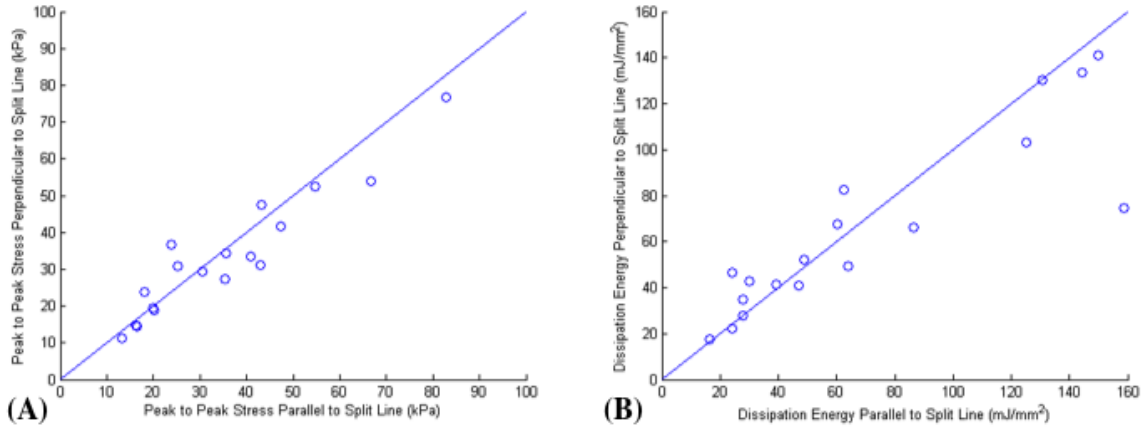

Figure 5.7: Relationship between values obtained parallel or perpendicular to split line direction at 5% strain **(A)** Peak to Peak Stress **(B)** Dissipation Energy

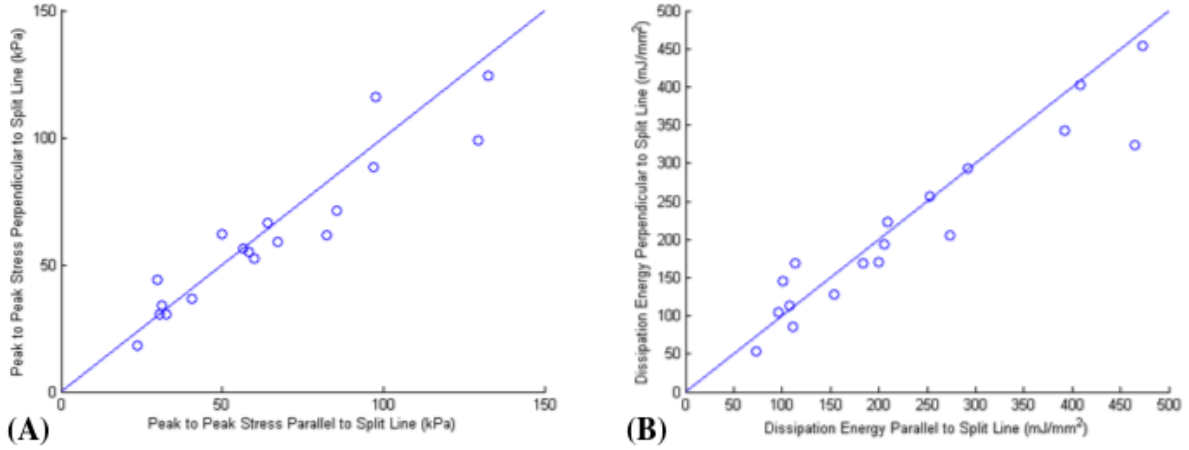

Figure 5.8: Relationship between values obtained parallel or perpendicular to split line direction at 10% strain. **(A)** Peak to Peak Stress **(B)** Dissipation Energy

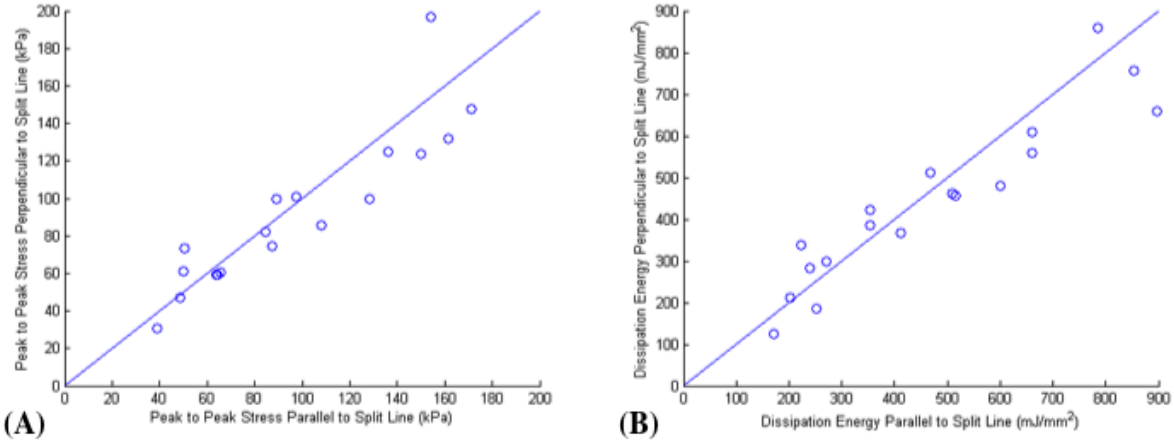

Figure 5.9: Relationship between values obtained parallel or perpendicular to split line direction at 15% strain. **(A)** Peak to Peak Stress **(B)** Dissipation Energy

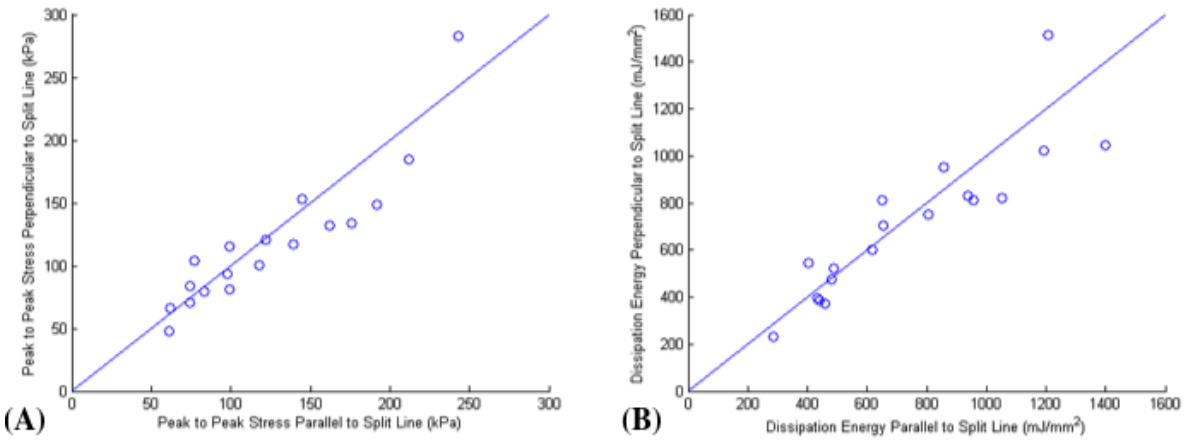

Figure 5.10: Relationship between values obtained parallel or perpendicular to split line direction at 20% strain. **(A)** Peak to Peak Stress **(B)** Dissipation Energy

5.2.3 Effects of Joint Contact Region on Peak to Peak Stress and Dissipation Energy

Tables 5.12 - 5.13 give the ANOVA results between joint contact region and peak to peak stress and dissipation energy, be strain level, from the ANOVA tests and Tukey's HSD tests.

Strain(%)	p-value Parallel	Significance	p-value Perpendicular	Significance
5	0.23	None	0.11	None
10	0.07	None	0.04	2-3
15	0.03	2-3	0.02	2-3
20	0.07	None	0.03	2-3

Table 5.12: Analysis of the association between joint contact region and peak to peak stress, by strain level, using ANOVA and Tukey's HSD. p-values less than 0.05 are significant.

Strain(%)	p-value Parallel	Significance	p-value Perpendicular	Significance
5	0.56	None	0.71	None
10	0.45	None	0.33	None
15	0.19	None	0.18	None
20	0.17	None	0.08	None

Table 5.13: Analysis of the association between joint contact region and dissipation energy, by strain level, using ANOVA and Tukey's HSD. p-values less than 0.05 are significant.

5.2.4 Effects of Contact Stress Region on Peak to Peak Stress and Dissipation Energy

Tables 5.14 - 5.15 give the ANOVA results between contact stress region and peak to peak stress and dissipation energy, by strain level, from the ANOVA tests and Tukey's HSD tests.

Strain(%)	p-value Parallel	Significance	p-value Perpendicular	Significance
5	0.12	None	0.20	None
10	0.19	None	0.26	None
15	0.31	None	0.44	None
20	0.40	None	0.44	None

Table 5.14: Analysis of the association between contact stress region and peak to peak stress using ANOVA and Tukey's HSD. p-values less than 0.05 are significant.

5.2.5 Effects of Sample Thickness on Peak to Peak Stress and Dissipation Energy

Tables 5.16 - 5.17 examines the correlation between explant thickness and peak to peak stress and dissipation energy, by strain level, using Pearson's correlation.

Strain(%)	p-value Parallel	Significance	p-value Perpendicular	Significance
5	0.21	None	0.09	None
10	0.06	None	0.09	None
15	0.12	None	0.30	None
20	0.19	None	0.29	None

Table 5.15: Analysis of the association between contact stress region and dissipation energy using ANOVA and Tukey's HSD. p-values less than 0.05 are significant.

	Parallel		Perpendicular	
Strain(%)	r-value	p-value	r-value	p-value
5	-0.61	0.01	-0.53	0.02
10	-0.52	0.03	-0.53	0.02
15	-0.51	0.03	-0.52	0.03
20	-0.60	0.01	-0.54	0.02

Table 5.16: Correlation between thickness and peak to peak stress for shear applied parallel and perpendicular to the split line direction using Pearson's correlation test.

	Parallel		Perpendicular	
Strain(%)	r-value	p-value	r-value	p-value
5	-0.64	0.00	-0.66	0.00
10	-0.69	0.00	-0.66	0.00
15	-0.62	0.01	-0.67	0.00
20	-0.65	0.00	-0.61	0.01

Table 5.17: Analysis of correlation between thickness and dissipation energy for shear applied parallel and perpendicular to the split line direction using Pearson's correlation test.

Fig.5.11 shows the relationship between sample thickness and peak to peak stress and dissipation energy for all strain values both parallel and perpendicular to the split line.

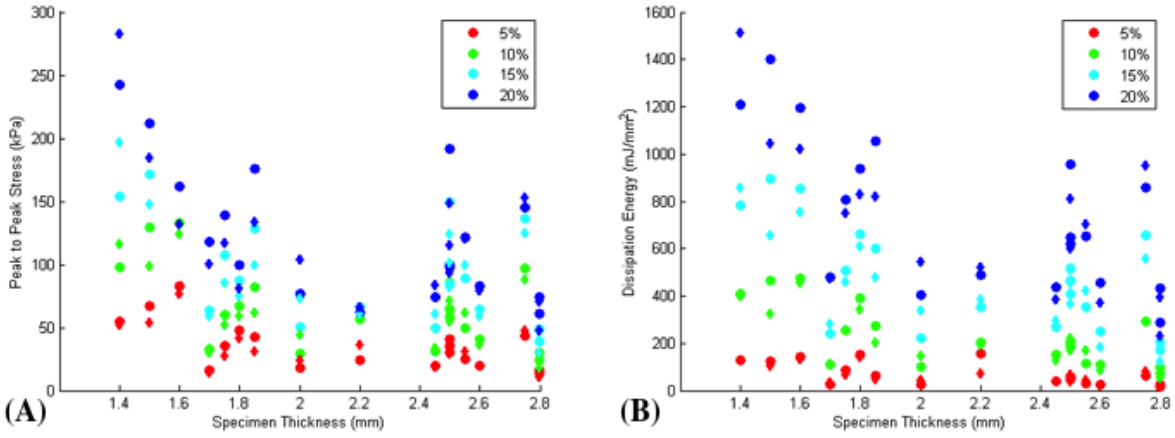

Figure 5.11: Relationship between sample thickness for all applied strain levels. Circular markers indicate shear parallel to the split line direction. Diamond markers indicated shear perpendicular to the split line direction. **(A)** Peak to Peak Stress **(B)** Dissipation Energy

6 Discussion

6.1 Discussion of Results

Fig. 5.1 shows the raw force data obtained from the experimental apparatus. In some patients, the equilibrium axis shifted slightly in a linear increase or decrease. This phenomenon is marginally apparent in Fig. 5.1, but more apparent in a different specimen shown in Fig. 6.1. A linear shift to compensate for this drift was applied to each data point in every specimen. The maximum shift from any sample as a compensation of $0.2\,\mathrm{kPa}$, which does not affect the validity of the results. Data were approximately centered around $0\,\mathrm{N}$. The researchers have no explanation for the shift at this time. Further work will be conducted to determine variables that influence the presence and magnitude of the shift. Fig. 5.2 shows the preconditioning cycles for a representative specimen. Three preconditioning loops were selected after confirmation of visual evidence of hysteresis loop repeatability after the third cycle. The hysteresis is clear evidence of viscoelasticity. The repeatability after preconditioning can be seen in a comparison between Fig. 5.2 and Fig. 5.3. The curve lines are more consistent, and produce less variability in dissipation energy between individual cycles. The dissipation energy is calculated by the area within the hysteresis loop.

Comparing values of peak to peak stress parallel and perpendicular to the split line from

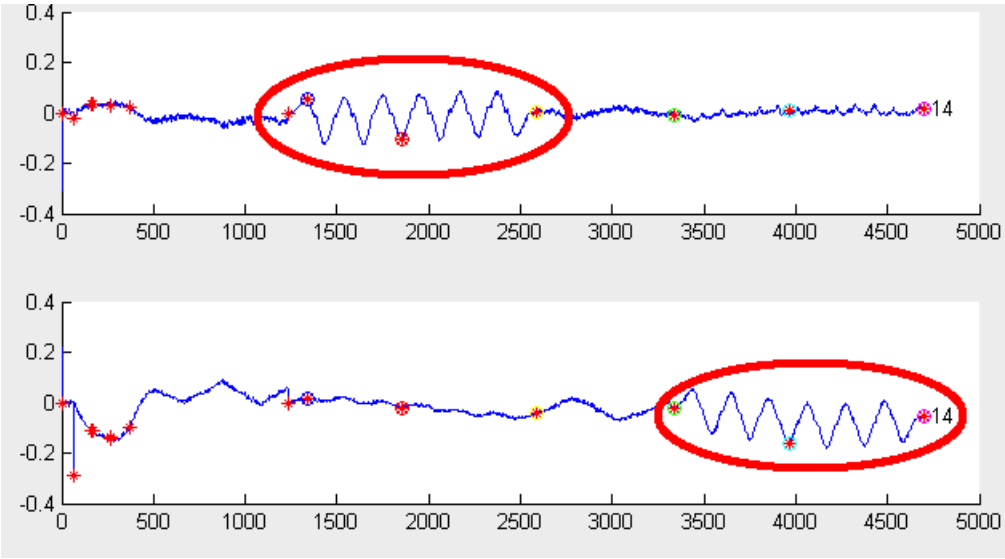

Figure 6.1: Raw force data from the triaxial machine showing the drift shift circled in red in both the parallel (top) and perpendicular (bottom) directions.

Table 5.1, initial overall impressions show peak to peak stress values to be slightly higher during shear applied parallel to the split line than perpendicularly. Energy dissipation values in Table 5.2 follow the same overall trend. This implies a marginal increased stiffness during for shear loads applied parallel to the split line than perpendicular. Correlations are discussed further in the section Differences Between Applied Shear Parallel or Perpendicular to the Split Line.

At 5% shear strain, $G = 412.1 \pm 214.4$ kPa. Buckley et al. (2008) report a range of 100 to 700 kPa for bovine tissue at 5 to 6 % shear and 10% compression. Our G falls within this range. Furthermore, Nguyen and Levenston (2012) report that increased compression correlates with an increased shear modulus. This further supports our findings for G, conducted at 1% compression, and indicate our value more closely aligns with the reported lower bound.

6.1.1 Inter-patient Variability

From Table 5.7, for shear strains applied in both parallel and perpendicular directions, the p-values are all greater than 0.05. Thus, there were no statistically significant differences between patients for peak to peak stress values. Similarly, in Table 5.8, only at 5% shear was there slight statistical significance between patients 1 and 2. Overall, with only 1/4 of the p-values being statistically significant, it is insufficient to say there is any statistically significant correlation between the patient and the dissipation energy. These statements prove each patient is sufficiently different from the other, and validates the claim that the groups are independent. This proves that, for example, if a peak to peak value or dissipation energy value is selected at random, it cannot be traced back to the patient without knowing the label; any trends of higher or lower average values for peak to peak stress or dissipation energy are not statistically significant.

From Fig. 5.5 we can confirm independence by the nature of the least-squares line fit to the average peak to peak and dissipation energy data. There is no relationship or proportionality between patient lines. We do note however that patient 2 has overall lower values in all categories for all strain values.

6.1.2 Differences Between Applied Shear Parallel or Perpendicular to the Split Line

Fig. 5.5 also alludes to relationships between values parallel and perpendicular to the split line. From the figure, the dotted lines fitting data from the perpendicular direction are closely aligned with with the solid lines fitting data from the parallel direction, indicating no considerable difference between shear applied parallel and perpendicular to the split line. This is

confirmed from similar means and median values in the box plot in Fig. 5.6, as well as Tables 5.10 - 5.11. From the Pearson's correlation test, the p-values are all < 0.0001 indicating a strong correlation between parallel and perpendicular values. This is further confirmed by the paired t-test, where the p-values indicate there is no statistically significant difference between the values obtained from applied shear in the parallel or the perpendicular direction with respect to the split line. This implies that the peak stresses and dissipation energies are irrespective of the split-line. This is corroborated visually by the virtually linear one-to-one relationships apparent in Figs. 5.7 - 5.10.

6.1.3 Effects of Joint Contact Region on Peak to Peak Stress and Dissipation Energy

There are distinct differences in data in Tables 5.12 - 5.13. Considering peak to peak stress, the majority of the reported p-values show statistical signficance between regions 2 and 3. Physiologically, this corresponds to flexion at $45°$ and $90°$. This indicates there is no statistically significant difference between the peak to peak stresses during flexion greater than $45°$. An interesting point to note is that in Table 5.12, any significance between joint contact region and the peak to peak stress occurs at strains 10% or higher. This may confirm there are notable behavioral differences between small and large strain, and validate the need for further experimental tests at large strains. Conversely, there is no statistical significance between the three joint contact regions with respect to dissipation energy. Thus, the joint contact region, thereby the degree of flexion, does not affect the magnitude of the area enclosed by the hysteresis loop.

6.1.4 Effect of Contact Stress Region on Peak to Peak Stress and Dissipation Energy

In Tables 5.14 - 5.15, there are no statistically significant differences between any of the contact stress regions. The marginal increase in both peak to peak stress and dissipation energy in the parallel direction over the perpendicular is not statistically significant. This could be due to the large standard deviations reported in the tables.

6.1.5 Effects of Sample Thickness on Peak to Peak Stress and Dissipation Energy

For both peak to peak stress and dissipation energy, there is a significant statistical correlation with the explant thickness. Specifically, smaller thicknesses have a higher peak to peak stress and dissipation energy than thicker samples. The p-values were reported in Tables 5.16 - 5.17 and are all below 0.05. It is worth noting the r-values are considerably low, indicating there is low agreement or precision between the trendline and the data points. Further testing could confirm or debunk this statement.

6.1.6 Summary

The degree of flexion and the cartilage thickness have a significant effect on shear stress and viscoelastic trends. Additionally, considerations of split line directions are not statistically significant. This confirms claims by Silverberg et al. (2014) and others that there are weak correlations between the collagen fiber orientation and shear modulus. This pilot study opens the door for larger studies with a greater number of patients, specimens, and comparisons be-

tween species. Further analysis can be conducted to extract shear moduli and other parameters for computational modeling.

6.2 Limitations and Potential Applications

As seen in Tables 5.1 - 5.6, large standard deviations were reported. This could overshadow any statistical significance overlooked by the SAS® program. Inspecting Table 5.1, patient 2 exhibited lower peak to peak stress values than patients 1 and 3. This is further apparent in Table 5.2. An in-depth OARSI score and grade using methods in Pritzker et al. (2006) could be taken to assure the patients are healthy. Patients were deemed healthy by inpsection of fibrillation at the surface; however OARSI scores could reveal patient 2 to have a degree of OA that would explain the overall lower peak to peak stresses and dissipation energies, as well as the large standard deviations due to potential localized OA.

Previous studies have shown a significant decrease in shear modulus (from 2.67 MPa to 1.72 MPa) when using thawed samples stored in Ringer's solution (Hayes and Bodine 1978). Future works include comparing obtained data with fresh bovine tissue.

In healthy joints, cartilage is continuously hydrated by synovial fluid; however in this *in vitro* study, the sample was exposed to the air during sample preparation, where dehydration and potential damage can occur. Dehydration has been found to influence mechanical properties, thus, if drying did occur, results could be tainted (Smyth et al. 2014).

For this test, we assumed a uniform shear stress as a function of depth. It is possible slight non-uniformity at the shearing plates could occur (Buckley et al. 2013). Future confirmation of a uniform stress field will be by conducting high resolution imaging and analyzing surface deformation. Results will be compared with cartilage and a rubber sample to confirm any non-

uniformity is negligible.Additionally, several groups report strain stiffening at large strains (Silverberg et al. 2014); however, this was not the case in this pilot study.

The results from these experiments are very exciting for the field of biomechanics. Understanding how physiological conditions correlate with mechanical behavior within the tissue allow engineers and scientists to determine more accurate markers for diseases such as OA, and potentially predict the onset of these diseases, creating better preventative and diagnostic measures for all.

Bibliography

Adams, M. A. (2006). The mechanical environment of chondrocytes in articular cartilage. *Biorheology*, 43(3-4):537–545.

Amos, J. R., Li, S., Yost, M., Phloen, H., and Potts, J. D. (2009). Limb bud mesenchyme cultured under tensile strain remodel collagen type i tubes to produce fibrillar collagen type ii. *Biorheology*, 46(6):439–450.

Archer, C. W. and Francis-West, P. (2003). The chondrocyte. *The International Journal of Biochemistry & Cell Biology*, 35(4):401–404.

Asanbaeva, A., Tam, J., Schumacher, B. L., Klisch, S. M., Masuda, K., and Sah, R. L. (2008). Articular cartilage tensile integrity: Modulation by matrix depletion is maturation-dependent. *Archives of Biochemistry and Biophysics*, 474(1):175–182.

Ateshian, G. A., Warden, W. H., Kim, J. J., Grelsamer, R. P., and Mow, V. C. (1997). Finite deformation biphasic material properties of bovine articular cartilage from confined compression experiments. *Journal of Biomechanics*, 30(11-12):1157–1164.

Athanasiou, K. A., Darling, E. M., Hu, J. C., DuRaine, G. D., and Reddi, A. H. (2013). *Articular Cartilage*. CRC Press, Hoboken.

Athanasiou, K. A., Rosenwasser, M. P., Buckwalter, J. a., Malinin, T. I., and Mow, V. C. (1991). Interspecies comparisons of in situ intrinsic mechanical properties of distal femoral cartilage. *Journal of Orthopaedic Research*, 9(3):330–340.

Atkinson, T. S., Haut, R. C., and Altiero, N. J. (1998). An investigation of biphasic failure criteria for impact-induced fissuring of articular cartilage. *Journal of biomechanical engineering*, 120:536–537.

Bae, W. C., Wong, V. W., Hwang, J., Antonacci, J. M., Nugent-Derfus, G. E., Blewis, M. E., Temple-Wong, M. M., and Sah, R. L. (2008). Wear-lines and split-lines of human patellar cartilage: relation to tensile biomechanical properties. *Osteoarthritis and Cartilage*, 16(7):841–845.

Bar-On, B. and Daniel Wagner, H. (2012). Elastic modulus of hard tissues. *Journal of Biomechanics*, 45(4):672–678.

Barbucci, R., Lamponi, S., Borzacchiello, A., Ambrosio, L., Fini, M., Torricelli, P., and Giardino, R. (2002). Hyaluronic acid hydrogel in the treatment of osteoarthritis. *Biomaterials*, 23(23):4503–4513.

Below, S., Arnoczky, S. P., Dodds, J., Kooima, C., and Walter, N. (2002). The split-line pattern of the distal femur. *Arthroscopy: The Journal of Arthroscopic & Related Surgery*, 18(6):613–617.

Billiar, K. L. and Sacks, M. S. (1999). Biaxial mechanical properties of the natural and glutaraldehyde treated aortic valve cusp - part i: Experimental results. *Journal of Biomechanical Engineering*, 122:23–30.

Blackburn, T. A. and Craig, E. (1980). Knee anatomy: A brief review. *Phys. Ther.*, 60:1556–1560.

Blankevoort, L., Kuiper, J., Huiskes, R., and Grootenboer, H. (1991). Articular contact in a three-dimensional model of the knee. *Journal of Biomechanics*, 24(11):1019–1031.

Boschetti, F., Gervaso, F., Pennati, G., Peretti, G. M., Vena, P., and Dubini, G. (2006). Poroelastic numerical modelling of natural and engineered cartilage based on in vitro tests. *Biorheology*, 43(3-4):235–247.

Boschetti, F., Pennati, G., Gervaso, F., Peretti, G. M., and Dubini, G. (2004). Biomechanical properties of human articular cartilage under compressive loads. *Biorheology*, 41:159–166.

Brault, M., Hootman, J., Helmick, C., Theis, K., and Armour, B. (2009). Prevalence and most common causes of disability among adults. *MMWR*, 58(16):421–426.

Broom, N. D. (1986). The Collagenous Architecture of Articular Cartilage- A Synthesis of Ultrastructure and Mechanical Function. *Journal of Rheumatology*, 13(1):142–152.

Buckley, M. R., Bergou, A. J., Fouchard, J., Bonassar, L. J., and Cohen, I. (2010). High-resolution spatial mapping of shear properties in cartilage. *Journal of Biomechanics*, 43(4):796–800.

Buckley, M. R., Bonassar, L. J., and Cohen, I. (2013). Localization of viscous behavior and shear energy dissipation in articular cartilage under dynamic shear loading. *Journal of biomechanical engineering*, 135(3):31002.

Buckley, M. R., Gleghorn, J. P., Bonassar, L. J., and Cohen, I. (2008). Mapping the depth

dependence of shear properties in articular cartilage. *Journal of biomechanics*, 41(11):2430–7.

Buckwalter, J., Mow, V., and Ratcliffe, A. (1994). Restoration of Injured or Degenerated Articular Cartilage. *The Journal of the American Academy of Orthopaedic Surgeons*, 2(August 1994):192–201.

Buckwalter, J. A. (1997). Articular cartilage. part ii- degeneration and osteoarthrosis, repair, regeneration, and transplantation. *The Journal of Bone and Joint Surgery*, 79-A(4):612–632.

Buckwalter, J. A. and Mankin, H. J. (1998). Articular Cartilage: tissue design and chondrocyte matrix interactions. *AAOS Instructional Course Lectures*, 47:477–486.

Buckwalter, J. A. and Martin, J. A. (1995). Degenerative joint disease. *Clinical Symposia*, 47(2):1–32.

Buckwalter, J. A. and Martin, J. A. (2006). Osteoarthritis. *Advanced drug delivery reviews*, 58(2):150–67.

Capistrant, B. D., Glymour, M. M., and Berkman, L. F. (2014). Assessing mobility difficulties for cross-national comparisons: results from the World Health Organization Study on Global AGEing and Adult Health. *Journal of the American Geriatrics Society*, 62(2):329–35.

Carballido-Gamio, J., Bauer, J. S., Stahl, R., Lee, K. Y., Krause, S., Link, T. M., and Majumdar, S. (2008). Inter-subject comparison of MRI knee cartilage thickness. *Medical image analysis*, 12(2):120–35.

Charlebois, M., McKee, M. D., and Buschmann, M. D. (2004). Nonlinear tensile properties of bovine articular cartilage and their variation with age and depth. *Journal of biomechanical engineering*, 126(April):129–137.

Chen, S. S., Falcovitz, Y. H., Schneiderman, R., Maroudas, a., and Sah, R. L. (2001). Depth-dependent compressive properties of normal aged human femoral head articular cartilage: Relationship to fixed charge density. *Osteoarthritis and Cartilage*, 9(6):561–569.

Clements, K. M., Bee, Z. C., Crossingham, G. V., Adams, M. a., and Sharif, M. (2001). How severe must repetitive loading be to kill chondrocytes in articular cartilage? *Osteoarthritis and Cartilage*, 9:499–507.

DiSilvestro, M. R. and Suh, J. K. (2001a). A cross-validation of the biphasic poroviscoelastic model of articular cartilage in unconfined compression, indentation, and confined compression. *Journal of Biomechanics*, 34(4):519–525.

DiSilvestro, M. R., Zhu, Q., Wong, M., Jurvelin, J. S., and Suh, J. K. (2001b). Biphasic poroviscoelastic simulation of the unconfined compression of articular cartilage: I–Simultaneous prediction of reaction force and lateral displacement. *Journal of biomechanical engineering*, 123(2):191–197.

Eisenfeld, J., Mow, V. C., and Lipshitz, H. (1978). Mathematical Analysis of Stress Relaxation in Articular Cartilage During Compresion. *Mathematical biosciences*, 39(1-2):97–112.

Ewers, B., Dvoracek-Driksna, D., Orth, M. W., and Haut, R. C. (2001). The extent of matrix damage and chondrocyte death in mechanically traumatized articular cartilage explants depends on rate of loading. *Journal of orthopaedic research : official publication of the Orthopaedic Research Society*, 19(5):779–84.

Eyre, D. R. (1991). The collagens of articular cartilage. *Seminars in arthritis and rheumatism*, 21(3 Suppl 2):2–11.

Fan, J. C. Y. and Waldman, S. D. (2010). The Effect of Intermittent Static Biaxial Tensile Strains on Tissue Engineered Cartilage. *Annals of biomedical engineering*, 38(4):1672–1682.

Fischenich, K. M., Lewis, J., Kindsfater, K. A., Bailey, T. S., and Haut Donahue, T. L. (2015). Effects of degeneration on the compressive and tensile Properties of Human meniscus. *Journal of Biomechanics*, 48(8):1407–1411.

Frank, E. H., Jin, M., Loening, A. M., Levenston, M. E., and Grodzinsky, A. J. (2000). A versatile shear and compression apparatus for mechanical stimulation of tissue culture explants. *Journal of Biomechanics*, 33(11):1523–1527.

Frisbie, D. D., Cross, M. W., and McIlwraith, C. W. (2006). A comparative study of articular cartilage thickness in the stifle of animal species used in human pre-clinical studies compared to articular cartilage thickness in the human knee. *Veterinary and Comparative Orthopaedics and Traumatology*, 19(3):142–146.

Gelse, K., Poschl, E., and Aigner, T. (2003). Collagens—structure, function, and biosynthesis. *Advanced Drug Delivery Reviews*, 55(12):1531–1546.

Greaves, G. N., Greer, A. L., Lakes, R. S., and Rouxel, T. (2011). Poisson's ratio and modern materials. *Nature Materials*, 10(11):823–837.

Griffin, D. J., Vicari, J., Buckley, M. R., Silverberg, J. L., Cohen, I., and Bonassar, L. J. (2014). Effects of enzymatic treatments on the depth-dependent viscoelastic shear properties of ar-

ticular cartilage. *Journal of orthopaedic research : official publication of the Orthopaedic Research Society*, 32(12):1652–7.

Grodzinsky, A. J., Levenston, M. E., Jin, M., and Frank, E. H. (2000). Cartilage Tissue Remodeling in Response to Mechanical Forces. *Annu. Rev. Biomed. Eng.*, 2(2000):691–713.

Guilak, F. and Mow, V. C. (2000). The mechanical environment of the chondrocyte: A biphasic finite element model of cell-matrix interactions in articular cartilage. *Journal of Biomechanics*, 33(12):1663–1673.

Hardingham, T. E., Muir, H., Kwan, M. K., Lai, W. M., and Mow, V. C. (1987). Viscoelastic Properties of Proteoglycan Solutions with Varying Proportions Present as Aggregates. *Journal of Orthopaedic Research*, 5(1):36–46.

Hayes, W. C. and Bodine, A. J. (1978). Flow-independent viscoelastic properties of articular cartilage matrix. *Journal of Biomechanics*, 11(8-9):407–419.

Hayes, W. C., Keer, L. M., Herrmann, G., and Mockros, L. F. (1972). A mathematical analysis for indentation tests of articular cartilage. *Journal of Biomechanics*, 5(5):541–551.

Heinegård, D. and Paulsson, M. (1987). Cartilage. In Cunningham, L. W., editor, *Structural and Contractile Proteins Part E: Extracellular Matrix*, volume 145 of *Methods in Enzymology*, pages 336 – 363. Academic Press.

Jin, M., Emkey, G. R., Siparsky, P., Trippel, S. B., and Grodzinsky, A. J. (2003). Combined effects of dynamic tissue shear deformation and insulin-like growth factor I on chondrocyte

biosynthesis in cartilage explants. *Archives of Biochemistry and Biophysics*, 414(2):223–231.

Jin, M., Frank, E. H., Quinn, T. M., Hunziker, E. B., and Grodzinsky, a. J. (2001). Tissue shear deformation stimulates proteoglycan and protein biosynthesis in bovine cartilage explants. *Archives of biochemistry and biophysics*, 395(1):41–48.

Julkunen, P., Wilson, W., Isaksson, H., Jurvelin, J. S., Herzog, W., and Korhonen, R. K. (2013). A review of the combination of experimental measurements and fibril-reinforced modeling for investigation of articular cartilage and chondrocyte response to loading. *Computational and mathematical methods in medicine*, 2013:326150.

Jurvelin, J. S., Buschmannf, M. D., Hunziker, E. B., Medicine, N., and Polytechnique, E. (1997). Optical and mechanical determination of poisson's ratio of adult bovine humeral articular cartilage. *Journal of biomechanics*, 30(3):235–241.

Kallemeyn, N. A., Grosland, N. M., Pedersen, D. R., Martin, J. A., and Brown, T. D. (2006). Loading and boundary condition influences in a poroelastic finite element model of cartilage stresses in a triaxial compression bioreactor. *The Iowa orthopaedic journal*, 26(319):5–16.

Kamalanathan, S. and Broom, N. D. (1993). The biomechanical ambiguity of the articular surface. *J. Anat.*, 183(3):567–578.

Kempson, G. E. (1982). Relationship between the tensile properties of articular cartilage from the human knee and age. *Annals of the Rheumatic Diseases*, 41(5):508–511.

Kempson, G. E., Freeman, M. A., and Swanson, S. A. (1971). The determination of a creep

modulus for articular cartilage from indentation tests of the human femoral head. *Journal of biomechanics*, 4(4):239–250.

Kempson, G. E., Muir, H., Swanson, S. A., and Freeman, M. A. (1970). Correlations between stiffness and the chemical constituents of cartilage on the human femoral head. *Biochimica et biophysica acta*, 215(1):70–77.

Korenchenko, A. E. and Beskachko, V. P. (2008). Determining the shear modulus of water in experiments with a floating disk. *Journal of Applied Mechanics and Technical Physics*, 49(1):80–83.

Korhonen, R. K., Laasanen, M. S., Töyräs, J., Rieppo, J., Hirvonen, J., Helminen, H. J., and Jurvelin, J. S. (2002). Comparison of the equilibrium response of articular cartilage in unconfined compression, confined compression and indentation. *Journal of Biomechanics*, 35(7):903–909.

Krishnan, R., Park, S., Eckstein, F., and Ateshian, G. A. (2003). Inhomogeneous cartilage properties enhance superficial interstitial fluid support and frictional properties, but do not provide a homogeneous state of stress. *Journal of biomechanical engineering*, 125(October 2003):569–577.

Lawson, H. (1873). *A manual of popular physiology, being an attempt to explain the science of life in untechnical language*. Putnam's popular manuals. New York, Putnam, United States.

Lees, C., Vincent, J. F. V., and Hillerton, J. E. (1991). Poisson's ratio in skin. *Biomedical Materials and Engineering*, 1(1):19–23.

Li, L., Soulhat, J., Buschmann, M., and Shirazi-Adl, A. (1999). Nonlinear analysis of cartilage in unconfined ramp compression using a fibril reinforced poroelastic model. *Clinical Biomechanics*, 14(9):673 – 682.

Li, L. P., Herzog, W., Korhonen, R. K., and Jurvelin, J. S. (2005). The role of viscoelasticity of collagen fibers in articular cartilage: Axial tension versus compression. *Medical Engineering and Physics*, 27(1):51–57.

Logerstedt, D. S., Snyder-Mackler, L., Ritter, R. C., and Axe, M. J. (2010). Knee pain and mobility impairments: meniscal and articular cartilage lesions. *The Journal of orthopaedic and sports physical therapy*, 40(6):A1–A35.

Lyyra, T., Jurvelin, J. S., Pitkanen, P., Vaatainen, U., and Kiviranta, I. (1995). Indentation instrument for the measurement of cartilage stiffness under arthroscopic control. *Medical engineering & physics*, 17(5):395–399.

Mansour, J. M. (2003). Biomechanics of Cartilage. In Oatis, C. A., editor, *Kinesiology: The Mechanics and Pathomechanics of Human Movement*, chapter 5, pages 66–79. Lippincott Williams and Wilkins, Philadelphia, 1 edition.

Mauck, R. L., Soltz, M. A., Wang, C. C., Wong, D. D., Chao, P. H., Valhmu, W. B., Hung, C. T., and Ateshian, G. A. (2000). Functional tissue engineering of articular cartilage through dynamic loading of chondrocyte-seeded agarose gels. *Journal of biomechanical engineering*, 122(3):252–260.

Meachim, G. (1972). Light microscopy of Indian ink preparations of fibrillated cartilage. *Annals of the Rheumatic Disease*, 31(6):457–464.

Mononen, M. E., Mikkola, M. T., Julkunen, P., Ojala, R., Nieminen, M. T., Jurvelin, J. S., and Korhonen, R. K. (2012). Effect of superficial collagen patterns and fibrillation of femoral articular cartilage on knee joint mechanics-a 3D finite element analysis. *Journal of biomechanics*, 45(3):579–87.

Moody, H. R., Brown, C. P., Bowden, J. C., Crawford, R. W., McElwain, D. L. S., and Oloyede, A. O. (2006). In vitro degradation of articular cartilage: Does trypsin treatment produce consistent results? *Journal of Anatomy*, 209:259–267.

Moreira, D. and Nunes, L. (2013). Comparison of simple and pure shear for an incompressible isotropic hyperelastic material under large deformation. *Polymer Testing*, 32(2):240–248.

Motavalli, M., Whitney, G. A., Dennis, J. E., and Mansour, J. M. (2013). Investigating a continuous shear strain function for depth-dependent properties of native and tissue engineering cartilage using pixel-size data. *Journal of the mechanical behavior of biomedical materials*, 28:62–70.

Mow, V. C., Gibbs, M. C., Lai, W. M., Zhu, W. B., and Athanasiou, K. A. (1989). Biphasic indentation of articular cartilage–II. A numerical algorithm and an experimental study. *Journal of biomechanics*, 22:853–861.

Mow, V. C., Gu, W. Y., and Chen, F. H. (2005). Structure and Function of Articular Cartilage and Meniscus. In Mow, V. C. and Huiskes, R., editors, *Basic Orthopaedic Biomechanics and Mechano-biology*, chapter 5, pages 180–258. Lippincott Williams and Wilkins, 3rd edition.

Mow, V. C., Holmes, M. H., and Lai, W. M. (1984). Fluid transport and mechanical properties of articular cartilage: a review. *Journal of biomechanics*, 17(5):377–394.

Mow, V. C., Kuei, S. C., Lai, W. M., and Armstrong, C. G. (1980). Biphasic creep and stress relaxation of articular cartilage in compression: Theory and experiments. *Journal of Biomechanical Engineering*, 102(1):73–84.

Nguyen, A. M. and Levenston, M. E. (2012). Comparison of osmotic swelling influences on meniscal fibrocartilage and articular cartilage tissue mechanics in compression and shear. *Journal of Orthopaedic Research*, 30(1):95–102.

Park, S. and Ateshian, G. a. (2006). Dynamic response of immature bovine articular cartilage in tension and compression, and nonlinear viscoelastic modeling of the tensile response. *Journal of biomechanical engineering*, 128(4):623–630.

Park, S., Hung, C. T., and Ateshian, G. a. (2004). Mechanical response of bovine articular cartilage under dynamic unconfined compression loading at physiological stress levels. *Osteoarthritis and Cartilage*, 12(1):65–73.

Parsons, J. R. and Black, J. (1977). The viscoelastic shear behavior of normal rabbit articular cartilage. *Journal of biomechanics*, 10(1):21–29.

Peat, G., Mccarney, R., and Croft, P. (2001). Knee pain and osteoarthritis in older adults: a review of community burden and current use of primary health care. *Annals of the Rheumatic Disease*, 60(2):91–97.

Pritzker, K. P. H., Gay, S., Jimenez, S. A., Ostergaard, K., Pelletier, J.-P., Revell, P. A., Salter, D., and van den Berg, W. B. (2006). Osteoarthritis cartilage histopathology: grading and staging. *Osteoarthritis and cartilage / OARS, Osteoarthritis Research Society*, 14(1):13–29.

Purslow, P. P., Wess, T. J., and Hukins, D. W. (1998). Collagen orientation and molecular

spacing during creep and stress-relaxation in soft connective tissues. *The Journal of Experimental Biology*, 201:135–142.

Ramos-Pichardo, J. D., Cabrero-García, J., González-Llopis, L., Cabañero Martínez, M. J., Muñoz Mendoza, C. L., Sanjuan-Quiles, A., Richart-Martínez, M., and Reig-Ferrer, A. (2014). What do older people understand by mobility-related difficulties? *Archives of Gerontology and Geriatrics*, 59(1):122–30.

Sasazaki, Y., Shore, R., and Seedhom, B. B. (2006). Deformation and failure of cartilage in the tensile mode. *Journal of Anatomy*, 208(6):681–694.

Seror, J., Merkher, Y., Kampf, N., Collinson, L., Day, A. J., Maroudas, A., and Klein, J. (2012). Normal and shear interactions between hyaluronan-aggrecan complexes mimicking possible boundary lubricants in articular cartilage in synovial joints. *Biomacromolecules*, 13(11):3823–3832.

Setton, L., Mow, V. C., and Howell, D. S. (1995). Mechanical Behavior of Articular Cartilage in Shear is Altered by Transection of the Anterior Cruciate Ligament. *Journal of Orthopaedic Research*, 13(4):473–482.

Setton, L., Tohyama, H., and Mow, V. C. (1998). Swelling and Curling Behaviors of Articular Cartilage. *Journal of biomechanical engineering*, 120(3):355–361.

Shen, Z. L., Dodge, M. R., Kahn, H., Ballarini, R., and Eppell, S. J. (2008). Stress-strain experiments on individual collagen fibrils. *Biophysical journal*, 95(8):3956–3963.

Silverberg, J. L., Barrett, A. R., Das, M., Petersen, P. B., Bonassar, L. J., and Cohen, I. (2014).

Structure-Function Relations and Rigidity Percolation in the Shear Properties of Articular Cartilage. *Biophysical Journal*, 107:1721–1730.

Silverberg, J. L., Dillavou, S., Bonassar, L., and Cohen, I. (2013). Anatomic variation of depth-dependent mechanical properties in neonatal bovine articular cartilage. *Journal of Orthopaedic Research*, 31(May):686–691.

Simon, W., Katter, R., and Brown, N. (1982). The production of shear fatigue in bovine articular cartilage. *Transactions of the annual meeting of the Orthopaedic Research Society*, 6:148.

Smyth, P. A., Rifkin, R., Jackson, R. L., and Hanson, R. R. (2014). The average roughness and fractal dimension of articular cartilage during drying. *Scanning*, 36(3):368–375.

Soltz, M. A. and Ateshian, G. A. (1998). Experimental verification and theoretical prediction of cartilage interstitial fluid pressurization at an impermeable contact interface in confined compression. *Journal of Biomechanics*, 31:927–934.

Soltz, M. A. and Ateshian, G. A. (2000). A Conewise Linear Elasticity Mixture Model for the Analysis of Tension-Compression Nonlinearity in Articular Cartilage. *Bioengineering*, 122(December 2000):576–586.

Sommer, G., Eder, M., Kovacs, L., Pathak, H., Bonitz, L., Mueller, C., Regitnig, P., and Holzapfel, G. a. (2013). Multiaxial mechanical properties and constitutive modeling of human adipose tissue: a basis for preoperative simulations in plastic and reconstructive surgery. *Acta biomaterialia*, 9(11):9036–48.

Spanos, P. (2003). Cure system effect on low temperature dynamic shear modulus of natural rubber.

Stannard, J. P. and Luck, J. V., editors (2015). *Journal of Knee Surgery*, chapter Cover Art. Thiele Publishers.

Stein, A. M., Vader, D. A., Weitz, D. A., and Sander, L. M. (2010). The Micromechanics of Three-Dimensional Collagen-I Gels. *Complexity*, 16(4):22–28.

Tang, S., Kobayashi, M., Miura, S., Fijuki, H., Iwabuchi, K., and Oomori, S. (2001). Texture and cross slip effects on ultrasonic wave velocity changes under simple and pure shear states. *Japan Society of Mechanical Engineers Proceedings*, 67(660):1402–1408.

Tang, Y., Ballarini, R., Buehler, M. J., and Eppell, S. J. (2010). Deformation micromechanisms of collagen fibrils under uniaxial tension. *Journal of the Royal Society, Interface / the Royal Society*, 7(46):839–850.

Thomas, G. C., Asanbaeva, A., Vena, P., Sah, R. L., and Klisch, S. M. (2009). A nonlinear constituent based viscoelastic model for articular cartilage and analysis of tissue remodeling due to altered glycosaminoglycan-collagen interactions. *Journal of biomechanical engineering*, 131(10):101002.

Toolbox, T. E. (2012). Tensile modulus - modulus of elasticity or young's modulus - for some common materials. http://www.engineeringtoolbox.com/young-modulus-d_417.html. Accessed: 2015-06-02.

Waldman, S. D., Couto, D. C., Grynpas, M. D., Pilliar, R. M., and Kandel, R. a. (2007). Multi-

axial mechanical stimulation of tissue engineered cartilage: Review. *European Cells and Materials*, 13(613):66–73.

Waldman, S. D., Spiteri, C. G., Grynpas, M. D., Pilliar, R. M., and Kandel, R. a. (2003). Long-term intermittent shear deformation improves the quality of cartilaginous tissue formed in vitro. *Journal of orthopaedic research : official publication of the Orthopaedic Research Society*, 21(4):590–6.

Wang, C. C. B., Chahine, N. O., Hung, C. T., and Ateshian, G. A. (2003). Optical determination of anisotropic material properties of bovine articular cartilage in compression. *Journal of Biomechanics*, 36(3):339–353.

Wang, C. C. B., Hung, C. T., and Mow, V. C. (2001). An analysis of the effects of depth-dependent aggregate modulus on articular cartilage stress-relaxation behavior in compression. *Journal of Biomechanics*, 34(1):75–84.

Wartella, K. A. and Wayne, J. S. (2009). Bioreactor for biaxial mechanical stimulation to tissue engineered constructs. *Journal of biomechanical engineering*, 131(4):044501.

Weightman, B. (1976). Tensile fatigue of human articular cartilage. *Journal of biomechanics*, 9(4):193–200.

Williamson, A. K., Chen, A. C., Masuda, K., Thonar, E. J. M. A., and Sah, R. L. (2003). Tensile mechanical properties of bovine articular cartilage: Variations with growth and relationships to collagen network components. *Journal of Orthopaedic Research*, 21(5):872–880.

Wilson, W., Huyghe, J. M., and van Donkelaar, C. C. (2006). A composition-based cartilage

model for the assessment of compositional changes during cartilage damage and adaptation. *Osteoarthritis and cartilage / OARS, Osteoarthritis Research Society*, 14(6):554–60.

Wong, B. L., Bae, W. C., Chun, J., Gratz, K. R., Lotz, M., and Sah, R. L. (2008). Biomechanics of cartilage articulation: Effects of lubrication and degeneration on shear deformation. *Arthritis and Rheumatism*, 58(7):2065–2074.

Wong, B. L. and Sah, R. L. (2010). Mechanical asymmetry during articulation of tibial and femoral cartilages: local and overall compressive and shear deformation and properties. *Journal of biomechanics*, 43(9):1689–95.

Woo, S. L., Akeson, W. H., and Jemmott, G. F. (1976). Measurements of nonhomogeneous, directional mechanical properties of articular cartilage in tension. *Journal of biomechanics*, 9(12):785–791.

Woo, S. L. Y., Lubock, P., Gomez, M. a., Jemmott, G. F., Kuei, S. C., and Akeson, W. H. (1979). Large Deformation Nonhomogeneous and Directional Properties of Articular Cartilage in Uniaxial Tension. *Journal of Biomechanics*, 12(6):437–446.

Zhu, W. B., Mow, V. C., Koob, T. J., and Eyre, D. R. (1993). Viscoelastic Shear Properties of Articular Cartilage and the Effects of Glycosidase Treatments. *Journal of Orthopaedic Research*, 11(6):771–781.